Vapor Pressures of Hydrogen, Deuterium, and Hydrogen Deuteride and Dew-Point Pressures of Their Mixtures[1]

Harold J. Hoge[2] and Robert D. Arnold

The vapor pressures of H_2, HD, and D_2 have been measured from near their triple points to their critical points. The H_2 and D_2 samples were catalyzed to ortho-para equilibrium at 20.4° K. Tables suitable for interpolation have been prepared to represent the results both in centimeter-gram-second and in engineering units.

Measurements of dew-point pressures of several binary mixtures have been made at several pressures below atmospheric. Observed pressures were about 3 percent above those predicted by the law of ideal solutions.

1. Introduction

Many papers dealing with the vapor pressures of various isotopic varieties of hydrogen have appeared since Dennison [1][3] correctly explained the behavior of ortho and para forms in 1927, and since Urey, Brickwedde, and Murphy [2] announced the concentration of deuterium in 1932. So far as we are aware, however, no measurements extending above the range of ordinary mercury manometry had been reported until quite recently, when White, Friedman, and Johnston [3] published data for normal hydrogen extending up to the critical point, and a preliminary report of the present work appeared [4]. Grilly [5] has measured the vapor pressures of the normal varieties of hydrogen, deuterium, and tritium up to approximately 3 atm. Vapor pressures of mixtures had been neglected, there being no information on deviations from the laws of ideal solutions other than that published by Woolley, Scott, and Brickwedde [6, p. 454] for mixtures of ortho and para hydrogen.

The present paper, and one on critical constants [7], being published simultaneously, comprise a full report of a program of determination of the properties of the hydrogens undertaken at the Bureau early in 1950. The work reported in this paper consisted of two parts: the measurement of vapor pressures of H_2, HD, and D_2 from low pressures to their critical points; and the measurement of the dew points of a number of binary mixtures of the same substances at pressures below 1 atm. The vapor-pressure measurements and the dew-point measurements were performed with different apparatuses, and are discussed separately, the vapor-pressure measurements being presented in section 2 and the dew-point measurements in section 3. Except for a few preliminary measurements, all the vapor pressures reported for H_2 and D_2 are for samples catalyzed to ortho-para equilibrium at the boiling point of normal hydrogen (20.4° K). Hydrogen so catalyzed (0.979 para-H_2, 0.021 ortho-H_2) has been designated e-H_2 [6]. Likewise, deuterium catalyzed to equilibrium at 20.4° K (0.022 para-D_2, 0.978 ortho-D_2) is designated e-D_2. It is worth while to emphasize that e-H_2 and e-D_2 were in ortho-para equilibrium only at 20.4° K, and that the composition did not change as the temperature was raised or lowered during the course of the measurements. It had been hoped to measure the vapor pressure of normal, or high-temperature-equilibrium hydrogen (0.25 para-H_2, 0.75 ortho-H_2) and deuterium (0.3333 para-D_2, 0.6667 ortho-D_2), but time did not permit. There are no separate ortho and para varieties of HD.

2. Vapor-Pressure Measurements

2.1. Apparatus and Methods

The apparatus and methods were substantially the same as those recently used to measure the vapor pressure of oxygen and are described in reference [8]. The diaphragm cell used for part of the work on oxygen was not employed.

After part of the present work was completed, it was noted that the floating nickel sleeves and magnetic detectors were not indicating correctly the difference in height of the two mercury meniscuses inside the stainless steel U-tube. This was verified by taking X-ray pictures of the meniscuses. The nickel sleeve at the Hg-H_2O interface (height h_2) was found to be functioning properly, supported entirely above the mercury by the surface tension of the latter. The sleeve at the Hg-H_2 interface (height h_1), however, had been wetted by the mercury and had sunk into it. Measurements affected by this difficulty were calculated from the value of h_2 only, by using a curve of h_1+h_2 versus h_2 plotted from data taken before the trouble developed. There was a considerable range of overlap of the piston-gage measurements with the mercury manometer and the mercury manometer-barometer measurements, in which the various methods were cross-checked from time to time.

The resistance thermometer (L14) that developed a leak during the O_2 measurements was removed and replaced by L11 and L28. With the exception of a few check measurements, all the temperatures in the

[1] This research was supported in part by the Atomic Energy Commission.
[2] Present address, Leeds & Northrup Co., Philadelphia, Pa.
[3] Figures in brackets indicate the literature references at the end of this paper.

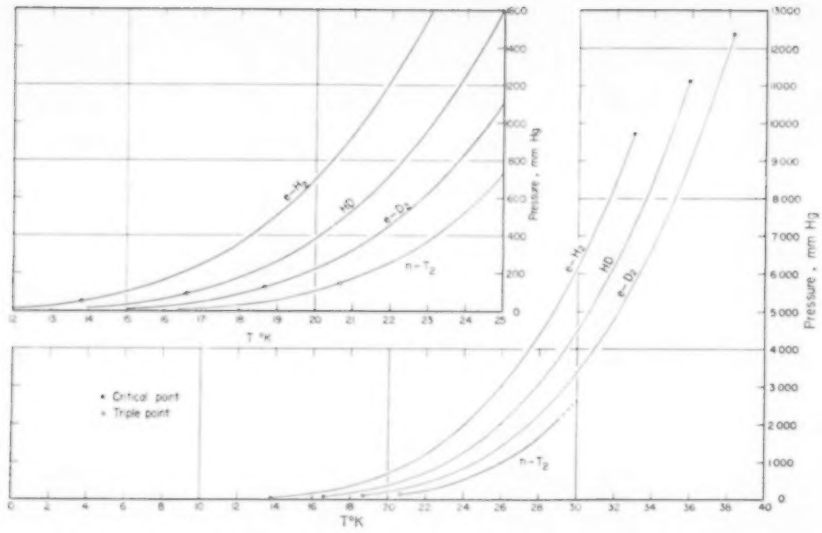

FIGURE 1. *A comparison of the vapor pressures of ordinary hydrogen, hydrogen deuteride, deuterium, and tritium.*

present work were measured with platinum resistance thermometer L11. This thermometer is one of the original group used to define the Bureau's temperature scale below 90° K. Its calibration is discussed in [9].

One improvement was made over the methods used in the oxygen measurements. Rather than make alternate measurements of pressure and of thermometer resistance, it was found more accurate and more convenient to observe the resistance thermometer continuously, keeping the piston gage balanced, until conditions had been steady for several minutes. A valve in the pressure-transmitting line was then closed, after which all the readings associated with the pressure measurement could be made at leisure.

The method of computing pressures was the same as that used for O_2 except that no correction was made for the hydrostatic pressure of hydrogen vapor. The maximum correction (at the critical point) in the case of O_2 was 6.5 mm Hg. It was estimated that the corresponding figure for D_2 would be about 1 mm Hg, with the values for HD and H_2 proportionately less.

Preparation and purity of the samples. The H_2 was taken from the supply generated by electrolysis of H_2O for use in this laboratory's hydrogen liquefier. The HD was prepared for us by Abraham Fookson, Philip Pomerantz, and Edwin H. Rich, who used the reaction

$$LiAlH_4+4D_2O \longrightarrow LiOD+Al(OD)_3+4HD.$$

The D_2 was obtained from the Stuart Oxygen Co. Both the HD and the D_2 were purified by distillation by Fookson, et al. A more complete report of their work is published elsewhere [10].

A number of samples taken at various stages of the vapor-pressure measurements were submitted to the Mass Spectrometry Section of the Bureau for analysis. The results are presented in connection with the discussion of the measurements on each particular substance.

2.2. Ortho-para Catalysis

The catalyst was Nd_2O_3 furnished by the Bureau's Inorganic Chemistry Section. It was a pale blue powder prepared by firing neodymium oxalate at 800° C. To avoid contaminating the H_2 with D_2, the catalyst used for D_2 was removed and replaced by a fresh sample before measurements on H_2 were begun. Each sample was contained in a cylindrical glass chamber of about 1.6-cm inside diameter and 15-cm³ volume. Connections were made by two glass tubes, one ending at the top and the other near the bottom of the chamber. About 10 cm³ of catalyst was placed in each chamber and confined with plugs of glass wool. The catalyst was prepared for use by evacuating for several hours near 440° C, and flushing with small portions of the H_2 (or D_2) to be measured. It was surrounded by liquid hydrogen before use, after which the entire sample of H_2 or D_2 to be measured was condensed on it. A toepler pump was used to circulate the gas so that all the material would come in contact with the catalyst. When gas was transferred from the catalyzing chamber to the cryostat, it was removed through the tube extending to the bottom of the chamber, so that only material that had been in close contact with the catalyst would be obtained. During the catalytic conversion, samples were condensed in the cryostat from time to time and their vapor pressures were observed; they were then recirculated until no further change in vapor pressure was observed. The time required to reach ortho-para equilibrium in the presence of the catalyst at 20.4° K appeared to be short compared to the time required to introduce and remove the sample.

2.3. The Data

Figure 1 gives a general picture of the temperature dependence of the vapor pressures of e-H_2, HD, e-D_2, and n-T_2. The curve for tritium is plotted from the data of Grilly [5]; the rest are our own data. On the scale of this graph, curves for different ortho-para compositions of the same isotope would scarcely be distinguishable.

The experimental data are given in tables 1, 2, 3, and 4. The first three contain the measurements on e-H_2, HD, and e-D_2, respectively. Table 4 contains the results of the first run, which was made on an uncatalyzed sample of D_2 taken directly from the supply cylinder. Presumably this sample was normal D_2, and since no other measurements were made on n-D_2 these preliminary data are being reported. The supply was analyzed by mass spectrometer, the mole fraction of D_2 being 0.99_2; and that of HD, 0.008. The data of table 4 are plotted in figure 3.

Column 1 of each table contains the run number (preceding the decimal point) and the observation number (following the decimal point) of each datum. Runs are numbered chronologically, as are the observations of a given run. Column 2 of each table shows the type of pressure-measuring equipment used. This was either a mercury manometer (Hg), mercury manometer plus barometer (HgB), or piston gage (PG). Columns 3 and 4 of each table contain the observed temperature and the corresponding observed pressure. From the original data in tables 1, 2, and 3, three new tables (5, 6, and 7) were derived giving values of $\log_{10}P$ at uniform values of $200/T$, for e-H_2 HD, and e-D_2, respectively. These tables are suitable for interpolation, and represent the results in essentially the same way that an equation might represent them. Deviations of the experimental data from these tables are given in the final columns of tables 1, 2, and 3. These deviations are plotted in figure 2. Consecutive points of each run have been joined by straight lines where this could be done without cluttering the graphs too much. A few of the deviations were too large to fall within the range of the graphs. Each of these is indicated by a line extending in the direction of the missing point, and the corresponding deviation can be found in table 1, 2, or 3. Near the critical point, where isotherms were also measured, all points inside the liquid-vapor dome are included. Where there was more than one point of a run on the horizontal portion of an isotherm, the temperature and pressure given in tables 1, 2, or 3 were obtained by averaging.

After the single run on uncatalyzed (normal) D_2, the measurements on HD were begun. Having no ortho and para forms, this substance requires no catalyst, but the measurements were complicated by slow conversion of HD into H_2 and D_2. This is shown best in figure 2 by the rise in pressure in the neighborhood of 31° K between successive runs. When liquid hydrogen was not available to keep the cryostat cold, it was our practice not to return the sample to the supply bulb, but to lower the mercury meniscus, h_1, so that the sample occupied most of one arm of the stainless steel U-tube. Returning the material to the supply bulb would have made it necessary to remeasure the mass in use for each successive run, and would have lowered the reproducibility of data obtained in the critical region. The pressure of the confined sample rose to about 30 atm when the cryostat rose to liquid-air temperatures. It is thought that the breakdown of HD to form H_2 and D_2 occurred principally during periods when most of the sample was inside the stainless steel tube and all of it was at relatively high pressure. In addition to stainless steel, the HD was in contact with nickel, copper, brass, and silver-solder. On completion of the measurements on HD, two samples were taken for mass-spectrometer analysis, one from the 5-liter glass bulb containing the unused portion of the original supply, and another from the sample on which measurements had been made. The analysis of the first sample was 0.99_8 HD, 0.001 H_2, and 0.001 D_2, in substantial agreement with an earlier analysis made at the time of distillation.

TABLE 1. *Observations of the vapor pressure of* e-H_2

The column headed ΔP contains deviations of the observed values from table 5.

Observation number	Pressure-measuring system	T	P (observed)	ΔP (observed − calculated)
		°K	mm Hg	mm Hg
14.1	Hg	17.8294	338.4	−0.1
14.2	Hg	18.5812	442.1	−.3
14.3	Hg	19.1245	530.7	−.1
14.4	Hg	20.0401	707.7	−.1
14.5	Hg	20.4089	789.6	.2
14.6	Hg	20.5118	813.7	−.2
14.7	Hg	16.9549	241.4	−.2
14.8	Hg	20.2648	757.1	.1
14.9	HgB	20.5167	815.2	.1
14.10	HgB	20.8655	900.7	.0
14.11	HgB	21.2046	989.8	−.1
15.1	HgB	20.9513	922.1	−.6
15.2	HgB	21.3379	1026.8	.2
15.3	PG	23.6441	1827.1	−.5
15.4	PG	24.4501	2189.4	−.1
15.5	PG	24.9003	2414.1	1.7
15.6	PG	25.5711	2773.5	0.2
15.7	PG	26.1980	3142.6	−.7
15.8	PG	26.7811	3517.5	.4
15.9	PG	27.4083	3952.7	.0
15.10	PG	28.3858	4705.7	.8
15.11	PG	29.3956	5583.9	.2
15.12	PG	30.3776	6544.6	.5
15.13	PG	31.4021	7660.2	−4.9
16.3	Hg	16.9752	243.1	−0.5
16.4	Hg	15.8414	149.7	−.3
16.5	PG	22.2604	1308.4	.2
16.6	PG	22.9058	1534.9	−.2
16.7	PG	25.0473	2488.5	.0
16.8	PG	27.8744	4288.6	−.2
16.9	PG	29.9173	6080.2	−.3
16.10	PG	30.9020	7102.8	.8
16.11	PG	31.8910	8255.1	7.7
17.1	PG	22.2800	1313.8	−0.9
17.2	PG	22.5792	1416.1	−1.0
17.3	PG	28.8797	5121.5	0.2
17.4	PG	31.0820	7302.5	1.5
18.1	PG	20.9534	922.5	−0.7
18.2	PG	21.6873	1127.2	−.4
18.3	PG	25.8955	2960.3	−.4
[a] 18.6	PG	32.8933	9566.2	3.1
19.1	PG	32.8836	9564.4	0.6
[b] 19.4	PG	32.8926	9559.3	−2.9
19.5	PG	32.6457	9219.5	−2.2
19.6	PG	32.3853	8875.1	0.3
19.7	PG	32.1392	8557.7	−.5

[a] Average of four observations.

[b] Average of three observations.

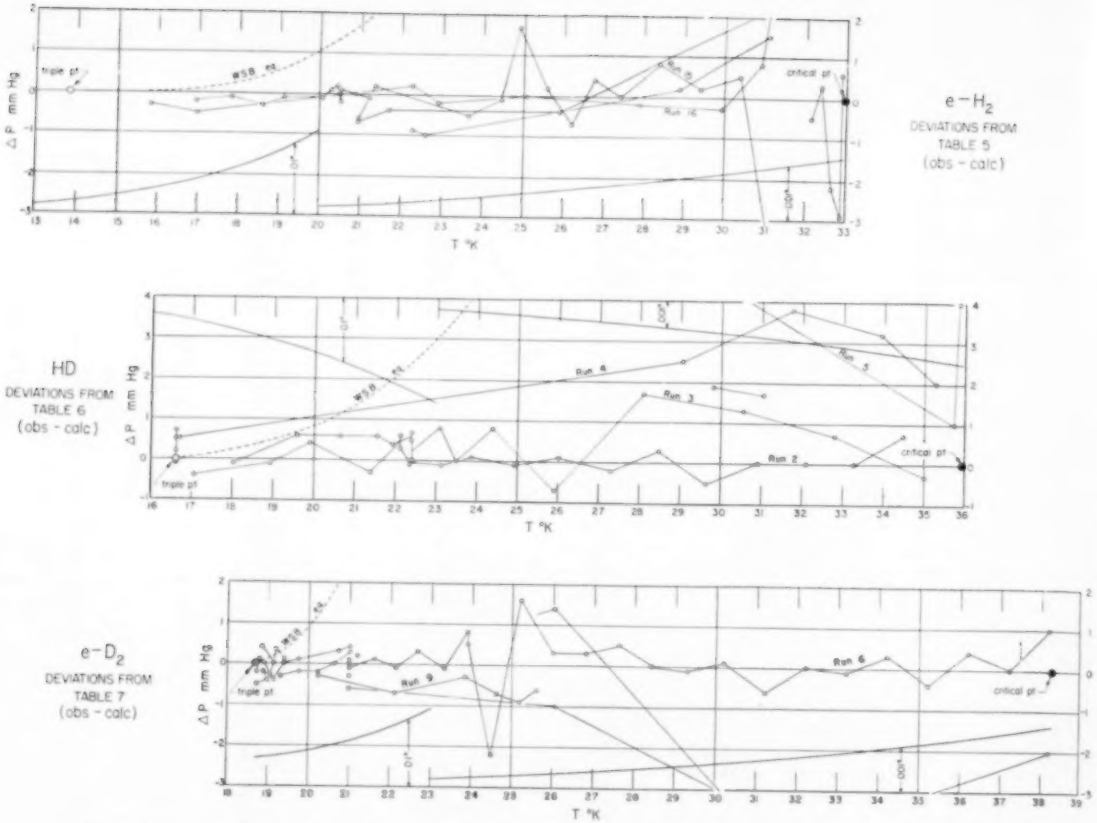

FIGURE 2. *Deviations of the experimental data in tables 1, 2, and 3 from tables 5, 6, and 7, respectively.*

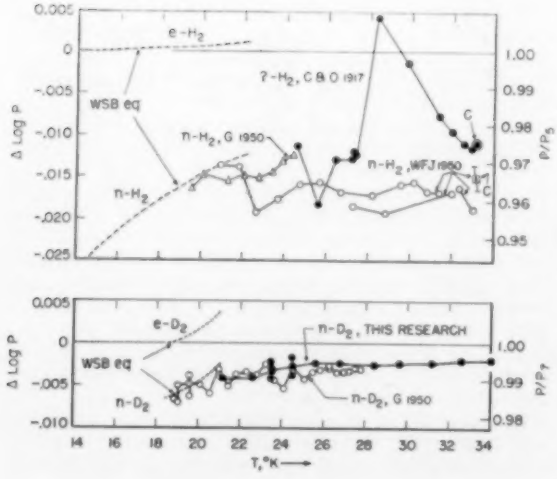

FIGURE 3. *Published vapor-pressure data compared with tables 5 and 7.*

Above: Published data for n-H_2 compared with table 5. $\Delta\log P = \log P$ (observed) minus $\log P$ (table 5). $P/P_5 = P$ (observed) / P (table 5). Below: Published data for n-D_2 compared with table 7. $\Delta\log P = \log P$ (observed) minus $\log P$ (table 7). $P/P_7 = P$ (observed) / P (table 7). Note that agreement is not to be expected, since in each case the table refers to the *equilibrium* variety, whereas the plotted points are the normal variety. The lower graph contains one set of data obtained in this research—those of table 4. C & O, Cath and Onnes; G, Grilly; WFJ, White, Friedman, and Johnston. C, Critical point.

TABLE 2. *Observations of the vapor pressure of* HD

The column headed ΔP contains deviations of the observed values from table 6.

Observation number	Pressure-measuring system	T	P (observed)	ΔP (observed−calculated)
		° K	*mm* Hg	*mm* Hg
2.1	Hg	17.046	114.5	−0.4
2.2	Hg	18.935	257.6	−.1
2.3	Hg	19.895	368.5	.4
2.4	Hg	21.388	604.5	−.3
2.5a	Hg	22.121	755.3	.3
2.5b	PG	22.121	755.6	.6
2.6a	Hg	22.364	810.2	−.1
2.6b	PG	22.364	810.3	.0
2.7	PG	23.108	997.9	−.1
2.8	PG	23.861	1218.2	.1
2.9	PG	24.920	1584.0	−.1
2.10	PG	26.024	2042.4	.1
2.11	PG	27.288	2673.9	−.2
2.12	PG	28.492	3393.1	.3
2.13	PG	29.652	4202.9	−.5
2.14	PG	30.889	5208.5	.0
2.15	PG	32.098	6344.7	.0
2.16	PG	33.285	7623.9	.0
2.17	PG	34.489	9105.5	.7
3.1	PG	31.049	5351.5	1.7
3.2	PG	29.814	4328.3	1.9
3.3	Hg	18.007	176.6	−0.1
3.4	Hg	19.580	329.2	.6
3.5	Hg	20.638	475.7	.6
3.6	Hg	21.554	637.4	.6
3.7	Hg	21.933	714.6	.4
3.8a	PG	22.394	817.8	.5
3.8b	Hg	22.394	818.0	.7
3.8c	PG	22.395	817.6	.0
3.9	PG	23.090	993.9	.8
3.10	PG	23.506	1110.4	.0
3.11	PG	24.390	1393.1	.8
3.12	PG	25.919	1994.4	−.7
3.13	PG	28.096	3144.8	1.7
3.14	PG	30.565	4931.8	1.3
3.15	PG	32.814	7096.6	0.7
[a] 3.16	PG	35.0334	9842.1	−.3
4.2a	Hg	[b] 16.5958	93.2	.7
4.2b	Hg	[b] 16.5966	93.0	.5
4.2c	Hg	[b] 16.5982	93.0	.5
4.4a	Hg	[b] 16.5980	92.9	.3
4.4b	Hg	[b] 16.5982	92.5	−.1
4.5	Hg	16.6718	96.5	.5
4.6	PG	29.035	3759.6	2.5
4.7	PG	31.763	6017.5	3.8
4.8	PG	33.948	8418.3	3.2
4.9	PG	35.276	10188	2
5.1	PG	30.374	4775.8	4.2
[a] 5.2	PG	35.7493	10887	1
[d] 5.3	PG	35.8797	11090	4

[a] Average of five observations.
[b] Triple point.
[c] Average of six observations.
[d] Average of two observations.

TABLE 3. *Observations of the vapor pressure of* e-D_2

The column headed ΔP contains deviations of the observed values from table 7.

Observation number	Pressure-measuring apparatus	T	P (observed)	ΔP (observed−calculated)
		° K	*mm* Hg	*mm* Hg
6.1d	Hg	20.9914	323.1	0.0
6.1e	Hg	20.9909	323.1	.1
6.1f	Hg	20.9909	322.9	−.1
6.2	Hg	21.6127	402.0	.1
6.3	Hg	22.1477	480.5	−.1
6.4	Hg	22.6805	570.1	.3
6.5	Hg	23.3317	694.7	−.1
6.6a	PG	23.8950	819.2	.8
6.6b	Hg	23.8953	818.9	.5
6.7	PG	24.4938	964.4	−2.2
6.8	PG	25.1942	1165.6	1.6
6.9	PG	25.9961	1424.5	0.3
6.10	PG	26.7961	1723.6	.3
6.11	PG	27.5954	2064.5	.5
6.12	PG	28.3966	2450.9	.0
6.13	PG	29.3002	2945.8	−.1
6.14	PG	30.1943	3501.4	.1
6.15	PG	31.1991	4209.2	−.6
6.16	PG	32.1980	5008.4	.0
6.17	PG	33.1984	5910.1	−.1
6.18	PG	34.1968	6929.7	.3
6.19	PG	35.1947	8048.2	−.4
6.20	PG	36.1982	9311.3	.4
[a]6.21	PG	37.1987	10708	0
6.22c	PG	38.2017	12274	1
7.1	Hg	20.9935	323.1	−0.2
7.2	PG	26.0185	1437.4	1.4
7.3	PG	32.2375	5036.8	−5.3
8.1	Hg	20.9875	322.0	−0.6
8.2	PG	26.0569	1444.5	−1.0
8.3	PG	32.2532	5051.4	−4.1
[b]8.6	PG	38.2034	12274	−2
9.1	Hg	20.9927	323.3	0.1
9.15	Hg	20.2347	243.3	−.3
9.16	Hg	22.1128	474.4	−.7
9.17	Hg	23.8370	804.6	−.3
9.18	HgB	24.6055	995.7	−.7
9.19	HgB	25.1752	1157.5	−.9
9.20	HgB	25.5973	1289.5	−.6
10.1	Hg	20.9991	324.3	.3
10.2	Hg	20.6377	283.8	.0
10.3	Hg	20.2178	241.8	−.2
10.4	Hg	19.7467	200.7	−.2
10.5	Hg	19.3116	167.7	−.3
10.7	Hg	21.1878	346.8	.2
11.1a	Hg	20.9935	323.0	−.3
11.1b	Hg	20.9944	323.7	.3
12.1	Hg	21.0145	326.2	.4
12.2	Hg	20.7220	293.1	.3
12.3	Hg	19.7457	200.9	.1
12.4	Hg	19.3730	172.4	.0
12.5	Hg	19.1332	155.4	−.4
12.6	Hg	18.8678	138.7	−.2
12.7	Hg	18.9821	145.6	−.4
12.8	Hg	18.7098	129.1	−.5
13.1	Hg	19.3963	174.2	.1
13.2	Hg	19.2038	160.8	.3
13.3	Hg	19.0467	149.8	−.3
13.4	Hg	18.9056	141.2	.0
13.5	Hg	18.7684	132.9	.1
13.6	Hg	18.7063	129.2	−.2
13.20	Hg	19.1459	156.9	.0
13.21	Hg	18.8379	137.5	.4

[a] Average of three observations.
[b] Average of two observations.

The analysis of the material removed from the cryostat, however, was 0.971 HD, 0.015 H_2, and 0.014 D_2. A calculation showed that this amount of decomposition of HD would raise the vapor pressure about twice as much as was actually observed. This is not surprising, for one would expect a fractionation of the isotopic impurities as the measurements proceeded. Run 2 was made immediately after introduction of HD into the apparatus, and hence presumably before any appreciable decomposition had occurred. Therefore it has been given a much greater weight than any of the other runs in determining the table to represent the vapor pressure of HD.

The measurements on e-D_2 were made following removal of HD from the apparatus. It was found desirable to recatalyze both e-D_2 and e-H_2 to ortho-para equilibrium at 20.4° K whenever any substantial part of the sample had been at room temperature for periods longer than an hour or two. On some occasions the change of vapor pressure resulting from catalysis of previously uncatalyzed samples was observed, and found to be in substantial agreement with the differences in vapor pressure of normal and equilibrium varieties found by Brickwedde and Scott [6, p. 452]. On removal from the apparatus the mass-spectrometer analysis of the sample was 0.995 D_2 and 0.005 HD. We were somewhat disappointed in this purity, but have no reason to

TABLE 4. *Observations of the vapor pressure of* n-D_2

Assumed to be n-D_2 because no catalyst was used

Observation number	Pressure-measuring system	T	P (observed)
		°K	mm Hg
1.1	Hg	21.124	335.6
1.2	Hg	22.612	552.5
1.3a	Hg	23.563	738.2
1.3b	PG	23.560	737.3
1.3c	PG	23.510	729.0
1.3d	Hg	23.511	725.5
1.4a	HgB	24.545	974.1
1.4b	PG	24.546	976.9
1.4c	HgB	24.560	975.6
1.5	PG	25.596	1283.0
1.6	PG	26.787	1710.6
1.7	PG	28.454	2466.1
1.8	PG	29.639	3131.4
1.9	PG	31.216	4201.0
1.10	PG	32.604	5337.2
1.11	PG	34.110	6800.6

doubt the accuracy of this analysis. Some memory effect was present in the mass spectrometer, but this was eliminated by use of a reference sample, which, by repeated runnings, was found to have a purity of 0.998 D_2. Analysis of our sample was then made by comparing it with the reference sample. We feel that the sample was at least as pure as the analysis indicated. No correction has been made for impurity.

A large number of measurements were made on e-D_2 near the triple point, both on the solid and on the liquid. Unfortunately, the apparatus was found to be poorly suited to rapid work in this region. Unless the apparatus was cooled very slowly, a section of the pressure-transmitting tube would become colder than the equilibrium chamber and the tube would become plugged with solid. As a result, the fraction of the observations below the triple point that were obviously bad was so large that all have been rejected. Just above the triple point the situation was better, but a considerable number of observations have been rejected. The deviations of the rejected points were almost all very large compared to those of the points plotted in figure 2. They were almost always negative, indicating that the plug of solid in the tube remained for some time below the temperature of the equilibrium chamber.

Before introducing H_2, the final substance, into the apparatus, the catalyzing chamber used for e-D_2 was removed and a similar one containing fresh catalyst substituted. No attempt was made to carry the measurements on e-H_2 very near to the triple point. When removed from the apparatus, the sample on which measurements had been made was analysed by mass spectrometer. The analysis was 0.999 H_2 and 0.001 HD. The only known source of deuterium contamination was desorption of the previous sample from the interior of the apparatus, which would hardly be expected to yield 1 per mill of HD. However, 1 per mill is the estimated uncertainty of the mass-spectrometer analyses, so this amount of HD is hardly a cause for concern.

2.4. Deriving the Smoothed Tables

Tables 5, 6, and 7, used in lieu of equations to represent the vapor-pressure-versus-temperature relation for each substance, were derived from the original data by the use of deviation plots. Various forms of equation were used. For e-H_2, for example, the equation of Woolley, Scott, and Brickwedde [6, p. 454] was used below about 28° K, in which range the observed values of $\log_{10}P$ do not deviate from the equation by more than about 0.00300. Between 28° and the critical point a different form of equation was used that had a smaller curvature near the critical point. Deviations of the observations from the equations were plotted versus the temperature, with a considerable range of overlap of the two equations. Smooth curves were drawn through the points. On these the temperatures corresponding to the values of $200/T$ appearing in table 5 were marked. At each of these temperatures the ordinate ($\log_{10}P_{obs}-\log_{10}P_{calc}$) was read and recorded. The equation was evaluated at the same temperatures and the ordinates of the smooth deviation curve added to the corresponding values of the equation.

The resulting table was differenced to third differences on an Underwood-Sundstrand automatic accounting machine. The table was smoothed by inspection of the differences, and redifferenced. The final result was table 5. Similar procedures, with minor variations, led to tables 6 and 7. For HD, the equation

$$\log_{10} P = A + (B/T) + C\left(\frac{100}{T} - D\right)^{\alpha}$$

was used throughout the entire liquid range. Above 24° K it represents the data almost within the experimental error, and the deviations at lower temperatures are small enough for satisfactory plotting. The value of D used was 2.5, or approximately $90/T_c$, and the exponent, α, was 0.71.

Tables 5, 6, and 7 are given in pressure units of millimeters of mercury, atmospheres, and pounds per square inch absolute; and in temperature units of degrees Kelvin and Rankine having been prepared in this form for inclusion in the NBS-NACA series of Tables of Thermal Properties of Gases [11]. For purposes where accurate interpolation is not necessary, it is more convenient to have tables with T as argument rather than $200/T$. Hence table 8, giving vapor pressures of all three varieties at temperature intervals of 1 deg K has been calculated from tables 5, 6, and 7. Table 9 contains the triple points and boiling points. Critical points are given in reference [7].

2.5. Comparison With Previous Work

The survey paper of Woolley, Scott, and Brickwedde [6], which appeared in 1948, contains an adequate summary of vapor-pressure data for the hydrogens published up so that time. Their paper

TABLE 5. *Vapor pressure of liquid* e-H_2 *(for interpolation)*

Interpolation with $200/T$ as argument is more accurate and also more convenient than interpolation with T as argument. Linear interpolation introduces no significant errors below about 23° K. Between 23° and 30° K linear interpolation is slightly inferior to higher-order interpolation, and above 30° K higher-order interpolation should be used if accurate values are required

$\frac{200}{T}$	T	$\text{Log}_{10}P$			Δ	T	$\frac{360}{T}$
°K^{-1}	°K	*mm Hg*	*atm*	*psia*		°*R*	°R^{-1}
14.5	13.793	(1.7176)	a(8.8368)	(0.0040)	242	24.828	14.5
14.4	13.889	1.7418	8.8610	.0282	242	25.000	14.4
14.3	13.986	1.7660	8.8852	.0524	242	25.175	14.3
14.2	14.085	1.7902	8.9094	.0766	242	25.352	14.2
14.1	14.184	1.8144	8.9336	.1008	243	25.532	14.1
14.0	14.286	1.8387	8.9579	.1251	243	25.714	14.0
13.9	14.388	1.8630	8.9822	.1494	244	25.899	13.9
13.8	14.493	1.8874	9.0066	.1738	244	26.087	13.8
13.7	14.599	1.9118	9.0310	.1982	244	26.277	13.7
13.6	14.706	1.9362	9.0554	.2226	244	26.471	13.6
13.5	14.815	1.9606	9.0798	.2470	245	26.667	13.5
13.4	14.925	1.9851	9.1043	.2715	245	26.866	13.4
13.3	15.038	2.0096	9.1288	.2960	245	27.068	13.3
13.2	15.152	2.0341	9.1533	.3205	246	27.273	13.2
13.1	15.267	2.0587	9.1779	.3451	247	27.481	13.1
13.0	15.385	2.0834	9.2026	.3698	246	27.692	13.0
12.9	15.504	2.1080	9.2272	.3944	247	27.907	12.9
12.8	15.625	2.1327	9.2519	.4191	247	28.125	12.8
12.7	15.748	2.1574	9.2766	.4438	248	28.346	12.7
12.6	15.873	2.1822	9.3014	.4686	248	28.571	12.6
12.5	16.000	2.2070	9.3262	.4934	249	28.800	12.5
12.4	16.129	2.2319	9.3511	.5183	249	29.032	12.4
12.3	16.260	2.2568	9.3760	.5432	250	29.268	12.3
12.2	16.393	2.2818	9.4010	.5682	250	29.507	12.2
12.1	16.529	2.3068	9.4260	.5932	250	29.752	12.1
12.0	16.667	2.3318	9.4510	.6182	251	30.000	12.0
11.9	16.807	2.3569	9.4761	.6433	251	30.253	11.9
11.8	16.949	2.3820	9.5012	.6684	252	30.508	11.8
11.7	17.094	2.4072	9.5264	.6936	252	30.769	11.7
11.6	17.241	2.4324	9.5516	.7188	253	31.034	11.6
11.5	17.391	2.4577	9.5769	.7441	254	31.304	11.5
11.4	17.544	2.4831	9.6023	.7695	254	31.579	11.4
11.3	17.699	2.5085	9.6277	.7949	255	31.858	11.3
11.2	17.857	2.5340	9.6532	.8204	255	32.143	11.2
11.1	18.018	2.5595	9.6787	.8459	256	32.432	11.1
11.0	18.182	2.5851	9.7043	.8715		32.728	11.0
11.0	18.182	2.58503	9.70425	.87144	2564	32.728	11.0
10.9	18.349	2.61070	9.72989	.89708	2571	33.028	10.9
10.8	18.519	2.63641	9.75560	.92279	2578	33.334	10.8
10.7	18.692	2.66219	9.78138	.94857	2585	33.646	10.7
10.6	18.868	2.68804	9.80723	.97442	2591	33.962	10.6
10.5	19.048	2.71395	9.83314	1.00033	2598	34.286	10.5
10.4	19.231	2.73993	9.85912	1.02631	2606	34.616	10.4
10.3	19.417	2.76599	9.88518	1.05237	2613	34.951	10.3
10.2	19.608	2.79212	9.91131	1.07850	2621	35.294	10.2
10.1	19.802	2.81833	9.93752	1.10471	2628	35.644	10.1
10.0	20.000	2.84461	9.96380	1.13099	2637	36.000	10.0
9.9	20.202	2.87098	9.99017	1.15736	2646	36.364	9.9
9.8	20.408	2.89744	0.01663	1.18382	2654	36.734	9.8
9.7	20.619	2.92398	.04317	1.21036	2663	37.114	9.7
9.6	20.833	2.95061	.06980	1.23699	2672	37.499	9.6
9.5	21.053	2.97733	.09652	1.26371	2682	37.895	9.5
9.4	21.277	3.00415	.12334	1.29053	2692	38.299	9.4
9.3	21.505	3.03107	.15026	1.31745	2702	38.709	9.3
9.2	21.739	3.05809	.17728	1.34447	2712	39.130	9.2
9.1	21.978	3.08521	.20440	1.37159	2723	39.560	9.1
9.0	22.222	3.11244	.23163	1.39882	2735	40.000	9.0
8.9	22.472	3.13979	.25898	1.42617	2746	40.450	8.9
8.8	22.727	3.16725	.28644	1.45363	2758	40.909	8.8
8.7	22.989	3.19483	.31402	1.48121	2770	41.380	8.7
8.6	23.256	3.22253	.34172	1.50891	2783	41.861	8.6
8.5	23.529	3.25036	.36955	1.53674	2797	42.352	8.5
8.4	23.810	3.27833	.39752	1.56471	2810	42.858	8.4
8.3	24.096	3.30643	.42562	1.59281	2825	43.373	8.3
8.2	24.390	3.33468	.45387	1.62106	2839	43.902	8.2
8.1	24.691	3.36307	.48226	1.64945	2854	44.444	8.1
8.0	25.000	3.39161	.51080	1.67799	2869	45.000	8.0
7.9	25.316	3.42030	.53949	1.70668	2886	45.569	7.9
7.8	25.641	3.44916	.56835	1.73554	2903	46.154	7.8
7.7	25.974	3.47819	.59738	1.76457	2919	46.753	7.7
7.6	26.316	3.50738	.62657	1.79376	2936	47.369	7.6
7.5	26.667	3.53674	.65593	1.82312	2954	48.001	7.5
7.4	27.027	3.56628	.68547	1.85266	2973	48.649	7.4
7.3	27.397	3.59601	.71520	1.88239	2993	49.315	7.3
7.2	27.778	3.62594	.74513	1.91232	3016	50.000	7.2
7.1	28.169	3.65610	.77529	1.94248	3040	50.704	7.1

TABLE 5. *Vapor pressure of liquid* e-H_2 *(for interpolation)*—Continued

$\frac{200}{T}$	T	$\text{Log}_{10}P$			Δ	T	$\frac{360}{T}$
°K^{-1}	°K	*mm Hg*	*atm*	*psia*		°*R*	°R^{-1}
7.0	28.571	3.68650	0.80569	1.97288		51.428	7.0
6.9	28.986	3.71716	.83635	2.00354	3066	52.175	6.9
6.8	29.412	3.74808	.86727	2.03446	3092	52.942	6.8
6.7	29.851	3.77927	.89846	2.06565	3119	53.732	6.7
6.6	30.303	3.81073	.92992	2.09711	3146	54.545	6.6
6.5	30.769	3.84246	.96165	2.12884	3173	55.384	6.5
6.4	31.250	3.87451	.99370	2.16089	3205	56.250	6.4
6.3	31.746	3.90688	1.02617	2.19336	3247	57.143	6.3
6.2	32.258	3.94001	1.05920	2.22639	3303	58.064	6.2
6.1	32.787	3.97382	1.09301	2.26020	3381	59.017	6.1
6.0	33.333	(4.00869)	(1.12788)	(2.29507)	3487	60.000	6.0
5.9	33.898	(4.04498)	(1.16417)	(2.33136)	3629	61.016	5.9

a Figures in parentheses are extrapolated values, to facilitate interpolation.

contains equations and tables giving what the authors judged to be the best values of the vapor pressures of e-H_2, n-H_2, HD, e-D_2, and n-D_2 up to about 1 atm. Tables 5, 6, and 7 are consistent with the triple-point temperatures and pressures accepted by Woolley, Scott, and Brickwedde (WSB) [6, p. 453]. On the basis of the present data alone, slightly different triple points are obtained for HD and e-D_2 (the triple point of e-H_2 was not measured), but the differences are so small that the WSB triple points have been retained. It has not, however, been possible to retain the same boiling points. Above the triple points, the WSB vapor pressures are higher than the present ones. This is shown by the three dotted curves in figure 2 labeled WSB equation. If expressed in terms of temperature, the deviations of the WSB equations for e-H_2 and HD from tables 5 and 6 are nearly the same, both equations being about 4 mdeg low at 19° K and 9 mdeg low at 22° K. Such a discrepancy is probably due to a difference in temperature scales. In this connection it should be pointed out that most of the data on which the WSB equations are based were taken *before* this Bureau's temperature scale [9] below 90° K was established. They were for the most part expressed as differences of vapor-pressures of different modifications, as a function of the vapor pressure of a particular modification. Part of the WSB data, however, related the resistance of thermometer L6 or L3 to the vapor pressure of hydrogen (generally e-H_2), and these were used to establish the temperatures of all the measurements. A discrepancy of up to 9 mdeg between the present temperature scale and that of the WSB equations seems large, but it unquestionably exists.

The deviation of the WSB equation for e-D_2 from the present results increases much more rapidly than the deviations for e-H_2 and HD. However, the WSB data for e-D_2 covered a range of less than 2 degrees K (18.691° to 20.4° K), whereas their measurements on liquid HD covered a range of nearly 4 degrees K, and on liquid e-H_2 of more than 6 degrees K. It is not surprising that the equation based on the

TABLE 6. *Vapor pressure of liquid* HD *(for interpolation)*

Interpolation with $200/T$ as argument is more accurate and also more convenient than interpolation with T as argument. Linear interpolation introduces no significant errors below about 25° K. Between 25° and 32° K linear interpolation is slightly inferior to higher-order interpolation, and above 32° K higher-order interpolation should be used if accurate values are required.

$\frac{200}{T}$	T	$\text{Log}_{10}P$			Δ	T	$\frac{360}{T}$
$°K^{-1}$	$°K$	*mm Hg*	*atm*	*psia*		$°R$	$°R^{-1}$
12.1	16.529	(1.9516)	*(9.0708)	(0.2380)	295	29.572	12.1
12.0	16.667	1.9811	9.1003	.2675	296	30.001	12.0
11.9	16.807	2.0107	9.1299	.2971	297	30.253	11.9
11.8	16.949	2.0404	9.1596	.3268	297	30.508	11.8
11.7	17.094	2.0701	9.1893	.3565	297	30.769	11.7
11.6	17.241	2.0998	9.2190	.3862	298	31.034	11.6
11.5	17.391	2.1296	9.2488	.4160	299	31.304	11.5
11.4	17.544	2.1595	9.2787	.4459	298	31.579	11.4
11.3	17.699	2.1893	9.3085	.4757	299	31.858	11.3
11.2	17.857	2.2192	9.3384	.5056	300	32.143	11.2
11.1	18.018	2.2492	9.3684	.5356	300	32.432	11.1
11.0	18.182	2.2792	9.3984	.5656	301	32.728	11.0
10.9	18.349	2.3093	9.4285	.5957	301	33.028	10.9
10.8	18.519	2.3394	9.4887	.6258	301	33.334	10.8
10.7	18.692	2.3695	9.4589	.6559	302	33.646	10.7
10.6	18.868	2.3997	9.4887	.6861	303	33.962	10.6
10.5	19.048	2.4300	9.5492	.7164	303	34.286	10.5
10.4	19.231	2.4603	9.5795	.7467	304	34.616	10.4
10.3	19.417	2.4907	9.6099	.7771	304	34.951	10.3
10.2	19.608	2.5211	9.6403	.8075	305	35.294	10.2
10.1	19.802	2.5516	9.6708	.8380	305	35.644	10.1
10.0	20.000	2.5821	9.7013	.8685		36.000	10.0
10.0	20.000	2.58207	9.70126	.86845	3057	36.000	10.0
9.9	20.202	2.61264	9.73183	.89802	3063	36.364	9.9
9.8	20.408	2.64327	9.76246	.92965	3070	36.734	9.8
9.7	20.619	2.67397	9.79316	.96035	3077	37.114	9.7
9.6	20.833	2.70474	9.82393	.99112	3084	37.499	9.6
9.5	21.053	2.73558	9.85477	1.02195	3091	37.895	9.5
9.4	21.277	2.76649	9.88568	1.05288	3097	38.299	9.4
9.3	21.505	2.79746	9.91665	1.08384	3104	38.709	9.3
9.2	21.739	2.82850	9.94769	1.11488	3111	39.130	9.2
9.1	21.978	2.85961	9.97880	1.14599	3119	39.560	9.1
9.0	22.222	2.89080	0.00999	1.17718	3128	40.000	9.0
8.9	22.472	2.92208	.04127	1.20846	3137	40.450	8.9
8.8	22.727	2.95345	.07264	1.23983	3148	40.909	8.8
8.7	22.989	2.98493	.10412	1.27131	3156	41.380	8.7
8.6	23.256	3.01649	.13568	1.30287	3165	41.861	8.6
8.5	23.529	3.04814	.16733	1.33452	3176	42.352	8.5
8.4	23.810	3.07990	.19909	1.36628	3188	42.858	8.4
8.3	24.096	3.11178	.23097	1.39816	3199	43.373	8.3
8.2	24.390	3.14377	.26296	1.43015	3208	43.902	8.2
8.1	24.691	3.17585	.29504	1.46223	3218	44.444	8.1
8.0	25.000	3.20803	.32722	1.49441	3229	45.000	8.0
7.9	25.316	3.24032	.35951	1.52670	3243	45.569	7.9
7.8	25.641	3.27275	.39194	1.55913	3255	46.154	7.8
7.7	25.974	3.30530	.42449	1.59168	3267	46.753	7.7
7.6	26.316	3.33797	.45716	1.62435	3281	47.369	7.6
7.5	26.667	3.37078	.48997	1.65716	3297	48.001	7.5
7.4	27.027	3.40375	.52994	1.69013	3311	48.649	7.4
7.3	27.397	3.43686	.55605	1.72324	3326	49.315	7.3
7.2	27.778	3.47012	.58931	1.75650	3342	50.000	7.2
7.1	28.169	3.50354	.62273	1.78992	3358	50.704	7.1
7.0	28.571	3.53712	.65631	1.82350	3375	51.428	7.0
6.9	28.986	3.57087	.69006	1.85725	3394	52.175	6.9
6.8	29.412	3.60481	.72400	1.89119	3415	52.942	6.8
6.7	29.851	3.63896	.75815	1.92534	3438	53.732	6.7
6.6	30.303	3.67334	.79253	1.95972	3461	54.545	6.6
6.5	30.769	3.70795	.82714	1.99433	3486	55.384	6.5
6.4	31.250	3.74281	.86200	2.02919	3514	56.250	6.4
6.3	31.746	3.77795	.89714	2.06433	3546	57.143	6.3
6.2	32.258	3.81341	.93260	2.09979	3579	58.064	6.2
6.1	32.787	3.84920	.96839	2.13558	3614	59.017	6.1
6.0	33.333	3.88534	1.00453	2.17172	3654	60.000	6.0
5.9	33.898	3.92188	1.04107	2.20826	3700	61.016	5.9
5.8	34.483	3.95888	1.07807	2.24526	3757	62.069	5.8
5.7	35.088	3.99645	1.11564	2.28283	3829	63.158	5.7
5.6	35.714	4.03474	1.15393	2.32112	3919	64.285	5.6
5.5	36.364	(4.07393)	(1.19312)	(2.36031)	4031	65.455	5.5
5.4	37.037	(4.11424)	(1.23343)	(2.40062)		66.667	5.4

* Figures in parentheses are extrapolated values, to facilitate interpolation.

TABLE 7. *Vapor pressure of liquid* e-D_2 *(for interpolation)*

Interpolation with $200/T$ as argument is more accurate and also more convenient than interpolation with T as argument. Linear interpolation introduces no significant errors below about 27° K. Between 27° and 33.5° K linear interpolation is slightly inferior to higher-order interpolation, and above 33.5° K higher-order interpolation should be used if accurate values are required.

$\frac{200}{T}$	T	$\text{Log}_{10}P$			Δ	T	$\frac{360}{T}$
$°K^{-1}$	$°K$	*mm* Hg	*atm*	*psia*		$°R$	$°R^{-1}$
10.8	18.519	(2.0783)	(9.1945)	(0.3617)	337	33.334	10.8
10.7	18.692	2.1060	9.2282	.3954	338	33.646	10.7
10.6	18.868	2.1428	9.2620	.4292	338	33.962	10.6
10.5	19.048	2.1766	9.2958	.4630	339	34.286	10.5
10.4	19.231	2.2105	9.3297	.4969	340	34.616	10.4
10.3	19.417	2.2445	9.3637	.5309	341	34.951	10.3
10.2	19.608	2.2786	9.3978	.5650	341	35.294	10.2
10.1	19.802	2.3127	9.4319	.5991	342	35.644	10.1
10.0	20.000	2.3469	9.4661	.6333	342	36.000	10.0
9.9	20.202	2.3811	9.5003	.6675	344	36.364	9.9
9.8	20.408	2.4155	9.5347	.7019	344	36.734	9.8
9.7	20.619	2.4499	9.5691	.7363	344	37.114	9.7
9.6	20.833	2.4843	9.6035	.7707	346	37.499	9.6
9.5	21.053	2.5189	9.6381	.8053		37.895	9.5
9.5	21.053	2.51889	9.63808	.80527	3461	37.895	9.5
9.4	21.277	2.55350	9.67269	.83988	3464	38.299	9.4
9.3	21.505	2.58814	9.70733	.87452	3468	38.709	9.3
9.2	21.739	2.62282	9.74201	.90920	3472	39.130	9.2
9.1	21.978	2.65754	9.77673	.94392	3476	39.560	9.1
9.0	22.222	2.69230	9.81149	.97868	3483	40.000	9.0
8.9	22.472	2.72713	9.84632	1.01351	3490	40.450	8.9
8.8	22.727	2.76203	9.88122	1.04841	3497	40.909	8.8
8.7	22.989	2.79700	9.91619	1.08338	3504	41.380	8.7
8.6	23.256	2.83204	9.95123	1.11842	3512	41.861	8.6
8.5	23.529	2.86716	9.98635	1.15354	3519	42.352	8.5
8.4	23.810	2.90235	0.02154	1.18873	3527	42.857	8.4
8.3	24.096	2.93762	.05681	1.22400	3536	43.373	8.3
8.2	24.390	2.97298	.09217	1.25936	3546	43.902	8.2
8.1	24.691	3.00844	.12763	1.29482	3555	44.444	8.1
8.0	25.000	3.04399	.16318	1.33037	3564	45.000	8.0
7.9	25.316	3.07963	.19882	1.36601	3574	45.569	7.9
7.8	25.641	3.11537	.23456	1.40175	3585	46.154	7.8
7.7	25.974	3.15122	.27041	1.43760	3596	46.753	7.7
7.6	26.316	3.18718	.30637	1.47356	3607	47.369	7.6
7.5	26.667	3.22325	.34244	1.50963	3616	48.001	7.5
7.4	27.027	3.25941	.37860	1.54579	3626	48.649	7.4
7.3	27.397	3.29567	.41486	1.58205	3636	49.315	7.3
7.2	27.778	3.33203	.45122	1.61841	3648	50.000	7.2
7.1	28.169	3.36851	.48770	1.65489	3662	50.704	7.1
7.0	28.571	3.40513	.52432	1.69151	3676	51.428	7.0
6.9	28.986	3.44189	.56108	1.72827	3690	52.175	6.9
6.8	29.412	3.47879	.59798	1.76517	3706	52.942	6.8
6.7	29.851	3.51585	.63504	1.80223	3725	53.732	6.7
6.6	30.303	3.55310	.67229	1.83948	3745	54.545	6.6
6.5	30.769	3.59055	.70974	1.87693	3765	55.384	6.5
6.4	31.250	3.62820	.74739	1.91458	3785	56.250	6.4
6.3	31.746	3.66605	.78524	1.95243	3807	57.143	6.3
6.2	32.258	3.70412	.82331	1.99050	3831	58.064	6.2
6.1	32.787	3.74243	.86162	2.02881	3861	59.017	6.1
6.0	33.333	3.78104	.90023	2.06742	3892	60.000	6.0
5.9	33.898	3.81996	.93915	2.10634	3925	61.016	5.9
5.8	34.483	3.85921	.97840	2.14559	3961	62.069	5.8
5.7	35.088	3.89882	1.01801	2.18520	3998	63.158	5.7
5.6	35.714	3.93880	1.05799	2.22518	4038	64.285	5.6
5.5	36.364	3.97918	1.09837	2.26556	4085	65.455	5.5
5.4	37.037	4.02003	1.13922	2.30641	4151	66.667	5.4
5.3	37.736	4.06154	1.18073	2.34792	4208	67.925	5.3
5.2	38.462	(4.10422)	(1.22341)	(2.39060)	4437	69.232	5.2
5.1	39.216	(4.14859)	(1.26778)	(2.43497)		70.589	5.1

shortest range of experimental data is the least satisfactory for extrapolation.

There appear to be no other data at higher pressures for e-H_2, HD, or e-D_2. There are, however, data for n-H_2 and n-D_2 with which a comparison can be made. Figure 3 shows such a comparison. The upper diagram refers to H_2, the base line being table 5, which represents our results for e-H_2. It will be

TABLE 8. *Vapor pressures of liquid* e-H_2, HD, *and* e-D_2 *at intervals of 1 degree K*

T	20.4° K e-H_2 (0.21% o-H_2) P			Hydrogen deuteride, HD P			20.4° K e-D_2 (97.8% o-D_2) P			T
				Solid						
° K	*mm* Hg	*atm*	*psia*	*mm* Hg	*atm*	*psia*	*mm* Hg	*atm*	*psia*	° R
10	1.93	0.00254	0.0373	0.28	0.00037	0.0054	0.05	0.00007	0.0010	18.0
11	5.62	.00739	.109	.99	.00130	.0191	.21	.00028	.0041	19.8
12	13.9	.0183	.269	2.94	.00387	.0569	.75	.00099	.0145	21.6
13	30.2	.0397	.584	7.46	.00982	.144	2.20	.00289	.0425	23.4
14	.....	.....	.....	16.8	.0221	.325	5.57	.00733	.108	25.2
15	.....	.....	.....	34.4	.0453	.665	12.6	.0166	.244	27.0
16	.....	.....	.....	65.2	.0858	1.261	26.0	.0342	.503	28.8
17	.....	.....	.....	.....	.....	.....	49.6	.0653	.959	30.6
18	.....	.....	.....	.....	.....	.....	88.7	.1167	1.715	32.4
				Liquid						
14	58.8	0.0774	1.137	.....	.....	.....	.....	.....	.....	25.2
15	100.3	.1320	1.939	.....	.....	.....	.....	.....	.....	27.0
16	161.1	.2120	3.115	.....	.....	.....	.....	.....	.....	28.8
17	246.0	.3237	4.757	112.4	0.1479	2.173	.....	.....	.....	30.6
18	360.3	.4741	6.967	176.2	.2318	3.407	.....	.....	.....	32.4
19	509.5	.6704	9.852	264.2	.3476	5.109	147.1	0.1936	2.844	34.2
20	699.2	.9200	13.520	382.0	.5026	7.387	222.3	.2925	4.299	36.0
21	935.3	1.2307	18.086	534.9	.7038	10.343	324.1	.4264	6.267	37.8
22	1223.7	1.6101	23.663	728.5	.9586	14.087	457.8	.6024	8.852	39.6
23	1570.5	2.0664	30.369	969.0	1.2750	18.737	628.8	.8274	12.159	41.4
24	1981.8	2.6076	38.322	1262.3	1.6609	24.409	843.1	1.1093	16.303	43.2
25	2463.8	3.2418	47.642	1614.5	2.1243	31.219	1106.6	1.4561	21.398	45.0
26	3022.9	3.9775	58.45	2031.5	2.6730	39.283	1425.6	1.8758	27.567	46.8
27	3665.1	4.8225	70.87	2519.4	3.3150	48.717	1806.1	2.3764	34.924	48.6
28	4396.8	5.785	85.02	3084.6	4.0587	59.65	2253.5	2.9651	43.576	50.4
29	5227	6.877	101.07	3732.8	4.9116	72.18	2774.3	3.6504	53.65	52.2
30	6162	8.108	119.16	4470.8	5.883	86.45	3374.7	4.4404	65.26	54.0
31	7210	9.486	139.41	5306	6.982	102.61	4062.0	5.345	78.55	55.8
32	8383	11.031	162.10	6246	8.219	120.79	4842.4	6.372	93.64	57.6
33	.....	.....	.....	7301	9.607	141.18	5723	7.530	110.66	59.4
34	.....	.....	.....	8480	11.157	163.97	6712	8.832	129.79	61.2
35	.....	.....	.....	9796	12.889	189.42	7819	10.288	151.19	63.0
36	.....	.....	.....	.....	.....	.....	9051	11.909	175.02	64.8
37	.....	.....	.....	.....	.....	.....	10418	13.708	201.45	66.6
38	.....	.....	.....	.....	.....	.....	11943	15.714	230.94	68.4

TABLE 9. *Triple points and boiling points of* e-H_2, HD, *and* e-D_2

The triple points are the same as those of Woolley, Scott, and Brickwedde [6]

Modification	Triple point					Normal boiling point, T	
	T	P			T		
	° *K*	*mm* Hg	*atm*	*psia*	° *R*	° *K*	° *R*
e-H_2	13.81[1]	52.8	0.0695	1.02	24.86[1]	20.27[4]	36.50[2]
HD	16.60[4]	92.8	.1221	1.79	29.88[6]	22.14[4]	39.85[7]
e-D_2	18.69[3]	128.5	.1691	2.48	33.64[4]	23.63[7]	42.45[7]

seen from the auxiliary ordinate scale at the right-hand side of the graph that from the critical point down to the boiling point the vapor pressure of n-H_2 is about 3.5 percent lower than that of e-H_2, but that at lower temperatures the percentage difference increases. This is shown by the dotted line that represents the WSB equation for n-H_2. The data plotted include those of Cath and Onnes [12]. These are chiefly of historical interest, since the measurements were reported in 1917 before the existence of the ortho and para forms was recognized. The other data are all very recent, being those of Grilly [5], and of White, Friedman, and Johnston [3, 13]. The lower diagram refers to D_2, the base line being table 7, which represents our results for e-D_2. The data plotted in this graph are those of Grilly [5], and those of the present research given in table 4. In both researches the material was uncatalyzed and was assumed therefore to be n-D_2. In confirmation of this assumption it may be noted that at 21° K $[P(\text{e-}D_2)-P(\text{n-}D_2)]$ computed from figure 3 is roughly equal to the same quantity computed from the appropriate WSB vapor-pressure equations. The lack of complete agreement could be due to partial conversion of the n-D_2, but is just as likely to be due to incipient failure of the equations at the ends of their ranges. Above the boiling point, the vapor pressure of n-D_2 is about 0.5 percent lower than that of e-D_2. At lower temperatures the percentage difference increases.

It is possible to use table 5 for calculations involving n-H_2 by drawing a smooth curve to represent the values of $P(\text{n-}H_2)/P$(table 5). In a similar way table 7 may of course be used for calculations involving n-D_2.

2.6. Accuracy

The discussion of the accuracy of pressure measurements given in reference [8] is applicable to the present results. The uncertainties in the temperature scale are somewhat greater here than in the

measurements on oxygen, but since the same temperature scale was used for all the measurements, the relative accuracy of the temperatures is quite high. The e-H_2 and e-D_2 tables are more accurate than the HD table because of the decomposition of the latter during the measurements. The pressures given for e-H_2 and e-D_2 are believed to be accurate to 0.2 or 0.3 mm Hg up to about 1 atm. Above 1 atm the uncertainty gradually increases, reaching perhaps ± 8 mm Hg near the critical points. For HD the pressures up to 1 atm are probably equally accurate, but above 1 atm the uncertainty is larger, gradually increasing to perhaps ± 15 mm Hg near the critical point. Uncertainty in the temperature scale is perhaps ± 20 m deg.

3. Dew-Point Pressures of Mixtures

Since no information on the vapor pressures of mixtures of H_2, HD, and D_2 appears in the literature, it was thought worth while to determine approximately how far such mixtures depart from ideal solution behavior, even to the limited precision and within the limited range of temperature and composition allowed by the time available for this work. Experimental dew-point pressures of mixtures were compared with those predicted by the law of ideal solutions and discrepancies greater than the experimental error were found. Significant deviations from ideality in mixtures of ortho- and para-H_2 have been previously observed by Woolley, Scott and Brickwedde [6, p. 454].

3.1. The Law of Ideal Solutions

The applicability of the law of ideal solutions to a liquid mixture at a given temperature can be tested by measuring the dew-point pressure, at the given temperature, of a gaseous mixture of the same components in a known composition. In the derivation of the appropriate equation, the following symbols will be used: x_i, mole fraction of the ith component in the liquid phase; y_i, mole fraction of the ith component in the vapor phase; P_{oi}, vapor pressure of the ith component in pure form; P_v, total pressure of the vapor in equilibrium with the liquid mixture; $Z_i(P)$, value of PV/RT for the ith component in pure form at the pressure P, all at the same temperature. The law of ideal solutions states that in the vapor that is in equilibrium with an ideal liquid solution the partial pressure of the ith component is equal to x_iP_{oi}. Assuming that this partial pressure is also equal to y_iP_v, we have

$$x_iP_{oi}=y_iP_v. \tag{1}$$

Equating the sum of the y's to unity yields the expression for the vapor pressure of an ideal solution;

$$P_v=\Sigma x_iP_{oi}. \tag{2}$$

In the dew-point experiment the y's rather than the x's are known, and therefore the proper form of the expression is that obtained by equating the sum of the x's to unity;

$$1/P_v=\Sigma y_i/P_{oi}. \tag{3}$$

A more rigorous expression of the law would result from using fugacities in place of pressures in eq 1, but this refinement seems to have a negligible effect on P_v in the present instances. In an approximation sufficiently good to show the order of magnitude of the effect of using fugacities [see 14, p. 197 to 199, 221 to 227], eq 1 becomes

$$x_iP_{oi}Z_i(P_{oi})=y_iP_vZ_i(P_v). \tag{4}$$

By this substitution, eq 3 is changed to

$$1/P_v=\Sigma y_iZ_i(P_v)/P_{oi}Z_i(P_{oi}). \tag{5}$$

In order to evaluate eq 5 we take values of $Z(P)$ for H_2 and D_2 from reference [6] and, in the absence of experimental values for HD, assume $Z(P)$ for HD equal to the mean of the values for H_2 and D_2. Values of P_v calculated from eq 5 differ from those calculated from eq 3 by only about 0.2 mm Hg, which is small compared to the experimental deviations from ideality.

3.2. Apparatus and Method

The equipment consisted of a 3-liter gas reservoir (which also served as a mixing bulb), a 140-cm^3 temperature-controlled chamber, and a combination mercury pump and mercury manometer. There were three functions for the latter, first to measure the pressure in the reservoir during mixing, second to transfer measured quantities of gas from the reservoir to the constant-temperature chamber, and third to measure the pressure in the chamber. A vacuum-type adiabatic calorimeter that had been previously constructed at this laboratory by R. B. Scott [15] was used as the isothermal chamber. The connection of these components is shown in figure 4.

A run proceeded as follows. One component of the mixture to be tested was admitted to the reservoir (at room temperature), and the reservoir pressure was measured. Then the second component was admitted and the pressure again measured, the mercury level in the manometer being adjusted to keep the reservoir volume constant. The composition of the mixture was deduced from these pressures taking into consideration the slight isotopic impurities in the individual components as determined by mass-spectrometer analysis. (There were traces of HD in the D_2 samples and of H_2 and D_2 in the HD samples.) The gaseous mixture was allowed to flow into the chamber until the chamber pressure was about 30 mm Hg less than the expected dew-point pressure. A selected volume of the pump-manometer was then filled with gas from the reservoir, the quantity being determined by the pressure difference in the pump before and after filling. This

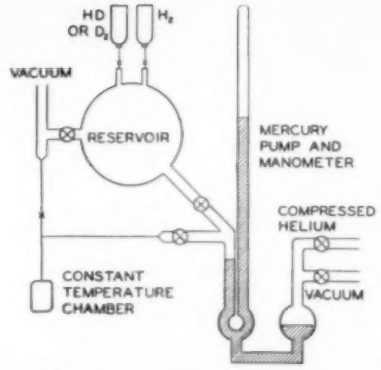

FIGURE 4. *Schematic drawing of the apparatus used in the dew-point pressure measurements.*

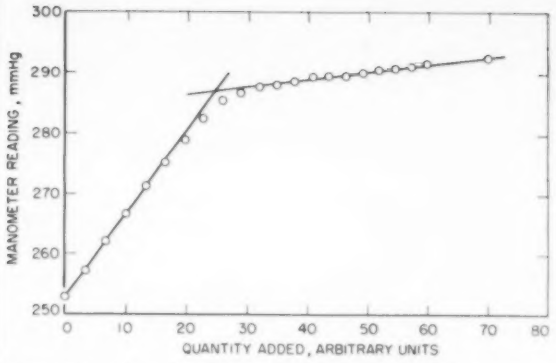

FIGURE 5. *Data of a run for the determination of the dew-point pressure of a mixture.*

Run L, 0.752 H_2, 0.248 HD, T=18.00° K.

quantity was then pumped into the chamber, and the chamber pressure was remeasured. Before each reading of the chamber pressure the chamber was brought to the temperature of the run and the mercury was brought to a selected level. Each reading was repeated after several minutes to make sure that equilibrium had been attained. By repeating this pumping operation a series of points of chamber pressure versus added quantity of mixture was obtained. Temperatures for all points in a run were equal within about 0.00_3 deg K to the average for the run. The thermometer used was L18, which has been calibrated against the Bureau's temperature scale [9], and which after these experiments checked satisfactorily at the ice point.

3.3. Results

Figure 5 is an example of a curve obtained in the manner described above. The dew-point pressure is taken to be the pressure at the intersection of the extrapolations of the two straight-line portions of the curve. Although the values of the abscissas are in error by that quantity of added material that went into the uncooled dead space of the apparatus (about 2% of the total quantity), the error is linear in terms of the pressure and hence has no effect upon the ordinate of the point of intersection. Manometer readings must be multiplied by 0.995 to convert to standard millimeters of mercury.

The results of seven runs are presented in table 10. Calculated pressures are taken from eq 3, using vapor pressures from reference [6, p. 454]. The ortho-para compositions are assumed to correspond to equilibrium at high temperature since no catalyst was used. This assumption is supported by the single-component dew-point pressures (runs E and H) observed with this apparatus. If these two pressures were plotted on the graphs of figure 3 they would fall within 0.0015 (in units of $\Delta\log_{10}P$) of the WSB curves for n-D_2 and n-H_2, respectively. The tabular entry $x_2(H_2)$ is calculated from eq 1.

Principal sources of error are (1) in $P_{obs.}$ the uncertainty in extrapolating the two straight lines to their intersection and (2) in $P_{calc.}$ the uncertainty in the composition. Estimated errors in $P_{obs.}$ are shown in the table. They are greater for the H_2-D_2 mixtures than for the H_2-HD mixtures because of the greater slope of the two-phase part of the isotherms of the former. Compositions of mixtures determined in the mass spectrometer differed from those determined by mixing pressures by an amount sufficient to cause the errors shown in the tabulated values of $P_{calc.}$ Mass-spectrometer compositions were thought to be slightly less reliable due to memory effect and to isotopic exchange in the spectrometer. The over-all estimated error is the sum of the errors in $P_{obs.}$ and $P_{calc.}$

TABLE 10. *Dew-point pressures of mixtures of* H_2, HD, *and* D_2 *in standard mm* Hg

Run	E	F	G	H	J	K	L
T(° K)	20.04	19.00	20.00	18.01	18.005	17.03	18.00
$y_1(H_2)$	0	0.499	0.440	1.00	0.503	0.503	0.752
y_2(HD)	0.008	.004	.004	0	.496	.496	.248
$y_3(D_2)$	.992	.497	.556	0	.001	.001	0
$x_1(H_2)$	.....	.23	.20	.....	.34	.33	0.61
$P_{ni}(H_2)$	.....	490.8	675.7	347.2	346.5	238.1	345.9
P_{ni}(HD)	388.2	264.7	382.8	.....	176.8	114.1	176.4
$P_{ni}(D_2)$	223.5	145.1	219.9	.....	87.5	50	.....
P_c,calc	224.3	224 ±2	313 ±2	347.2	234 ±2	154 ±2	279 ±2
P_c,obs	223.5	234 ±2	322 ±2	348.2	240 ±1	158 ±1	286 ±1
ΔP	−0.8	10 ±4	9 ±4	1.0	6 ±3	4 ±3	7 ±3
$100\Delta P/P$	−.35	4.4	2.8	0.3	2.5	2.6	2.5

Observed pressures are seen to be about 3 percent above those calculated from eq 3, with an estimated error in the deviations of about ±50 percent.

3.4. Discussion

The reason for the rounding of the experimental curves in the region of saturation is not clear, but several possibilities may be considered. These will be discussed with reference to the curve for pure H_2 (fig. 6) in which the rounding also occurs.

First consider the effect of nonideality of the gaseous hydrogen. This will cause the data to depart from a straight line in the same direction as that observed, but is much too small to account for the actual departure. A plot of the isotherm based on a three-term virial equation with the coefficients

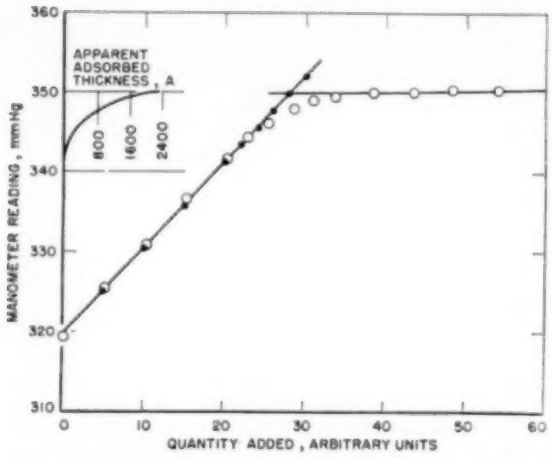

FIGURE 6. *Data of a run using pure H_2 in the dew-point pressure apparatus.*

Run H, T = 18.01° K, ●, from virial equation, ○, experimental.

taken from [6, p. 396] is superimposed on the experimental curve. The scale of the abscissa has been adjusted to force the two curves to match in position and slope at one point (330 mm Hg). The significant comparison is that while the virial-based isotherm falls within 0.1 mm Hg of a straight line, the experimental curve deviates more than 3 mm Hg from its extrapolated linear portion. It is of course possible that the three-term virial equation is inadequate to cover peculiar effects, such as molecular aggregation, at pressures very close to saturation.

A more likely cause of the rounding is adsorption of the gas on the walls of the container. (For a discussion of this phenomenon see [16, p. 317 to 329]). Assuming that the horizontal departure of the experimental curve from the straight line corresponds to the quantity of material adsorbed, that the effective adsorbing surface is equal to the macroscopic surface area in the chamber, and that the density of adsorbed material is the same as that of the liquid, the thickness of the adsorbed layer is, as shown in figure 6, up to about 2000 A near saturation. This appears to be excessive; however, the effective surface area is probably many times the macroscopic area, due to surface roughness, and there is in addition the possibility of capillary adsorption. The surface material was tinned copper sheet and tinned copper tubing. The chamber volume contains many baffles and also a close-wound helix of copper tubing, so the existence of many crevices at contact points of parts of the structure is quite probable. It seems reasonable that these conditions could account for the large apparent adsorption thickness. If we can accept the adsorption explanation, then the intersection of the extrapolated straight lines is the correct dew point for the mixtures.

The making of the measurements was greatly assisted by George T. Furukawa, Raymond A. Nelson, and Dino Zei.

4. References

[1] D. M. Dennison, A note on the specific heat of the hydrogen molecule. Proc. Roy. Soc. (London) **115**, 483 (1927).

[2] Harold C. Urey, F. G. Brickwedde, and G. M. Murphy, A hydrogen isotope of mass 2. Phys. Rev. **39**, 164 (1932).

[3] David White, Abraham Solomon Friedman, and Herrick L. Johnston, The vapor pressure of normal hydrogen from the boiling point to the critical point. J. Am. Chem. Soc. **72**, 3927 (1950).

[4] Robert D. Arnold and Harold J. Hoge, A test of ideal solution laws for H_2, HD, and D_2. Vapor pressures and critical constants of the individual components. J. Chem. Phys. **18**, 1295 (1950).

[5] E. R. Grilly, The vapor pressures of hydrogen, deuterium, and tritium up to three atmospheres. Los Alamos Report LADC–773 (July 11, 1950). Dr. Grilly has informed us by letter that he now has data on more highly purified tritium and obtains vapor pressures somewhat lower than those given in report LADC–773. The tritium curve of figure 1 is shifted slightly to agree with Grilly's later results.

[6] Harold W. Woolley, Russell B. Scott, and F. G. Brickwedde, Compilation of thermal properties of hydrogen in its various isotopic and ortho-para modifications. J. Research NBS **41**, 379 (1948) RP1932.

[7] Harold J. Hoge and James W. Lassiter, Critical temperatures, pressures, and volumes of hydrogen, deuterium, and hydrogen deuteride. J. Research NBS **47**, 75 (1951) RP2229.

[8] Harold J. Hoge, Vapor pressure and fixed points of oxygen and heat capacity in the critical region. J. Research NBS **44**, 321 (1950) RP2081.

[9] Harold J. Hoge and Ferdinand G. Brickwedde, Establishment of a temperature scale for the calibration of thermometers between 14° and 83°K. J. Research NBS **22**, 351 (1939) RP1188.

[10] A. Fookson, P. Pomerantz, and E. H. Rich, The preparation of high-purity hydrogen deuteride. Science **112**, 748 (1950).

[11] The NBS-NACA tables of thermal properties of gases. Table 7.50, Vapor pressure of three hydrogens. Compiled by Harold J. Hoge and Robert L. Powell. Preliminary issue (Sept. 1950).

[12] P. G. Cath and H. Kamerlingh Onnes, Vapor pressures of hydrogen in the neighborhood of the boiling point and between the boiling point and the critical temperature. Commun. Phys. Lab. Univ. Leiden 152a (1917).

[13] David White, Abraham Solomon Friedman, and Herrick L. Johnston, The direct determination of the critical temperature and critical pressure of normal hydrogen. J. Am. Chem. Soc. **72**, 3565 (1950).

[14] G. N. Lewis and M. Randall, Thermodynamics and the free energy of chemical substances (McGraw-Hill Book Co., Inc., New York, N. Y., 1923).

[15] R. B. Scott, C. H. Meyers, R. D. Rands, Jr., F. G. Brickwedde, and N. Bekkedahl, Thermodynamic properties of 1,3-butadiene in the solid, liquid, and vapor states, J. Research NBS **35**, 39 (1945) RP1661.

[16] S. Brunauer, The adsorption of gases and vapors, I (Princeton University Press, 1943).

WASHINGTON, January 22, 1951.

rnal of Research of the National Bureau of Standards Vol. 47, No. 2, August 1951 Research Paper 2229

Critical Temperatures, Pressures, and Volumes of Hydrogen, Deuterium, and Hydrogen Deuteride

Harold J. Hoge[1] and James W. Lassiter[2]

The critical temperatures, pressures, and volumes of H_2, HD, and D_2 have been determined by measuring short sections of P–V isotherms in the neighborhood of the critical points. The H_2 and D_2 samples were catalyzed to ortho-para equilibrium at 20.4° K and are designated e-H_2 and e-D_2. For e-H_2 the values found are $T_c = 32.9_{94}$° K, $P_c = 12.7_{70}$ atm, and $V_c = 65.5$ cm³ mole⁻¹. For HD the corresponding values are 35.9_{38}° K, 14.6_{45} atm, and 62.8 cm³ mole⁻¹; for e-D_2 the values are 38.2_{42}° K, 16.2_{82} atm, and 60.3 cm³ mole⁻¹. A method of correlating isotherm data for different substances, based on the use of graphs of log P versus log V, is described.

1. Introduction

The present paper and the accompanying one on vapor pressures and dew-point pressures [1][3] comprise a full report of a program of determination of properties of the hydrogens undertaken at the National Bureau of Standards early in 1950. The situation with regard to critical data at that time was very similar to the situation with regard to vapor pressures above 1 atm; the field having been neglected from the time of the last Leiden measurements [2] in 1917, until very recently, when White, Friedman, and Johnston [3] published critical data for normal hydrogen, and a preliminary report [4] was made of the present work.

2. Experimental Methods

The measurements were made with an apparatus used previously in an investigation of the vapor pressure of oxygen [5]. Minor modifications are mentioned in [1]. Pressure exerted by the hydrogen in the equilibrium chamber was transmitted out of the cryostat through a small metal tube that connected to one end of a U-tube of stainless steel (½-in. outside diameter). The lower-part of the U-tube contained mercury, and the arm not filled with hydrogen contained water through which the pressure was transmitted to oil and thence to the piston gage with which pressures were measured. By means of a pump, water could be forced into or removed from the line. This caused the mercury to rise in one side of the U-tube and to fall in the other, thus varying the space available for hydrogen in the U-tube and causing material to flow into or out of the equilibrium chamber. This made it possible to measure the sample in the equilibrium chamber at different molar volumes.

The experimental data are given in tables 1, 2, and 3. All observations are numbered in chronological order, with the run number preceding the decimal point. The directly observed (unadjusted) values of temperature and pressure are given in columns 2 and 3 of each table. Temperature variation among the points of a given isotherm was small; nonetheless, corrections were made to bring each group to a common temperature. This was accomplished by using appropriate values of $(1/P)(dP/dT)$ obtained whenever possible from tables 5, 6, and 7 of [1], which give log P as a function of $1/T$. Above the range of these tables, estimated values of $(1/P)(dP/dT)$ were used. The correction is exact only where two phases are present in the equilibrium chamber, but fortunately this is the place where the corrections are most important. Adjusted values of T and P are given in columns 4 and 5 of the tables. The adjustments seldom changed the pressure by more than 1 mm Hg.

The molar volume corresponding to each observation is the effective volume of the equilibrium chamber divided by the number of moles of hydrogen present in it when the observation was made. This quantity, V, is given in column 6 of the tables. The effective volume of the equilibrium chamber and the volumes of the various parts of the pressure-transmitting line were determined in a separate series of experiments. The number of moles of sample confined in the equilibrium chamber and in the pressure-transmitting line, including the U-tube, was determined separately for each run. For each observation of a given run, the number of moles not in the equilibrium chamber was computed by means of the gas laws, and subtracted from the total number to give the quantity actually inside the chamber.

All the necessary knowledge of volumes may be obtained after the apparatus is assembled, provided the inside diameter of the U-tube is known.

If n moles of gas are confined in a volume V_1 at temperature T_1, they satisfy the equation $PV_1 = nRT_1Z_1$, where the compressibility factor Z accounts for the deviation of the gas from ideality. If the volume containing the gas is not all at uniform temperature it must be divided into subvolumes. The number of moles of gas in the ith subvolume is

[1] Present address: Leeds & Northrup Company, Phila., Pa.
[2] Present address: U. S. Coast Guard, Cape May, N. J.
[3] Figures in brackets indicate the literature references at the end of this paper.

TABLE 1. *Isotherms of* e-H_2

Observations of the dependence of pressure on volume in the critical region

Observation number	T (unadjusted)	P (unadjusted)	T (adjusted)	P (adjusted)	V
	°K	mm Hg	°K	mm Hg	cm³ mole⁻¹
18. 6a	32. 8935	9654. 4		9653. 7	52. 07
18. 6b	32. 8933	9579. 8		9579. 4	55. 24
18. 6c	32. 8933	9566. 8		9566. 4	58. 61
19. 1g	32. 8936	9564. 4		9563. 6	60. 69
18. 6d	32. 8932	9566. 1		9565. 8	62. 50
19. 4h	32. 8897	9556. 0		9560. 6	62. 86
19. 4i	32. 8943	9561. 1	32. 893	9559. 7	66. 09
18. 6e	32. 8933	9565. 9	$(T/T_c=0.99694)$	9565. 5	66. 95
19. 4j	32. 8938	9560. 8		9559. 7	70. 23
18. 6f	32. 8933	9566. 0		9565. 6	71. 84
19. 4k	32. 8936	9558. 2		9557. 4	76. 81
19. 4l	32. 8936	9554. 6		9553. 8	80. 55
18. 5a	33. 0455	9925. 1		9924. 4	52. 20
18. 5b	33. 0463	9837. 0		9835. 1	55. 35
19. 3h	33. 0453	9815. 2		9814. 8	56. 58
18. 5c	33. 0455	9799. 7		9799. 0	58. 87
19. 3i	33. 0453	9784. 2		9783. 8	61. 95
18. 5d	33. 0458	9786. 7	33. 045	9785. 6	62. 79
18. 5g	33. 0452	9782. 5	$(T/T_c=1.00155)$	9782. 2	65. 12
18. 5e	33. 0457	9778. 8		9777. 8	67. 44
19. 3j	33. 0453	9774. 5		9774. 1	67. 49
19. 3k	33. 0453	9768. 7		9768. 3	71. 47
18. 5f	33. 0460	9769. 3		9767. 9	72. 70
19. 3l	33. 0456	9756. 3		9755. 4	76. 09
19. 3m	33. 0456	9731. 6		9730. 7	81. 17
17. 5e	33. 2935	10733		10732	[a] 48. 76
16. 12a	33. 2933	10755		10755	[a] 48. 77
19. 2q	33. 2928	10417		10417	52. 21
18. 4l	33. 2963	10390		10385	52. 26
17. 5f	33. 2933	10334		10334	[a] 53. 49
16. 12b	33. 2928	10324		10324	[a] 53. 50
18. 4m	33. 2931	10244		10244	56. 04
19. 2r	33. 2928	10238		10238	56. 52
16. 12c	33. 2944	10193		10191	[a] 58. 99
19. 2s	33. 2925	10177		10178	60. 24
18. 4n	33. 2935	10175	33. 293	10174	60. 47
19. 2t	33. 2925	10136	$(T/T_c=1.00906)$	10137	64. 97
16. 12d	33. 2939	10136		10135	[a] 65. 63
18. 4o	33. 2925	10133		10134	65. 74
17. 5g	33. 2942	10105		10103	[b] 70. 68
18. 4p	33. 2931	10091		10091	72. 40
19. 2u	33. 2925	10076		10077	74. 47
17. 5h	33. 2935	10055		10054	[b] 77. 56
19. 2v	33. 2922	10008		10009	82. 38
17. 5i	33. 2967	9983		9958	[b] 86. 28
17. 5j	33. 2938	9798		9797	[b] 96. 60
17. 5k	33. 2938	9543		9542	[b] 108. 67

[a, b] No measurements of mass of material were made corresponding to the two groups of observations marked respectively by a and b. Masses were determined as described in the text, from the superposition of graphs.

TABLE 2. *Isotherms of* HD

Observations of the dependence of pressure on volume in the critical region

Observation number	T (unadjusted)	P (unadjusted)	T (adjusted)	P (adjusted)	V
	°K	mm Hg	°K	mm Hg	cm³ mole⁻¹
3. 16b	35. 033	9844		9844	59. 48
3. 16c	35. 033	9841		9841	63. 60
3. 16a	35. 033	9841	35. 033	9841	68. 10
3. 16d	35. 034	9843	$(T/T_c=0.97563)$	9842	73. 23
3. 16e	35. 034	9841		9840	81. 75
5. 2h	35. 7499	10889		10888	57. 76
5. 2g	35. 7494	10886		10885	60. 91
5. 2f	35. 7494	10889		10888	64. 12
5. 2d	35. 7486	10887	35. 749	10888	67. 68
5. 2e	35. 7496	10885	$(T/T_c=0.99557)$	10884	67. 84
5. 2c	35. 7487	10886		10886	72. 11
5. 2b	35. 7486	10890		10881	75. 72
5. 2a	35. 7491	10890		10890	82. 59
5. 3a	35. 8798	11095		11095	57. 83
5. 3b	35. 8796	11091		11092	61. 04
5. 3c	35. 8798	11089	35. 880	11089	64. 68
5. 3d	35. 8796	11091	$(T/T_c=0.99922)$	11092	69. 36
5. 3e	35. 8795	11078		11079	74. 15
5. 3f	35. 8795	11056		11057	78. 75
5. 3g	35. 8793	11021		11022	82. 68
3. 17d	36. 022	11319		11321	59. 86
3. 17e	36. 023	11308	36. 023	11308	63. 22
3. 17c	36. 023	11298	$(T/T_c=1.00320)$	11298	66. 89
3. 17b	36. 023	11257		11257	73. 71
3. 17a	36. 023	11132		11132	86. 76
4. 10b	36. 250	11715		11715	57. 88
4. 10c	36. 251	11684		11682	60. 84
4. 10a	36. 251	11648		11646	65. 15
4. 10d	36. 250	11626	36. 250	11626	67. 87
4. 10e	36. 250	11603	$(T/T_c=1.00952)$	11603	70. 61
4. 10f	36. 249	11565		11567	74. 39
4. 10g	36. 249	11508		11510	79. 05
4. 10h	36. 249	11427		11429	84. 35

given by $n_iR=PV_i/T_iZ_i$, and summing over all subvolumes

$$nR=R\sum_i n_i=P\sum_i(V_i/T_iZ_i). \quad (1)$$

With all the volumes V_i at the same known temperature (room temperature), and with enough gas in the apparatus to obtain convenient pressures, the position of the mercury meniscus in the U-tube was varied and the resulting changes in P observed. In this way the total volume occupied by the sample was found to be

$$\sum_i V_i(\text{cm}^3)=84.66-0.0968h_1, \quad (2)$$

where h_1 was the scale reading in millimeters of the mercury meniscus in the arm of the U-tube containing hydrogen. Previously, when the apparatus had been used to measure the vapor pressure of oxygen [5], similar measurements had given 84.45 for the constant term. The agreement is considered satisfactory. Having obtained eq 2, the effective volume of the cryostat was determined by noting the pressure, first with all volumes at room temperature, and again after cooling the cryostat with liquid air, and applying eq 1 to the results. The volume was found to be 5.88 cm³.

Once the volumes were known, the number of moles of gas confined could be determined from any set of pressure and temperature readings, provided none of the sample was condensed. Normally, such a determination was made at the completion of each run, after the cryostat had warmed to liquid-air temperature and the pressure had risen to 25 to 35 atm. The molar volume V corresponding to each individual observation of the run could then be computed by summing eq 1 over all volumes except that of the cryostat itself, and subtracting the result from the total number of moles in the system. The temperature of the U-tube was indicated by a mercury-in-glass thermometer. The table of Z-values given by Woolley, Scott, and Brickwedde [6] was used for all three gases. The table is for H_2, but was considered adequate for HD and D_2 also, in view of the fact that other quantities involved in the calculation were not known with very high accuracy.

In two instances we failed to make any measurement of the total mass of sample in the system. The two groups of observations involved are for the highest isotherm of e-H_2 and are indicated in table 1. Calculations of the molar volume were made for these observations in the usual way, except that the unknown total number of moles appeared as an arbitrary constant. Graphs of pressure versus

TABLE 3. *Isotherms of* e-D_2

Observations of the dependence of pressure on volume in the critical region

Observation number	T (unadjusted)	P (unadjusted)	T (adjusted)	P (adjusted)	V
	° K	*mm* Hg	° K	*mm* Hg	$cm^3\ mole^{-1}$
6.21c	37.1983	10708	37.199	10709	63.74
6.21a	37.1988	10709	$(T/T_c=0.97222)$	10709	70.60
6.21b	37.1991	10708		10708	80.73
7.4a	38.2029	13969		13969	40.19
7.4b	38.2036	12292		12291	52.48
8.6a	38.2038	12276		12275	56.44
8.6b	38.2031	12272	38.203	12272	63.04
6.22c	38.2017	12274	$(T/T_c=0.99846)$	12276	64.20
6.22a	38.2022	12272		12273	72.35
6.22b	38.2018	12163		12165	84.13
8.7a	38.3978	12630		12630	54.12
8.7b	38.3979	12610		12610	57.15
8.7c	38.3978	12599	38.398	12599	60.49
8.7d	38.3977	12588	$(T/T_c=1.00155)$	12588	64.25
8.7e	38.3977	12570		12570	68.57
8.7f	38.3977	12536		12536	73.34
7.5a	38.5556	15010		15011	40.30
7.5b	38.5552	14236		14237	42.20
7.5c	38.5554	13654		13655	44.33
7.5d	38.5558	13295		13295	46.58
7.5e	38.5554	13106		13107	48.94
8.4a	38.5563	13003	38.556	13002	50.74
7.5f	38.5556	12991	$(T/T_c=1.00768)$	12992	51.85
7.5g	38.5554	12952		12953	53.46
8.4b	38.5566	12907		12906	55.57
8.4c	38.5566	12866		12865	60.28
8.4d	38.5565	12827		12826	65.72
8.4e	38.5563	12742		12742	73.99
7.6a	38.8794	15981		15982	40.37
7.6b	38.8766	15075		15082	42.40
7.6c	38.8795	14421		14422	44.67
7.6d	38.8794	14017		14018	47.05
7.6e	38.8794	13775		13776	49.53
8.5a	38.8801	13666	38.880	13666	50.86
7.6f	38.8794	13608	$(T/T_c=1.01615)$	13609	52.66
7.6g	38.8791	13545		13547	54.50
8.5b	38.8807	13492		13491	55.91
8.5c	38.8801	13399		13399	60.87
8.5d	38.8801	13312		13312	66.54
8.5e	38.8806	13155		13154	75.23
7.7a	39.1990	16937		16937	40.45
7.7b	39.1985	15878		15879	42.58
7.7c	39.1988	14113	39.199	14113	55.40
6.23c	39.1981	13839	$(T/T_c=1.02449)$	13841	64.74
6.23a	39.1995	13627		13626	73.54
6.23b	39.1980	13211		13213	87.00
6.24a	40.1960	14876	40.196	14876	74.98
6.24b	40.1959	14151	$(T/T_c=1.05055)$	14151	89.63
6.25a	41.2076	16066	41.208	16067	76.42
6.25b	41.2085	15020	$(T/T_c=1.07700)$	15019	92.33

number of moles of hydrogen in the equilibrium chamber were made on transparent paper for these data (with the zero of abscissas undetermined); and a similar graph was made of the rest of the data of the isotherm, for which the zero of abscissas was known. The graphs of the "unknown" data were superposed in turn on the graph of the "known" data, and moved along the axis of abscissas until known and unknown graphs merged into a single continuous curve. By comparing the two abscissa scales the total number of moles of sample employed in each unknown run was determined.

3. Analysis of the Data

The preliminary analysis of the isotherms was carried out in the usual way by plotting P versus V for each modification of hydrogen, drawing in the liquid-vapor domes, and taking the highest point of each dome as the critical point of that particular modification. It was difficult to determine the positions of the domes with the desired accuracy, however, so we sought some method of correlating the data for the three kinds of hydrogen in order to obtain more accurate critical constants for all. If the critical temperature and pressure of each variety were known, P/P_c could be plotted versus V/V_c with all three modifications on the same graph; and, if the law of corresponding states were obeyed all the isotherms would form a single family. Since only approximate values of P_c and V_c were available, this method of correlation could be used only by a process of successive approximations. However, it was recognized that this difficulty could be avoided by taking logarithms. If log (P/P_c) were plotted versus log (V/V_c), the isotherms of the three modifications would, of course, form a single family just as they would when the variables were P/P_c and V/V_c. But a graph of log (P/P_c) versus log (V/V_c) differs from a graph of log P versus log V only by a translation of $-\log P_c$ along the axis of ordinates and of $-\log V_c$ along the axis of abscissas. Hence, if separate graphs of log P versus log V for each modification are prepared on transparent stock, it should be possible to superpose them in such a way as to form a single family of isotherms, to draw a single liquid-vapor dome for the family, and thus to obtain critical constants for the three modifications with improved absolute accuracy and much greater relative accuracy than could otherwise be obtained.

The result of applying this type of correlation is shown in figure 1. The three sets of data were initially plotted on three separate sheets of tracing cloth and superposed for viewing by transmitted light. The graphs were shifted relative to each other along the axes of coordinates until they most nearly blended into a single family. The relation between the various coordinate scales was then noted and all the data plotted on a single sheet. On this graph the liquid-vapor dome was drawn and the critical point selected. The coordinates of this point with respect to the three original graphs give log P_c and log V_c for the three modifications of hydrogen. The corresponding critical temperatures were found by substituting each value of P_c into the appropriate vapor-pressure table (table 5, 6, or 7) of [1]. The critical constants are given in table 4. Values of the compressibility factor $Z=PV/nRT$ at the critical point are included. After the critical constants had been determined, T/T_c was computed for each isotherm of figure 1, and coordinate scales in terms of log (P/P_c) and log (V/V_c) were substituted for those originally used, so that the same scales could be used for all three modifications.

TABLE 4. *Critical constants of* e-H_2, HD, *and* e-D_2

	T_c	P_c			V_c	P_cV_c/RT_c
	°K	*mm* Hg	*atm*	*psia*	cm^3mole^{-1}	
e-H_2	32.994	9,705	12.770	187.67	65.5	0.309
HD	35.908	11,130	14.645	215.22	62.8	.312
e-D_2	38.262	12,374	16.282	239.27	60.3	.312

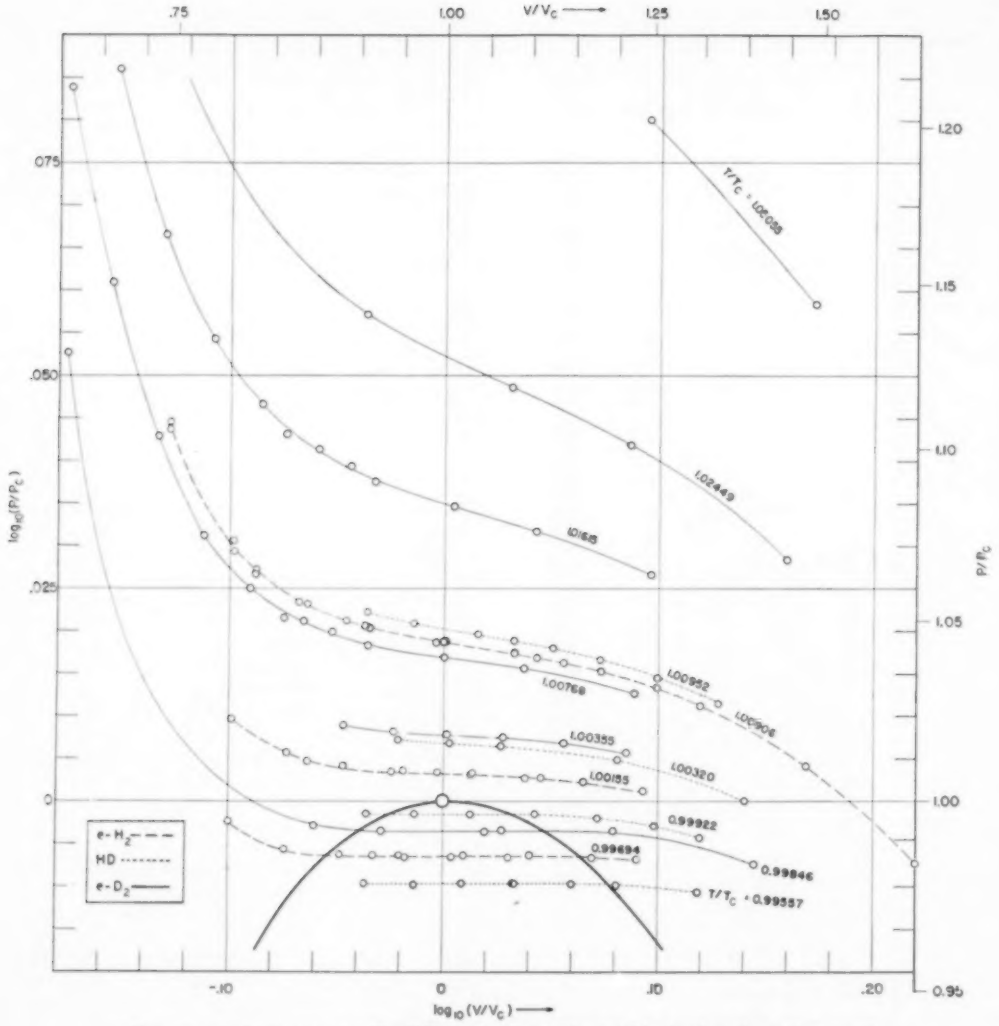

FIGURE 1. *Isotherms of* e-H_2, HD, *and* e-D_2 *in the neighborhood of the critical point.*

To help in properly drawing the liquid-vapor dome, several other sets of isotherm data were plotted on log P versus log V graphs and compared with our own results by superposition. The data plotted included those of Michels, Blaisse, and Michels for CO_2 [7], and those of Onnes, Crommelin, and Cath for hydrogen [2]. The isotherm data in the latter paper are given graphically rather than numerically, so the coordinates of the plotted points and of various points on the dome had to be read from the published graph. The dome drawn in figure 1 is in agreement with that of the Leiden observers within the accuracy of the observations. The CO_2 data could not be satisfactorily superposed on our hydrogen data because the dome was too wide. It was estimated that if for CO_2 one should plot log P versus 0.81 log V, the resulting graph could be superposed satisfactorily on the hydrogen graph. The difference in dome-shape of hydrogen and CO_2 is undoubtedly real. It would be interesting to compare the critical regions of other triatomic molecules, such as N_2O and SO_2 with that of CO_2, to see the extent to which triatomic molecules follow one law of corresponding states and diatomic molecules another.

The vapor-pressure tables of [1] are believed to be accurate near the critical point to ± 8 mm Hg in the case of e-H_2 and e-D_2, and to ± 15 mm Hg in the case of HD. The uncertainties of the critical constants are greater than these values, however, because they include the additional uncertainty in locating the proper spot on figure 1 to choose as the

critical point. It is estimated that the critical point selected is uncertain by ± 0.001 in log (P/P_c). This is equivalent to ± 22 mm Hg for e-H_2, ± 26 mm Hg for HD, and ± 28 mm Hg for e-D_2. To these may be added the estimated uncertainties in the vapor-pressure tables, giving (after rounding off) ± 30 mm Hg for e-H_2, ± 40 mm Hg for HD, and ± 35 mm Hg for e-D_2. Using values of dP/dT from the accepted vapor-pressure tables of [1], these uncertainties are approximately equivalent to ± 20 mdeg for e-H_2 and e-D_2, and to ± 25 mdeg for HD. An additional allowance of ± 20 mdeg must be made for uncertainty in the temperature scale.

The position of the critical point in figure 1 is uncertain by perhaps ± 0.005 in log (V/V_c), which is equivalent to slightly more than 1 percent in V. Errors in determining the volumes of the equilibrium chamber and the various parts of the pressure-transmitting line are not included in this figure. These would affect the determinations of the total mass of material employed in each run, and would introduce a systematic error into log (V/V_c). An uncertainty of ± 2 percent is thought to be adequate to cover errors due to all causes. The relative errors of the critical volumes of the three varieties are much smaller than the total errors. This type of error may be estimated from the accuracy with which the three original log P-log V graphs could be correctly superposed. It is estimated that the ratio of any two critical volumes is correct to 5 per mille. The relative accuracy of any two critical pressures is probably 1 per mille, and that of any two critical temperatures about 3 parts in 10,000.

The published critical data for hydrogen were summarized by Pickering [8] in 1926. He selected as best values: $t_c = -239.9°$ C, $P_c = 12.8$ atm, and $\rho_c = 0.0310$ g cm^{-3} (equivalent to $V_c = 65.0$ cm^3 mole^{-1}). These are essentially the values of Onnes, Crommelin, and Cath [2] for the critical temperature and pressure and that of Mathias, Crommelin, and Onnes [9], for the critical density. In [2] the critical temperature is given both in centigrade and in Kelvin units ($-239.91°$ C $= 33.18°$ K). Since the Leiden authors were unaware of the necessity of controlling ortho-para compositions, we may assume that they worked with normal (normal $= 0.25$ para-hydrogen, 0.75 orthohydrogen; see [1]) hydrogen, possibly with an appreciable conversion in the direction of equilibrium hydrogen. In the recent determination of critical constants at Ohio State University [3], normal hydrogen was also employed, so there are no published data exactly comparable with ours. The Ohio State values are $T_c = 33.24_4°$ K, and $P_c = 12.797$ atm.

The above critical points are shown in figure 3 of [1], which is a graph of deviations of observed vapor pressures from an accepted vapor-pressure table. Note that the n-H_2 data in this graph are not to be expected to give zero deviations because the table from which deviations are calculated represents not n-H_2 but e-H_2. To our knowledge there are no previous measurements of the critical constants of HD and e-D_2 with which our results may be compared.

The valuable assistance of Dino Zei and Raymond A. Nelson in making the measurements is acknowledged.

4. References

[1] Harold J. Hoge and Robert D. Arnold, Vapor pressures of hydrogen, deuterium, and hydrogen deuteride and dew-point pressures of their mixtures, J. Research NBS **47**, 63 (1951) RP2228.

[2] H. Kamerlingh Onnes, C. A. Crommelin, and P. G. Cath, A preliminary determination of the critical point of hydrogen, Commun. Phys. Lab. Univ. Leiden 151c (1917).

[3] David White, Abraham Solomon Friedman, and Herrick L. Johnston, The direct determination of the critical temperature and critical pressure of normal hydrogen, J. Am. Chem. Soc. **72,** 3565 (1950).

[4] Robert D. Arnold and Harold J. Hoge, A test of ideal solution laws for H_2, HD, and D_2. Vapor pressures and critical constants of the individual components, J. Chem. Phys. **18**, 1295 (1950).

[5] Harold J. Hoge, Vapor pressure and fixed points of oxygen and heat capacity in the critical region, J. Research NBS **44,** 321 (1950) RP2081.

[6] Harold W. Woolley, Russell B. Scott, and F. G. Brickwedde, Compilation of thermal properties of hydrogen in its various isotopic and ortho-para modifications, J. Research NBS **41,** 379 (1948) RP1932.

[7] A. Michels, B. Blaisse, and C. Michels, The isotherms of CO_2 in the neighborhood of the critical point and round the coexistence line, Proc. Roy. Soc. London **A160,** 358 (1937).

[8] S. F. Pickering, A review of the literature relating to the critical constants of various gases, BS Sci. Pap. **21,** 597 (1926) S541.

[9] E. Mathias, C. A. Crommelin, and H. Kamerlingh Onnes, The rectilinear diameter of hydrogen, Commun. Phys. Lab. Univ. Leiden 154b (1921).

Washington, April 27, 1951.

Journal of Research of the National Bureau of Standards Vol. 47, No. 2, August 1951 Research Paper 2230

A Photoelectric Recording Interferometer for Measurement of Dimensional Changes[1]

Richard N. Work

A method is given for the photoelectric recording of light intensity at a reference point in an image of an interference pattern for the automatic plotting of fringe count versus thermocouple electromotive force in interferometric dilatometry. Application of the technique to the measurement of coefficients of expansion and to the determination of transition temperatures in rubber-like materials over a temperature range of −185° to +185° C is given. Transitions can be located to a precision of ±0.5 degree C and coefficients of expansion found to a precision of ±5 percent.

1. Introduction

Many investigations require a study of the changes in dimension of a substance that take place upon a change in temperature. The temperatures at which phase transitions or second-order transitions occur may be located from such data, and the values of the expansivities at various temperatures may be found. Crystallization in rubber, for instance, has been studied by means of X-ray diffraction, birefringence, specific heat, interferometric, and volume dilatometric methods. The second-order transition of rubber has been studied by volume dilatometry, interferometry, specific heat, and index of refraction measurements.

The study of transition phenomena by the interferometric method requires no confining liquid, may be adapted to wide temperature ranges, and is semiautomatic in operation. The application is limited only to materials that do not flow under small stress.

This paper deals with an improved interferometric method of determining the relationship between length and temperature of solid materials. Novel features of the present work include the photoelectric counting of fringes, the automatic plotting of fringe count against thermocouple emf, and the easy adjustment of the fringe pattern. Illustrative data obtained from measurements on rubber are given, but the application of the method described is not restricted to this type of material.

Merritt [1][2] and Saunders [2] have described in detail the interferometric apparatus and procedure. The application of the method to measurements on rubber-like materials has been described by Wood, Bekkedahl, and Peters [3]. The method may be described very briefly as follows. If the separation of two optically flat, transparent plates is determined by the thickness of three spacers, a few millimeters thick but equal in thickness to within a few wavelengths of light, and if these plates are illuminated with parallel monochromatic light normal to the plane of their faces, a pattern of interference fringes will be observed. If, now, the thicknesses of the specimens are caused to change by a variation in temperature, the separation of the plates will be altered, and there will be a corresponding variation in the fringe pattern evidenced by a motion of the fringes. The change in separation of the plates at a given point is related to the motion of the fringes by the following relation

$$\Delta l = \frac{\Delta N \lambda}{2}, \tag{1}$$

where Δl is the change in separation; ΔN is the number of fringes passing the point of reference; and λ is the wavelength of light used. By the use of a suitable illuminating and viewing instrument, the motions of the fringe pattern can be measured quantitatively, and the change in dimension associated with a given temperature interval can be obtained from eq 1.

The visual interferometric method requires continuous and undivided attention, which may account for the fact that its adoption has been limited. Various photographic methods of recording the changes in the fringe pattern have been developed [4, 5, 6] to eliminate this objection. A photoelectric method of recording the fringe count shows certain advantages over the photographic methods, including the elimination of film-processing and the presentation of data on a strip chart in a form suitable for immediate determination of transition temperatures and estimates of expansivities. The quantitative determination of the coefficients of expansion requires less processing than other interferometric methods. The course of a measurement can be followed and the procedure modified when it is seen to be necessary. The speed to this photoelectric method can be made sufficiently high to be able to count the rapidly moving fringes during rapid change in volume that accompany phase transitions.

The photoelectric method utilizes the changes in light intensity at a reference point in the fringe pattern as the fringes move past this point. These changes are detected by a photomultiplier tube, and the amplified output of the tube is automatically plotted against time on a strip-chart recorder. A switch, actuated by the recorder movement, produces a current pulse upon the passage of each

[1] The work reported here was supported by the Office of Naval Research and the Office of the Quartermaster General as part of Project ONR (QMC) NR-033-314.

[2] Figures in brackets indicate the literature references at the end of this paper.

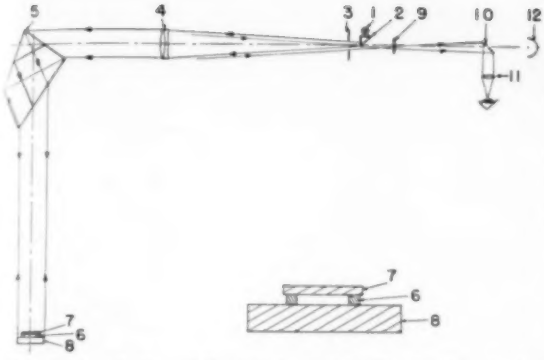

FIGURE 1. *Optics of the interferometric illuminating-viewing instrument.*

See text for explanation of numbered items. Enlarged section of 6, 7, and 8 is shown at the right.

fringe. Simultaneously, the temperature of the specimen, as indicated by the emf of a thermocouple embedded in a piece of material of similar size to the specimen, is plotted against fringe count on a second strip-chart recorder, which has been so modified that the current pulse from the time-intensity recorder actuates a mechanism that moves the chart a unit distance for each fringe.

2. Apparatus

2.1. Interferometer

A Pulfrich type [7] viewing instrument, similar to that described by Merritt and modified according to figure 1 forms the optical part of the apparatus used here. The light source is a helium tube, 1, located above a small right-angle reflecting prism, 2, which places the effective source very near to the optic axis of the instrument. After traversing an iris diaphragm, 3, which limits the effective size of the source, the rays are rendered parallel by the lens, 4. The light is deviated through approximately 90° and dispersed in passing through the Pellin-Broca prism, 5. By rotating this prism about an axis perpendicular to the plane of the paper, light of a wavelength corresponding to any one of the spectral lines in the source may be made to fall perpendicularly upon the interferometer plates, separated by three samples, 6. The rays reflected from the bottom surface of the top plate, 7, and from the top surface of the bottom plate, 8, interfere in a manner determined by the separation of the plates and form a pattern of interference fringes. The two surfaces of each interferometer plate are inclined at an angle of 20 minutes to eliminate unwanted reflections from the upper surface of the top plate and the lower surface of the bottom plate. The reflected light returns through the prism and collimating lens to form an image of the effective source in the lower half of the iris diaphragm, through which the light passes to the photoelectric detector. Images corresponding to other wavelengths present in the source fall above or below the opening and are stopped. An image of the interferometer plates is formed by lens, 9, and falls upon a mirror, 10, inclined at an angle of 45° to the beam. This mirror, which contains a small aperture about 0.1 mm in diameter, permits inspection of the image through the side tube with the aid of lens, 11. Light passing through the aperture, which is about one-fiftieth the diameter of the image, falls upon the photosensitive surface of the photo-multiplier tube, 12.

Of the various spectral lines present in the light from the helium discharge tube, the yellow line, 5876 A, is used because of its good visibility and because it shows the highest sensitivity-intensity product for the phototube used.

2.2. Specimen Holder

The specimen holder, figure 2, is designed for use with rubber and rubber-like materials to be measured over a temperature range from −185° to +185° C. The discussion of the apparatus is divided for convenience into two sections, optical and thermal.

a. Optical

For this experiment, a useful fringe pattern is obtained when the surfaces of the two transparent plates are flat within two to three wavelengths and parallel within 20 wavelengths. If these surfaces are not parallel within this limit, 40 or more fringes will be seen to traverse the 2-cm-diameter plates making visual observations difficult. A more serious effect lies in the fact that the aperture in the inclined mirror becomes large compared to the width of each fringe. The variation in transmitted light upon the passage of a fringe then becomes too small to be detected photoelectrically.

If the material under test is hard, say a metal or ceramic, a specimen may be ground to one of the forms recommended by Saunders [2], making three connected, supporting structures the same length within a few wavelengths. However, there is considerable difficulty in cutting or molding three specimens of a soft rubber-like material to the same thickness within the required tolerance. Accordingly, the specimen holder has been designed so that the three specimens are supported by fused-quartz wedges, which in turn rest upon the bottom interferometer plate. Then, if the specimens are fixed laterally while the wedges are movable along a radius, a vertical adjustment of the top plate is possible. This motion enables one to bring the top plate into parallelism with the bottom plate without having to cut the specimens to close tolerances.

The wedges are 5 mm in width and 15 mm in length and vary in thickness from 2.00 to 2.15 mm. The maximum travel of the wedge is of the order of 5 mm, allowing a maximum vertical adjustment of 0.05 mm. In practice, the maximum adjustment is used only for material that flows or creeps under the weight of the top plate, in which case the finding of an acceptable fringe pattern is fortuitous. Usually, however, vulcanized rubber samples and many unvulcanized materials can be easily cut or molded

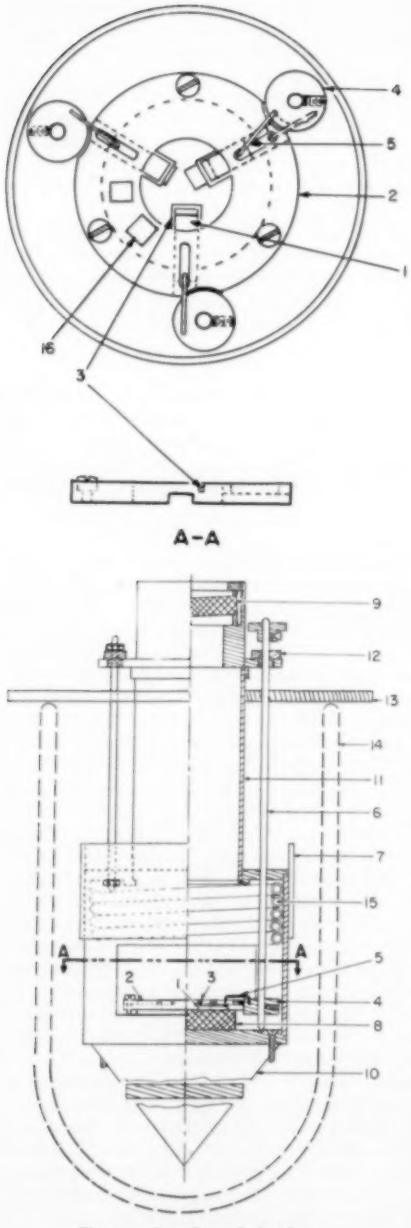

FIGURE 2. *Sample holder.*

See text for explanation of numbered items. Enlarged section of A–A is shown above.

to within 0.02 mm. The uncertainty in thickness is, therefore, less than 1 percent of the usual thickness of the specimens (2 to 5 mm).

The details of the wedge-adjusting mechanism are shown in figure 2. The wedges, 1, may be moved in radial slots milled in the brass plate, 2. The central portion of this brass plate has been cut out to allow light to reach the bottom interferometer plate. Square enclosures, or wells, 5 mm square, 3, are located above the inner ends of the wedges, which extend into the open portion in the center of the brass plate. The specimens lie upon the quartz wedges and in these wells, the walls of which restrain the motion of the specimens when the wedges are moved.

Motion of the wedges is achieved by a lever drive, 4, which is coupled to the wedge by means of a wire link, 5. The shaft, 6, fastened to the lever extends to the top of the holder where a knob allows the operator to make adjustments when the specimen is inaccessible. The side openings of the holder are closed by means of sleeve, 7.

A window, 9, forms a closure at the top of the specimen holder. To avoid the reduction in contrast of the image caused by reflections from the window surfaces, the window is tilted at a small angle to deflect the light out of view.

Fogging and frosting of the window at low temperatures are eliminated by passing a stream of dry air over it. Frosting of the interferometer plates is avoided by circulating dry air in the specimen chamber.

b. Thermal

The specimens are cooled by liquid nitrogen pumped from a reservoir by means of a pressure bulb into a Dewar, 14, surrounding the specimen holder. The rate of cooling is determined by the rate at which the liquid nitrogen is pumped into the Dewar. A triangular brass wedge, 10, ⅜ in. thick, 2 in. high, and 3-in. base is attached to the bottom of the specimen holder and acts as a heat transfer path of variable length and cross section to make the rate of cooling more nearly uniform with variation in liquid level. Unless such a device is used, the temperature in the sample chamber drops slowly until the liquid nitrogen level reaches the bottom of the specimen holder, at which time the temperature falls rapidly, making temperature control difficult.

Heat transfer to the surroundings is reduced by the use of a Bakelite tube, 11, as the center section of the specimen holder. Bakelite washers, 12, between the brass tie rods and the flange on the top of the specimen holder and between the wedge adjusting rods and the flange, reduce heat transfer along those paths. Further, closure of the space between the Dewar, 14, and the sample holder is made by means of a piece of Masonite, 13, lined with a soft plush cloth to make good contact with the edge of the Dewar. The amount of condensation and frosting on the exposed metal surfaces is small even when the sample is held near liquid nitrogen temperatures for several hours.

The temperature of the sample may be increased by means of a current in a resistance element located in the bottom of the Dewar. The heater current is adjusted with a variable transformer to obtain a suitable rate of heating.

Dry air passes through a copper tube, 15, a 5-turn helix inside the sample chamber with which it makes

good thermal contact. The air stream then flows into the sample chamber and stirs the air, insuring a uniform temperature in the chamber.

2.3. Amplifier

The fringe recording circuit consists of a 931A-photomultiplier tube to convert light changes into electric signals, suitable amplifier stages, and a strip-chart recorder.

The power supply for the photomultiplier tube is controlled with a variable transformer, allowing a wide range of gain. It is usually operated at about 90 v/dynode for optimum signal-to-noise ratio.

The variation in the phototube current is about 5×10^{-9} amp for the passage from a light band to a dark band of an interference fringe when operated at the conditions noted above. Noise currents from various sources, namely, the helium tube, phototube, stray fields, etc., are of the same order of magnitude. Therefore, a tuned circuit is employed in the amplifier to prevent the over loading of the amplifier by noise voltages. Since the helium tube is excited by a high-voltage transformer connected to the 60-cycle line, the light is modulated with a fundamental frequency of 120 c/s. A single-stage triode pre-amplifier is followed by a two-stage amplifier with negative feedback over a 120-cycle parallel T rejection network. This results in a sharp peak at 120 cycles in the gain-frequency characteristic of the amplifier. A reduction in noise due to stray coupling to the line and poor filtering of the power supply could be made by a choice of some other frequency than the line frequency for the excitation of the helium lamp. Such an expedient was found to be unnecessary. The tuned amplifier is followed by a phase inverter-detector stage, which converts a single ended alternating-current signal to a balanced direct-current output, whose level is proportional to the peak input-signal voltage. The detector stage is followed by a balanced direct-current amplifier with an adjustable time constant. A time constant of 1, 2, 4, 6, or 8 sec may be chosen by means of a selector switch. The relatively long time constants average any fluctuations (noise) in the output that are of higher frequency than 1 to 1/8 c/s. The available range permits the operator to choose a time constant that mostly corresponds to the frequency of variation of the desired signal, and that is sufficiently short so the signal is not appreciably attenuated. Normally the temperature is varied at a rate between 1/2 and 1 deg/min, which corresponds roughly to a fringe per minute for rubber specimens 2 to 5 mm thick. In this case the 8-sec time constant is used. However, if the sample undergoes rapid crystallization, the fringes may move at rates up to 10 or 20/min, in which case the 8-sec time constant would appreciably reduce the amplitude of the output. In this case, a shorter time constant is used.

The output of the amplifier actuates a strip-chart recorder yielding a plot of light intensity at the phototube aperture against time. The recorder mechanism is fitted with a switch that is closed once per fringe. The switch consists simply of a vertical wire, the end of which is engaged by a projection on the recorder movement so as to make a momentary connection with a fixed contact. Contact is made only for motions in one direction. The momentary closing of the switch operates a relay, which in turn operates the fringe-counting solenoid on the temperature recorder.

The temperature of the specimens is indicated by the emf of two copper-constantan thermocouples in series. The reference junctions are in an ice-water bath, whereas the other junctions are placed in specimens of the same or similar material and of similar size to those under test. These specimens are placed in the thermocouple wells, 16, figure 2. The emf is recorded continuously on a recording-potentiometer. The recorder scale was expanded to cover the temperature range $-185°$ to $+185°$ C in three spans. A precision of ±0.5 deg at the low-temperature end and ±0.2 deg at the high end is attainable. The potentiometer-recorder was calibrated with a laboratory potentiometer, and calibration scales were made. Emf's corresponding to temperatures at 1 deg intervals, the values of which were taken from the International Critical Tables, were impressed upon the input terminals of the recording-potentiometer. The potentiometer was allowed to come to balance at each value of emf and a mark made. The temperature corresponding to any point on the chart can then be found simply by aligning the scale on the chart and reading the temperature from the scale corresponding to the point on the chart.

The chart paper drive of the recorder was modified so that an impulse from the fringe counting solenoid would move the paper a constant distance. The Brown Electronik recorder, model 153X11, was found to be well suited for this modification of the chart mechanism. Other recorders are undoubtedly as well suited, but for explicitness, the details of the modification of the Brown recorder will be given.

The last six gears of the chart drive train were removed from their supporting shafts, the gear shafts and the automatic standardization gears being left in place. An adapter, figure 3, was made to mount a 17-tooth ratchet gear, 1, drive pawl, 2, and lever, 3, upon the shaft, 4, of the driving gear of the chart drum. The solenoid magnet, 5, and armature, 6, which operates the rachet lever is mounted upon a ¼-in. aluminum plate, 7, which in turn is screwed to the recorder chassis, using existing tapped holes in the chassis. A hold pawl, 8, has been mounted upon the aluminum plate to prevent the chart drum from being pulled back by the tension of the unwinding paper.

It is planned to replace the 17-tooth gear with a 48-tooth rachet and equip the solenoid with an adjustable stop. In this way the paper can be advanced in steps of multiples of 0.025 in., according to the number of ratchet teeth taken per step.

It is further planned to add a time-marking pen to the recorder so that the chart record will be complete, including temperature, fringe count, and time

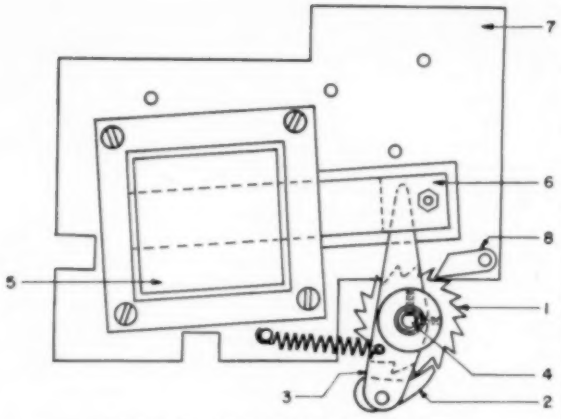

FIGURE 3. *Chart advancing mechanism.*
See text for explanation of numbered items.

3. Procedure

The sample of rubber to be tested can be cut from a molded sheet of rubber if it is of uniform thickness, or a slice may be cut with a razor from bulk material in an arrangement like a miter box. The faces of the slice should be nearly parallel. Three specimens about 4 mm square are then cut from the slice or molded sheet. The edges of the test specimens are trimmed to remove any feather-like protrusions that may be present.

The specimens are placed in the wells above the adjusting wedges in the specimen holder. The top interferometer plate is then placed upon the samples and with the eyepiece of the viewing instrument removed, the image reflected from the bottom of the top plate is brought into coincidence with the image from the top of the bottom plate by adjusting the positions of the quartz wedges. The eyepiece is inserted, and the fringe pattern, which is now visible, is adjusted until not more than 10 fringes are visible.

The openings on the side of the specimen holder are closed, and the Dewar is supported in place around the specimen holder. The tripod screws are adjusted to center the return image of the source upon the lower half of the aperture of the iris diaphragm.

Air dried over calcium chloride and dehydrated calcium sulfate is then passed into the chamber in a continuous stream at a pressure about 2 mm of mercury above atmospheric pressure. Ice is placed in the reference junction bath, and the temperature recording potentiometer is standardized. Liquid nitrogen is then slowly introduced into the Dewar. With a little practice a cooling rate between ½ and 1 deg C/min can be maintained.

It is necessary to adjust the leveling screws on the viewing instrument occasionally to insure that the image of the light source coincides with the lower half of the aperture of the iris diaphragm. This image moves slightly because of differential contraction of various parts of the specimen holder. The errors due to the image shifts introduced by the adjusting procedure are negligible compared to other errors in the procedure when measurements are made on rubber or other materials of high expansivity.

During the course of a run it will be noted that the number and orientation of the fringes gradually change. These changes are due to the tilting of the top plate relative to the bottom plate. The origin of the tilting is discussed in detail by Saunders [2], so only a brief account need be given here. First, since the samples are not necessarily equal in thickness and wedges are used to make up the difference, the magnitude of change in length of the three specimens will be different for a given change in temperature. It has already been noted that the error due to this cause is small, but it can be further reduced by placing the aperture in the viewing mirror near the image of one of the specimens and using the thickness of that specimen in the calculation of the coefficient of expansion.

Second, if sticking occurs between the samples and the interferometer plates, the specimens must tilt because of the difference between the expansions of the specimens and the interferometer plate upon a change in temperature. However, if one of the specimens is weighted more heavily than the others, the tilting will take place at the unweighted specimens. Therefore, by placing a small weight (about 1 g) upon the top plate above one of the specimens, and placing the aperture of the viewing mirror near that specimen, the tilting error can be reduced. Best practice is to locate the thickest specimen by noting the positions of the wedges and to place the weight above that specimen, since it will usually be found that the weight reduces the height of that specimen slightly. The effect of sticking of the specimens can further be reduced by coating them with graphite, as mentioned by Wood [3].

Occasionally, when going through a transition or when the specimens stick to the interferometer plates, it is found that the number of fringes becomes too great for the phototube to resolve the passage of a single fringe. This difficulty can be readily corrected by an appropriate adjustment of the quartz wedges. It should be noted, however, that such adjustments of the fringe pattern can be serious sources of error. Saunders [2] presents a thorough discussion of the errors introduced by tilting of the interferometer plate.

The effect of the change in dimensions of the quartz wedges can be taken into account, but since the coefficient of expansion of quartz is about one-thousandth that of rubber, no correction is considered necessary.

4. Treatment of Data

The second-order transition temperature or other transition temperatures can be obtained directly from the strip-chart record of fringe count versus thermocouple emf. The second-order transition temperature may be defined as the temperature at the intersection of the extrapolated straight portions

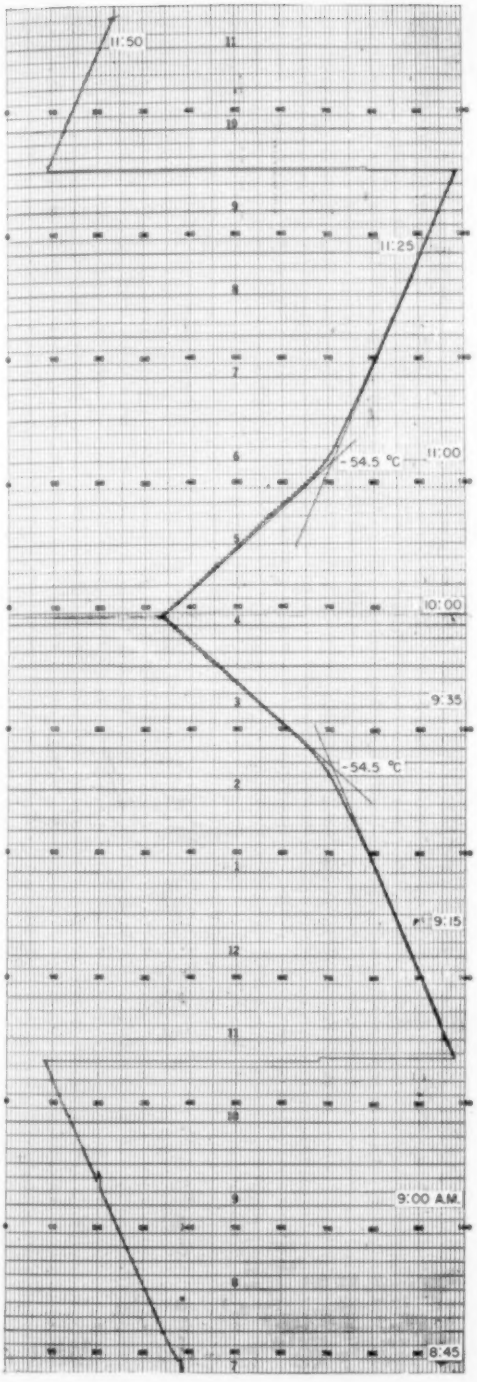

FIGURE 4. *Strip chart record, sodium-potassium catalyzed polybutadiene.*

of the record above and below the transition. The value of the emf corresponding to this point and the corresponding temperature may then be read directly from the chart with the aid of a calibrated scale.

A typical experimental strip-chart record showing the second-order transition at −54.5° C is given in fig. 4. The material tested is a polybutadiene polymerized at 5° C with a mixture of sodium and potassium as catalyst in a diluent composed of 150 parts pentane and 50 parts methylcyclohexane. The specimen thickness was 2.90 mm. The illumination was the yellow helium line, 5876 A. The top interferometer plate, 2 cm in diameter weighed 1.58 g. The second-order transition temperature has been indicated. Time has also been recorded at intervals during the run to indicate the rate of cooling or heating.

The data have been replotted as shown in fig. 5. The temperature has been obtained from the strip-chart by means of the calibrated scale for every tenth fringe in the linear portions and for every other fringe in the curved regions. The change in length in microns per centimeter, as computed by the method shown below, was then plotted against temperature. It is necessary that the data be treated in this manner if values of the coefficient of expansion are desired, as this method of calculation corrects for the nonlinearity of the temperature-emf curve of the thermocouples and for the change in wavelength of light as the index of refraction of the air in the interferometer changes with temperature.

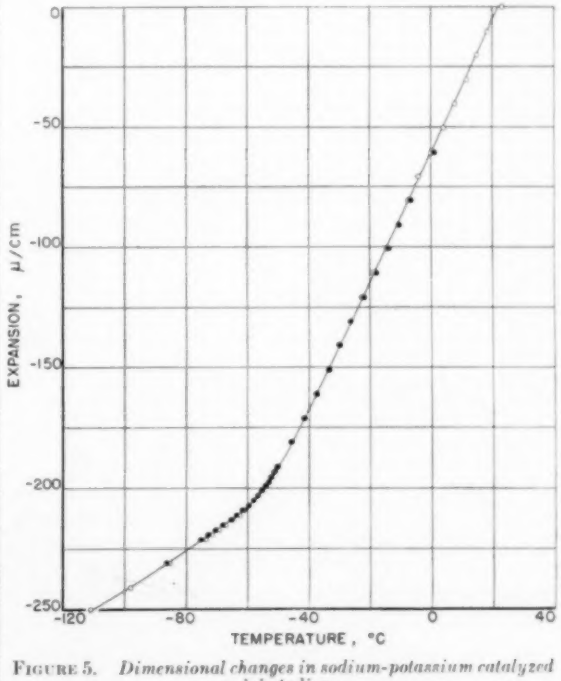

FIGURE 5. *Dimensional changes in sodium-potassium catalyzed polybutadiene.*

●, Increasing temperature; ○, decreasing temperature.

The expansion in microns per centimeter is calculated according to the following expression

$$\frac{\Delta L}{L_0}=\frac{\Delta N\lambda}{2L_0}+C, \tag{2}$$

where ΔL is the expansion of the sample over the temperature range T_0 to T; ΔN is the number of fringes passing the reference point, counting from T_0, between T_0 and T; λ is the wavelength of the light used in air at room temperature; L_0 is the length of the sample at T_0; and C is the correction for change in wavelength with temperature obtained from a table prepared by Merritt [1].

Experience shows the location of transition temperatures to be reproducible to ± 0.5 deg C, where the transition itself is sharp enough to be defined with equal or better precision. Measurements of expansivities of rubber show deviations of about ± 5 percent.

5. Other Applications

In the case of rubber-like materials of a given sample thickness, say 0.3 cm, the passage of 1 to 2 fringes corresponds to a 1 deg C change in temperature above the transition temperature while below the transition temperature, about half as many fringes correspond to the same temperature interval. Metals, however, have a coefficient about one-tenth and glasses about one twenty-fifth that of rubber. In tests on metals, the number of fringes passing the reference mark is reduced by the same factor for samples of the same thickness, and the number of experimental points along an expansion curve is correspondingly reduced. If the expansion curve is linear or only slightly curved, this is no disadvantage; however, in regions of high curvature it is desirable to have a sufficient number of points to define the curve with reasonable accuracy. The number of experimental points can be increased by increasing the thickness of the sample, but there is a limit to the thickness that can be used without too great a loss in fringe contrast unless a differential arrangement [8] is used. It is possible to increase the number of experimental points by arranging a number of switches on the time-intensity recorder spaced to count fractional fringes. It would be necessary before introducing this modification to provide additional stabilization of the power supply to prevent errors due to drift of the output indicator.

The measurement of creep under constant load and the measurement of Young's modulus under light compressive loads suggest themselves as additional applications of the photoelectric recording device.

6. Conclusions

The photoelectric fringe counting method can be used to advantage in survey work where it is desired to locate transitions in a large number of materials both rapidly and conveniently. The data can be processed with a minimum of effort and a precision of ± 0.5 deg C or better in the location of transition points can be realized. Values of coefficient of expansion in the case of rubber-like materials are reproducible to at least ± 5 percent.

7. References

[1] G. E. Merritt, An interference method of measuring thermal expansion, J. Research NBS **10,** 59 (1933) RP515.

[2] J. B. Saunders, Improved interferometric procedure with application to expansion measurements, J. Research NBS **23,** 179 (1939) RP1227.

[3] L. A. Wood, N. Bekkedahl, and C. G. Peters, Application of the interferometer to the measurement of dimensional changes in rubber, J. Research NBS **23,** 571 (1939) RP1253.

[4] J. B. Saunders, An instrument for photographing interference phenomena, J. Research NBS **35,** 157 (1945) RP1668.

[5] F. C. Nix and D. MacNair, Interferometric dilatometer with photographic recording, Rev. Sci. Instr. **12,** 66 (1941).

[6] A. Trobridge, Photograph of moving interference fringes, J. Opt. Soc. Am. **6,** 195 (1922).

[7] C. Pulfrich, The Abbe-Fizeau dilatometer, Z. Instrumentenk. **18,** 261 (1898).

[8] J. B. Saunders, Expansivity of Vycor brand glass, J. Research NBS **28,** 51 (1942) RP1445.

Washington, December 14, 1950.

Journal of Research of the National Bureau of Standards Vol. 47, No. 2, August 1951 Research Paper 2231

A Fiftyfold Momentary Beam Intensification for a High-Voltage Cold-Cathode Oscillograph[1]

John H. Park

A method for obtaining a momentary increase (up to 50 times the steady value) in the intensity of the electron beam obtained from a high-voltage cold-cathode discharge tube has been developed. Its application for increasing the recording speed of a high-voltage cathode-ray oscillograph is described. Oscillograms have been obtained in which the writing speed is about three-fourths the speed of light.

The intensification is caused by superposing a steeply rising voltage pulse on the normal steady voltage across the electrodes of the discharge tube serving as the electron beam source. The voltage pulse momentarily disrupts equilibrium conditions in the discharge and produces an intense discharge that lasts for about 2 microseconds. Measurements of the magnitude and duration of the superposed pulse and of the changes in discharge current have been made. A tentative explanation of the mechanism of intensification based on these measurements is given.

I. Introduction

High-voltage cold-cathode discharge tubes have long been used as sources of electron beams. One of their most important applications has been to supply the electron beam for high-speed cathode-ray oscillographs (CRO) used to record transient electric phenomena of very short duration. The establishment of a beam of high electron density is of paramount importance where very high "writing speeds" are required.

In the experimental work that will be described, the electron beam source[2] was a 1-in.-diameter Pyrex glass tube provided with two cylindrical electrodes spaced 4 in. apart. The air pressure in the tube was adjustable and was maintained at approximately 10μ of mercury. With a direct voltage of 50 kv applied between electrodes, a very narrow beam of visible discharge is obtained that originates in a bright spot at the center of the cathode and terminates at the anode. Since the mean free path for electrons in the discharge is approximately equal to the distance between electrodes, a large fraction of the electrons generated at the cathode are accelerated to a speed corresponding to full voltage between cathode and anode while travelling to the anode. A small hole in the center of the anode allows part of this electron beam to continue from the discharge tube into the main chamber of the CRO where the electrons pass through a beam trap, focusing coil, deflecting and sweep plates and finally strike the film or fluorescent viewing screen. The current in the discharge tube is very sensitive to small changes in air pressure. A fine control of pressure permits adjustment of the discharge current to values ranging from 0.1 to 0.8 ma. The portion of the electron beam passing through the hole in the anode and used for recording purposes is only about 1 percent of the total discharge-tube current.

In order to obtain useable records of electrical transients of very short duration, that is, high "writing speeds", a high electron density in the beam is required. Some of the various methods [3 4 5 6] that have been used to increase beam intensity are (1) shaping the electrodes, (2) using different gases in the discharge tube, and (3) using prefocusing coils placed around the discharge tube. Also the fine control of gas pressure that permits adjustment of current in the discharge tube can be used to increase beam intensity up to a certain point; but any attempt to establish a steady discharge current above approximately 0.8 ma destroys equilibrium and changes the type of discharge so that a steady beam cannot be maintained. These methods of intensification have proved moderately successful. However, it was found that by superposing a momentary pulse on the constant direct-current voltage applied to the discharge tube, the discharge current and beam intensity could be momentarily increased by a factor of 10 to 50 times the steady state value. The increased beam current persists only for a very short time and does not appreciably decrease the life of the cathode, but by proper synchronization with the phenomena being measured the increased beam intensity becomes useful for obtaining higher writing speeds.

2. Experimental Methods and Measurements

A momentary increase in current through the discharge tube and beam intensification occurs whenever a sudden increase of about 800 v or more is superposed on the normal steady value of 50 kv applied between the cathode and anode. The following methods of applying this pulse have been

[1] This investigation has been carried out as part of a cooperative program on basic instrumentation jointly sponsored at the National Bureau of Standards by the Office of Naval Research, the Office of Air Research, and the Atomic Energy Commission.

[2] A Westinghouse 50-kv cathode-ray oscillograph (with minor modifications) was used in all the experimental work.

[3] W. Rogowski, Limitations of cathode-ray oscillograph, Elektrotech. Z. **52** 1245 (Oct. 1931).

[4] F. Mölsch, Electron current density in CRO, Arch. Elektrotech. **27**, 642 (Sept. 1933).

[5] J. M. Bryant and M. Newman, Developments in high speed cathode ray oscillography, Univ. Minn. Engr. Expt. Sta. Tech. Pap. 27 (March 1942).

[6] E. T. Wade, T. J. Carpenter, and D. D. MacCarthy, Modern cathode-ray oscillograph for testing lightning arresters, Trans. AIEE **61**, 349 (May 1942).

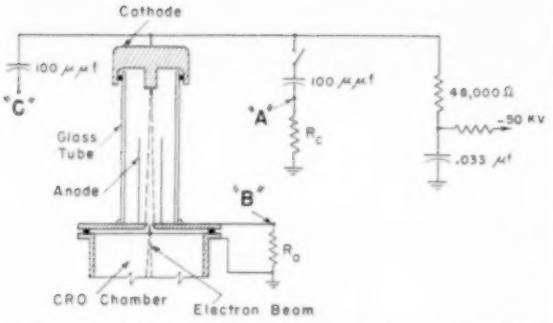

FIGURE 1. *Wiring diagram of circuits used for (1) applying the intensifying pulse to the discharge tube supply voltage and (2) obtaining measurements of this pulse and changes in current through the discharge tube.*

tried and all give the intensification: (1) A current pulse passed through a resistor between anode and ground return lead. (2) A voltage pulse capacitively coupled with the cathode. (3) A current pulse inductively coupled with the lead to the cathode or anode. Because of the difficulties encountered in the control and measurement of the applied voltage pulse for method (3), a detailed description of procedure and results will be given only for methods (1) and (2).

2.1. Current Pulse through Anode Resistor

Resistor R_a and connections at B and C (see fig. 1) were used for this method, and the single-pole switch just above A was open. The anode of the discharge tube was insulated from the grounded case of the CRO by removing the screws that clamp the rubber gasket separating the discharge chamber from the main CRO case. The anode was connected to ground through resistor R_a. By passing a current pulse through R_a the potential difference between anode and cathode could be given a similar pulse. The magnitude and wave shape of this pulse were measured by connecting B to the CRO deflecting plates. By connecting C to the deflecting plates and thus using the deflecting plates as the low side of a capacitance divider, a record of change in potential of the cathode was also obtained. This record of the change in cathode potential when divided by 48,000 is also a record of the change in current through the discharge tube, since for the short duration of the pulse the voltage of the cathode can only be changed by the same amount as the IR drop through the 48,000-ohm resistor, which is in series between the cathode and the 0.033-μf smoothing capacitor.

By connecting B to various points on the resistance network that supplies the Norinder [7] relay voltages for the CRO, the magnitude, duration, and polarity of E_a (voltage pulse applied to the anode) could be controlled. Records were obtained for various conditions, and two examples are shown in figure 2. The horizontal trace, nearest the time scale in each oscillogram, is the reference "zero line" obtained with the deflecting plates short-circuited. The voltage applied to the anode, E_a, rises to a maximum very rapidly ($<0.5\mu$sec) and decreases fairly slowly. The current, i_a, through the discharge tube increases from its low steady-state value of 0.1 ma to a fairly high value, approximately 7 ma, as soon as the anode voltage is applied. When the polarity of the anode pulse is positive (fig. 2, A), it increases the voltage between anode and cathode and a short time (about 1μsec) after application of the anode pulse (this delay time being shorter for higher anode voltages and for higher values of initial discharge current) the discharge current shows a second rapid rise and the intensity of the electron beam increases at the same time. As the discharge current decreases, the beam intensity also decreases. When the polarity of the anode pulse is negative (fig. 2, B), it decreases the voltage between anode and cathode. The net current in the discharge tube is temporarily reversed from its steady-state direction and is of a greatly increased magnitude. Nevertheless, a beam of electrons continues to flow in the original direction and is even somewhat intensified.

2.2. Voltage Pulse Capacitively Coupled With Cathode

For this method the single pole switch above A (see fig. 1) was closed, thus connecting the cathode to one terminal of a small high-voltage capacitor (actually consisting of a polyethylene-insulated wire with a braided sheath over the insulation). The other terminal of this capacitor was connected to ground through resistor R_c. With the steady direct-current voltage on the cathode this capacitor is charged to 50 kv, and when a current pulse is passed through R_c the cathode voltage is immediately changed by the drop through R_c. The duration of this change in cathode voltage is not fixed by the duration of the current pulse through R_c but is determined by the time it takes for the small high-voltage capacitor to assume a new value of charge, that is, by the time constant of the small capacitance in series with the 48,000-ohm resistor (the effective resistance of the discharge tube being much larger). A record of this change in cathode voltage was obtained by connecting C to the CRO deflecting plates. A record of the current through the discharge tube was obtained by making R_a 100,000 ohms and connecting B to the CRO deflecting plates.

By connecting A to various points on the resistance network that supplies the Norinder relay voltages for the CRO, the magnitude and polarity of E_c (change in cathode voltage) could be controlled. Records were obtained for various conditions, and two examples are shown in figure 3. With a negative pulse applied to the cathode (increase in voltage between cathode and anode) the discharge current increases to a high value immediately. Beam intensification and a second increase in discharge current occur a short time later. In the example shown in figure 3, A, the magnitude of the applied

[7] O. Ackermann, A cathode ray oscillograph with Norinder relay, Trans. AIEE 39, 467 (April 1930).

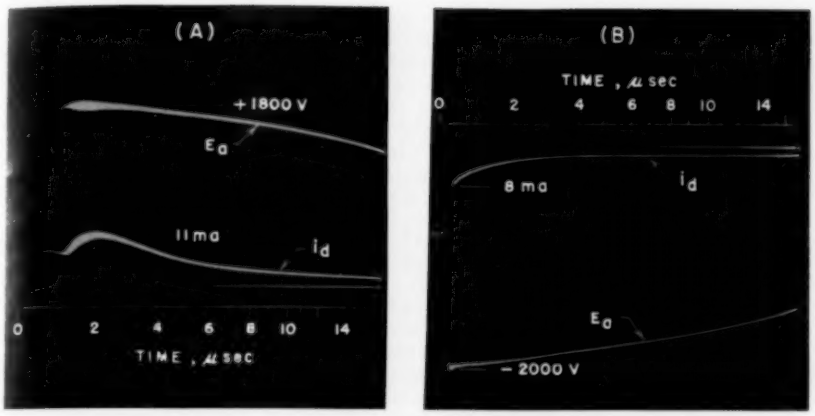

FIGURE 2. *Oscillograms of voltage pulses applied to the anode, E_a, and the corresponding changes in current through the discharge tube, i_d.*

(A) is for a positive polarity voltage pulse, and (B) is for a negative polarity voltage pulse.

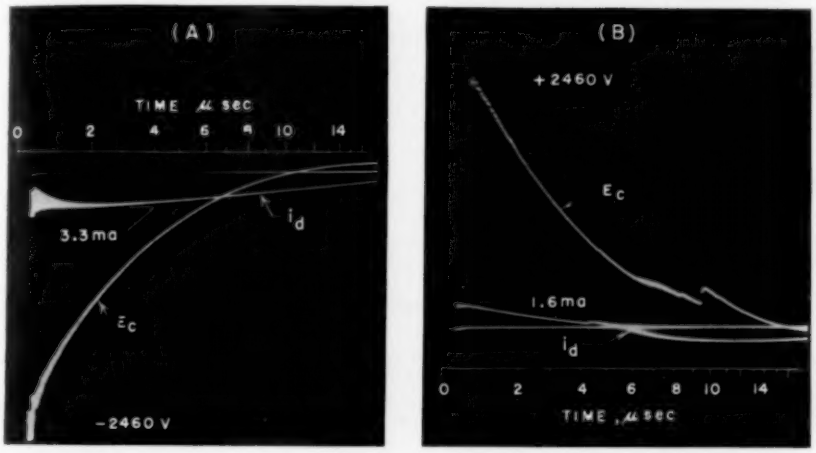

FIGURE 3. *Oscillograms of voltage pulses applied to the cathode, E_c, and the corresponding changes in current through the discharge tube, i_d.*

(A) is for a negative polarity voltage pulse, and (B) is for a positive polarity voltage pulse.

cathode pulse was so high that beam intensification and second increase in discharge current occur very quickly. The discharge current remains high even after the cathode voltage pulse has decreased to zero. Records with slower sweeps indicate that the discharge current and beam intensity continue to decrease and at a somewhat later time (approximately 200 μsec) the beam fails to leave a trace on the film. A momentary blink in the visible discharge can be observed when the cathode-anode voltage is suddenly increased by a large amount (2 kv or more). With a positive pulse applied to the cathode (decrease in voltage between cathode and anode) the discharge current immediately increases to a high value, reversed in direction from the steady-state discharge current. This current decreases as the cathode pulse voltage decreases, and unless the maximum value of the cathode pulse is above approximately 1,000 v, very little beam intensification occurs. For the example shown in figure 3, B, the cathode pulse was above this minimum value and beam intensification, and reversal of discharge current (to the normal steady state direction) occur about 5 μsec after cathode pulse is initiated. Oscillograms taken under other conditions indicate that this time delay decreases as the magnitude of the cathode pulse is increased and as the initial steady-state discharge current is increased.

3. Proposed Explanation of Experimental Measurements

The reversal in direction of current through the discharge tube (i. e., reversed from the normal steady-state condition) as shown in figures 2, B and 3, B, indicates that for short times, energy can be taken from the discharge without appreciably affecting the mechanism of beam generation, since the electron beam density remains nearly constant as shown by constant density in the trace on the oscillogram. Also, as shown in figure 2, A, with an applied pulse that increases cathode-anode voltage, energy can be fed into the discharge during the short period before beam intensification starts without affecting the recording electron beam. In order to explain these results, consider the variation of net space charge density in the discharge between

cathode and anode. There is a high concentration of both electrons and positive ions throughout the volume of the discharge. Electrons are being constantly fed into the region near the cathode, and since it takes a significant, even though short, time for them to be accelerated toward the anode by the impressed electric field, a large net negative space charge region is built up near the cathode. In the region near the anode, including the space inside the tube forming part of the anode, gas molecules are continually being ionized by the short-wave radiation produced by the impact of high-speed electrons on the anode. The slow electrons produced in this manner drift toward the anode and leave an excess of positive ions, which tend to be accelerated toward the cathode but in the meanwhile build up a high net positive space-charge region near the anode. These space-charge regions have very marked effects on the current fed into the discharge tube, especially during sudden changes in applied voltage. However, the current in the discharge is probably mainly determined by (1) the number of positive ions produced by the short-wave radiation caused by each high-speed electron reaching the anode, and (2) the number of electrons generated at the cathode by each of these positive ions. This process is dependent on gas density and makes the steady-state discharge current so sensitive to gas pressure.

Under steady-state conditions, with 50-kv direct current applied between cathode and anode and with the pressure in the discharge tube adjusted so that a normal electron beam is obtained (0.1 to 0.5 ma in the discharge), it may be assumed that the high concentration of negative space charge in the region near the cathode makes the gradient at the cathode quite small in comparison to the average gradient between electrodes. Similarly, the gradient near the anode should be quite small. When the voltage between cathode and anode is suddenly changed, an instantaneous change in charge distribution can only occur on the electrode surfaces. Since the electrodes more nearly approximate points than infinite planes, the sudden change in their surface charge causes a sudden increase of gradient, mainly in the regions near the electrodes. The sudden increase in gradient causes electrons or positive ions to be drawn from each space charge region toward the adjacent electrode. This flow of electrons and ions constitutes a current flow in the external supply circuit, which is superposed on the steady-state current in the discharge tube. If there is a sudden decrease in cathode-anode voltage, there will be a net flow of electrons from the cathode space-charge region to the cathode and a net flow of positive ions from the anode space-charge region to the anode; these constitute the "reversed" current illustrated in figure 2, B, which continues until the gradients near the electrodes are reduced to their normal low values.

If there is a sudden increase in the cathode-anode voltage, electrons and ions will flow in the direction to increase the negative space-charge density in the cathode region and to increase the positive space-charge density in the anode region. This is illustrated by the first part of the i_d trace in figure 2, A. A sudden increase of available electrons in the space near the cathode, if it is of sufficient magnitude, will disrupt the equilibrium conditions existing in the discharge as shown in figure 2, A, by the second increase in discharge current accompanied by beam intensification. A possible explanation of this sudden change in equilibrium conditions in the discharge is as follows: The increase of negative space charge in the region near the cathode causes an increase (probably gradual at first) in magnitude of the electron stream from cathode space-charge region to anode space-charge region. The greater the number of fast electrons reaching the anode the greater will be the intensity of the short-wave radiation that increases the supply of positive ions; and they will be accelerated toward the cathode and produce more electrons. Thus the action is cumulative. If the initial change is small or occurs at a low rate, a new equilibrium condition will be attained with little effect on the electron beam. If the initial disturbance is of sufficient magnitude and occurs suddenly the cumulative effect causes beam intensity and discharge current to increase rapidly (see fig. 2, A). This effect is stopped very soon because the number of positive ions that can be produced in this short time is limited by the low gas pressure (total number of gaseous molecules) in the tube. As the number of available positive ions is reduced, the beam intensity and discharge current gradually decrease and in some cases the discharge is momentarily extinguished.

When the sudden change in voltage between cathode and anode is a pulse of short duration, as illustrated in figure 3, the effects and their explanation are quite similar with one exception—that beam intensification as shown in figure 3, B, is obtained when the polarity of the voltage pulse is such as to *reduce* the cathode-anode voltage. Note here that the high intensification does not occur until the superposed voltage pulse has decreased to about one-sixth its peak value and that before this time the gradients at the electrodes have been in the direction to decrease the magnitude of total space charge in each space-charged region (as indicated by the reversed direction of discharge current). Intensification occurs as the cathode-anode voltage returns to its normal value, which for the reduced magnitudes of space charge at this instant is sufficient to cause high gradients near the electrodes in the direction to increase the magnitude of charge in the space-charge regions. Thus, the physical explanation for beam intensification and increase in discharge current is the same as that given above, except that the method of initiation is different. As already noted, the high value of discharge current shown in figure 3, A, persists even after the intensification has subsided and the disturbing voltage pulse has reached zero. This is additional evidence that the beam intensification and "second" increase in discharge current are caused by a "triggering" action that is initiated by the sudden increase in

negative space charge near the cathode.

Some beam intensification may be observed in figure 3, B, as soon as the voltage pulse is applied (the direction of the pulse being such as to decrease the cathode-anode voltage). This minor intensification might be accounted for by a concentrating effect on the beam caused by a temporary change in the shape of the electric field near the electrodes when the voltage between cathode and anode is suddenly changed.

4. Application to Cathode-Ray Oscillographs

The main reason for investigating the phenomena of momentary beam intensification was that such a study might lead to increased writing speed for the high-voltage CRO. The extremely high beam intensification lasts for about 2 μsec (see figs. 2 and 3) and can be made to come to full intensity within 0.25 μsec after initiation of the intensifying pulse. Oscillographs now available give satisfactory records for sweep times of 1 μsec or more. Improvement of writing speed is desired mainly for sweep times of less than 1 μsec. Thus the beam intensification is of sufficient duration provided it can be accurately synchronized with the CRO sweep.

The CRO employed in these beam-intensification studies uses pulses to supply the Norinder relay or beam unblocking plates and sweep plates. These pulses are obtained by discharging capacitors, charged to 3,000 v, through resistance or resistance-capacitance circuits as indicated in figure 4. The resistance circuit provided to supply voltages to the Norinder relay plates (used to unblock the beam for the short time required for one sweep of the beam across the film) may be conveniently used to supply the intensifying pulse. It is only necessary to connect from point *I* on this circuit to the sheath of the high-voltage (polyethylene-insulated) lead to the cathode. This connection gives positive synchronization of the intensification with the sweep, but since the time to attain maximum intensification is about 0.25 μsec, shorter sweep times would show no intensification. This timing discrepancy is compensated for by adding 0.25-μsec delay lines in the supply to the sweep plates as indicated in figure 4. This delay in sweep supply has the added advantage of allowing the voltage on the Norinder relay plates to reach a high uniformly changing value before the sweep is started, which is quite important for very short sweep times.

Examples of the records obtained by using the intensifying pulse on very fast sweeps (60 in./μsec) are shown in figures 5[8] and 6. Without the intensifying pulse the only record visible is a very faint zero line. The oscillogram shown in figure 5 was obtained by coupling the CRO deflecting plates with as short a loop as possible directly to the plate circuit of a 150-megacycle oscillator consisting of two 6J6 tubes in push-pull parallel. The deflection shown in figure 5 corresponds to 500 v rms on the deflecting plates, which was obtained by momentarily pulsing the plate supply of the oscillator to 1,200 v. This momentary high plate voltage was used not only in order to attain the high momentary output from the oscillator but also to prevent breakdown between the deflecting plates inside the CRO. It was found that a steady radio frequency as low as 100 v rms applied to the deflecting plates caused a gaseous discharge to appear between plates when

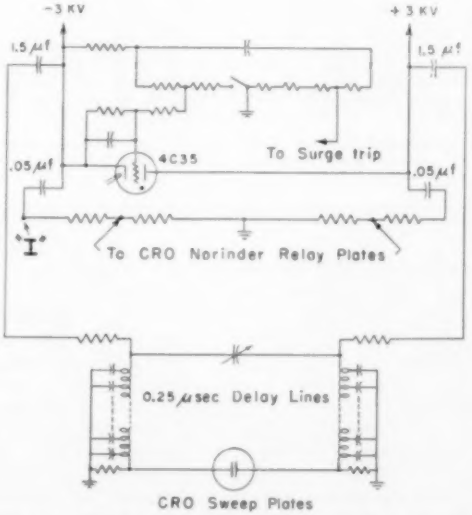

FIGURE 4. *Wiring diagram of circuits used to supply the voltage surges for the Norinder relay plates and sweep plates of the CRO.*

Intensifying pulse was obtained by connecting to point *I*.

[8] As seen from these records, the sweep speed is neither exactly uniform nor logarithmic. The slight packing of the time scale on the initial part of the sweep is introduced by the 0.25-μsec 10-section delay lines inserted in the sweep leads.

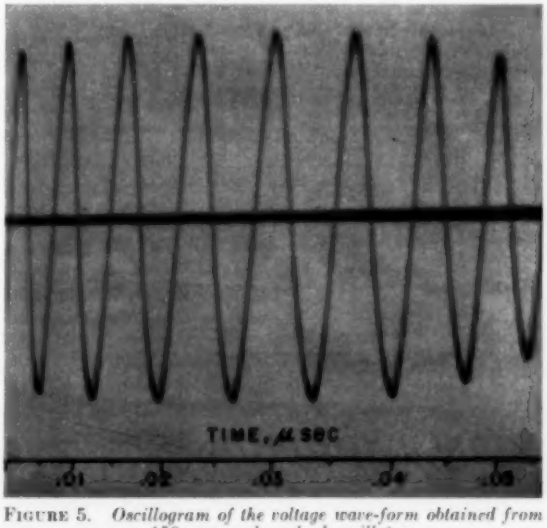

FIGURE 5. *Oscillogram of the voltage wave-form obtained from a 150-megacycle pulsed oscillator.*

The intensified beam was used to obtain this record.

the beam is unblocked. No discharge appears with direct-current or pulse voltages, whose magnitudes are 2,000 v or higher.

The oscillogram shown in figure 6 is one of a number taken in an attempt to determine the maximum writing speed attainable with the intensified beam. The deflecting plates were connected to a small neon tube lightning arrester (intended for use on telephone circuits), using the shortest leads possible. A steeply rising voltage pulse was applied to the arrester tube by connecting it across a 500-ohm resistor through which a capacitor was discharged. Figure 6 shows the initial part of the rise of this voltage. Breakdown of the arrester occurs after the voltage has gone off scale on the oscillogram. The subsequent oscillations shown on the record are produced when the deflecting plates are short-circuited by the arrester discharge, after being charged to a high voltage (about 6,000 v). This high value of charging voltage, which caused the initial rise of voltage and the first four oscillation peaks to go off scale on the oscillogram, was used in order to attain as high a rate of change of voltage on the deflecting plates as possible. As seen from the record, the beam intensity is sufficient to obtain a visible trace even with this high rate of change of voltage. The trace on the oscillogram is a record of the change of voltage with time and it is very nearly perpendicular to the time axis. Since a trace made on the film, with voltage on the deflecting plates only, was found to be not exactly perpendicular to the zero line, measurements of time between maximum deflection in one direction and maximum deflection in the opposite direction are not significant. This is accounted for by the fact that in order to have the record start at the left edge of the film the beam is deflected off the axis of the CRO by deflecting coils just before it passes through the deflecting plates, and this makes the beam travel through an unsymmetrical fringing field just as it leaves the deflecting plates. In order to obtain writing speeds corrected for this distortion, the time between the two vertical traces of a positive or negative half cycle whose peak was off the film was measured (1) at the zero line and (2) at the place where the trace just goes off the film. The difference between these two measured times is the time it takes the beam to travel from the zero line to the off-scale point and back to the zero line (a distance of 5½ in. on the film). Measurements of writing speed made by this method on the record reproduced in figure 6, and 10 other similar film records give an average writing speed for the trace appearing on the film during the first cycle of the oscillations of 9,100 in./μsec (about three-fourths the speed of light).

The value of writing speed given above is for a trace that is easily visible on the film, the maximum writing speed being fixed by (1) the maximum rate of change of deflection that can be imparted to the electron beam while traveling between the deflecting plates, and (2) the distance from the plates to the recording film. This maximum rate of change of deflection is limited by (1) the time of travel of the electrons of the beam through the deflecting plate field, and (2) the maximum rate of change of the electric field between the deflecting plates. The maximum rate of change of voltage between deflecting plates is attained when the plates are charged to the highest voltage possible and then discharged through the shortest leads possible. These conditions were fulfilled as nearly as possible in obtaining the record shown in figure 6. A computation of this rate of change of voltage was made by using (1) the measured value of capacitance between plates (10 μμf), (2) an estimated effective length of leads between the plates and the point at which these leads were short-circuited by the small neon tube arrester (8 in.), and (3) a maximum charging voltage on the plates of 6,000 v. Using this computed rate of

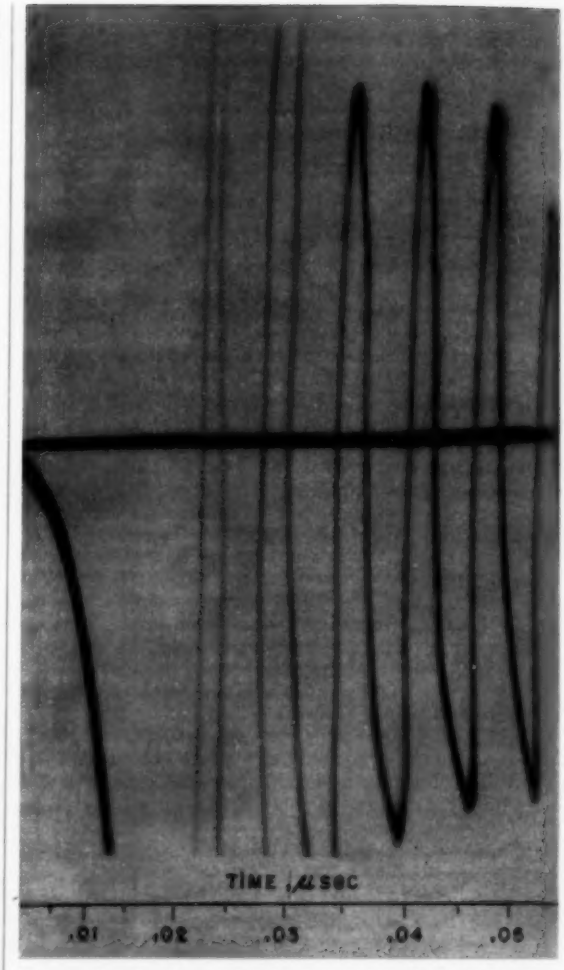

FIGURE 6. *Oscillogram of the oscillations obtained when the CRO deflecting plates are short-circuited after being charged to 6,000 volts.*

The maximum speed of the recording trace on this film was about 9,100 inches per microsecond.

change of voltage and taking into account the time of travel of electrons through the deflecting plate field and the distance between the deflecting plates and the recording film, a computed value of maximum writing speed for the CRO used in the experiments described above was found to be 9,700 in./μsec.

5. Conclusions

The computed and experimental values of maximum writing speed agree quite well, and as already noted this maximum value is determined by the design of the CRO used in these experiments rather than the intensity of the electron beam. The electron beam intensity as used in the experiments is probably sufficient to yield writing speeds greater than the speed of light if a CRO deflecting system, designed with this objective in mind, were used.

Thus the method of beam intensification described in this paper can be used to obtain extremely high writing speeds, and it can very easily be applied to a high-voltage cold-cathode CRO. Also, since the current in the discharge tube is maintained at a low steady value except for the very short time required to obtain the record, the problems of beam adjustment and life of cathode become of minor importance. It should be noted that the intensifying pulse increases the electron beam voltage slightly (about 2 to 5%, depending on the magnitude of the pulse being used). This decreases the voltage sensitivity of the CRO by the same percentage and suggests that a voltage calibration be made when the intensifying pulse is used if a higher percentage accuracy is desired from the CRO records.

In addition to its use for increasing the writing speed of a high-voltage CRO, the method described should be useful wherever a high-density electron beam of short duration (about 2 μsec.) is required.

WASHINGTON, February 15, 1951.

Journal of Research of the National Bureau of Standards Vol. 47, No. 2, August 1951 Research Paper 2232

Annealing of Platinum for Thermometry

Robert J. Corruccini

Experiments are described on the annealing of platinum wire in which the coefficient of resistance and thermal electromotive force were used as criteria of the physical state of the metal. It was found that platinum wire of the highest available purity almost completely recovers its electrical properties at a temperature as low as 300° C, although a slight further recovery occurs with increase of annealing temperature up to 1,450° C. On quenching heated wires in various gaseous media, changes in the electrical properties occur that are greater the more rapid the quenching and that are similar to the effect of strain.

The electrical properties of dilute alloys of gold, silver, and copper in platinum were measured. Contrary to prediction, the copper and silver alloys were thermoelectrically positive to platinum at ordinary temperatures. Thus far, no impurity other than gold has been found to lower the thermoelectric power of platinum.

It is apparently not possible to represent the kinetics of annealing in terms of a temperature activated process having a single value of activation energy. This result is interpreted in terms of the diffusion of dislocations.

1. Introduction

The metal, platinum, is used in resistance thermometers and in platinum versus platinum-rhodium thermocouples. These types of thermometers, when certain specifications are met, are used to define temperatures on the International Temperature Scale in the range −182.97 to +1,063° C [1].[1] Because both the resistivity and thermal electromotive force (emf) of platinum depend on the physical condition, the annealed condition is specified for platinum to be used in thermometry. This condition is produced by heating and is characterized by decreased tensile strength, hardness, and thermoelectric power and by increased coefficient of resistance compared to cold-drawn or cold-rolled platinum.

The published data on the conditions necessary for annealing are diverse, because the annealing temperature is a function of the amount of deformation in cold-working and the purity of the metal.[2] Thus, Wise and Vines [2] showed that there was an inverse relation between the amount of deformation produced in cold-rolling platinum to various degrees and the temperature required to restore the metal in 15 min to the hardness characteristic of annealed platinum. Earlier work by Tammann and Dreyer [3] failed to show such an effect for platinum or palladium, although it was demonstrated that the temperature required for recovery of the minimum hardness and resistivity of silver, copper, and gold varied inversely with the amount of previous deformation. A similar variation in the temperature for recovery of the thermoelectric power of silver was demonstrated by Tammann and Bandel [4]. Feussner [5] showed that the minimum annealing temperature of platinum is raised by additions of impurities.

The International Temperature Scale [1] recommends that platinum for thermometry should be annealed in air above the maximum temperature at which it is to be used (450° C or higher for standard resistance thermometers and about 1,100° C for standard thermocouples).

Since 1935, platinum versus platinum-rhodium thermocouples submitted to the Bureau for calibration have been annealed for 1 hr at 1,450° C before calibration, the temperature 1,450° being approximately the maximum temperature of calibration. The wires are annealed by hanging them between two binding posts in air and passing an electric current through them. A previous article [6] offers the following comments on this practice.

"There is some question as to the optimum temperature or length of time at which such couples should be annealed to produce the most constant characteristics in later use. As a matter of fact, there is some question as to whether annealing for for more than a few minutes is harmful or beneficial. Most of the mechanical strains are relieved during the first few minutes of heating at 1,400 to 1,500° C, but it has been claimed that the changes in the thermal emf of a couple in later use will be smaller if the wires are heated for several hours before calibration and use. The principal objection to annealing thermocouples for a long time at high temperatures aside from the changes in emf taking place, is that the wires are weakened mechanically as a result of crystal growth."

The lowest annealing temperature that has been advocated for thermometric platinum is 400° C [7]. Brenner states, "It was found that chemically pure platinum wire can be completely annealed at 400° C in one hour. Wire annealed slowly at this temperature *in air* (by heating it in a platinum dish in a furnace, not by resistance heating) shows an improved behavior with respect to contamination in subsequent service as compared to wire annealed (by electrical heating) at 1,450° C."

In an unpublished investigation at this Bureau in 1947, C. H. Meyers found that 0.003-in.-diameter

[1] Figures in brackets indicate the literature references at the end of this paper.

[2] Evaluation of published data on the conditions for annealing platinum is frequently difficult because information on the amount of deformation and the purity is not given. The purity of thermometric platinum is conveniently specified by a coefficient of resistance, in particular by the average coefficient over the interval, 0° to 100° C, which is defined as $(R_{100}-R_0)/100R_0=\alpha$. It would be desirable to have the value of this quantity always stated as a figure of merit for platinum of thermometric quality.

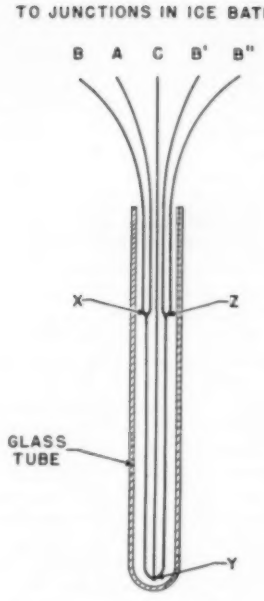

FIGURE 1. *Schematic diagram of sample and leads.*

AXYZ is the sample. Terminals B–A–B′–B″ were used when the portion XYZ was to be used as a four-lead resistor. Terminals A–C were used for determination of the thermal emf of portion AY versus the reference platinum wire CY.

platinum resistance-thermometer wire (cross-sectional area reduced 99+% in drawing) was almost completely annealed within 5 min. at 500° C. After heating for a few minutes in air at about 1,000° C, the value of $\alpha(=[R_{100}-R_0]/100R_0)$ decreased but increased again upon subsequent heating at 500° or 600° C. It was pointed out by Meyers that this effect would be of importance in using platinum-resistance-thermometers at high temperatures.

The present investigation had a twofold purpose at the start: (1) To find whether annealing for 1 hr at 1,450° C causes any further change in the electrical properties of platinum that has already been annealed at a lower temperature, and (2) to investigate the reversible decrease of the coefficient of resistance due to heating that was found by Meyers. An experimental arrangement was used that permitted measurement of both the coefficient of resistance, α, and the thermal emf (versus an arbitrary reference material) of samples of platinum after each of a series of heat treatments. Because the changes in α and thermal emf are related, measurement of both properties provides a valuable experimental check on the results. Since these electrical properties are sensitive to impurities, care was taken to avoid contamination of the platinum. During the course of this work, it was decided to investigate the effects of the impurities, gold, silver, and copper on the electrical properties of platinum and also the kinetics of annealing. These subjects are discussed later in separate sections.

2. Experimental Methods

Figure 1 shows the arrangement of the sample and leads used for most of the measurements. The length AXYZ was the sample. At X was welded a platinum lead BX, and at Z were welded two platinum leads B′Z, B″Z. The leads BX, B′Z, B″Z were platinum of ordinary quality. The wire CY was a reference wire for the measurement of thermal emf. The thermal emf of the sample versus the reference wire was measured, using terminals A-C. The length XYZ (16 in.) of the sample served as the element of a four-lead resistor for the determination of α, using terminals B-A-B′-B″. Most of the measurements were made using 0.020-in. thermocouple-grade platinum wire. The reference wire CY was an annealed 0.020-in. thermocouple-grade platinum wire. For measurement of the electrical properties, the sample, with leads attached as shown in figure 1, was inserted into a glass tube of 15-mm inside diameter with the wires separated by mica partitions.

The connections between the platinum wires and the copper leads to the measuring circuit were in an ice bath, except for sample 3. With this sample no thermal emf measurements were made, hence the reference wire CY was absent and the copper leads were soldered to short lengths of the four platinum leads inside the glass sample-tube. All electrical measurements were made with a Wenner thermocouple potentiometer. The resistance of the samples of 0.020-in. wire was about 0.2 ohm at the ice point. For measuring the resistance of the 0.020-in. wire, a current of 20 ma was used. It was found that the effect of the heating due to this measuring current was negligible. As the voltage drop across the resistor was only about 4 mv, care was taken to minimize residual emf in the system.[3] All connections between the potentiometer and the sample leads were of copper. By means of a four-pole double-throw switch of low contact resistance, the currents in the potentiometer and the sample could be reversed simultaneously. By averaging the emf readings obtained in this way, the residual emf in the sample and the measuring circuit was canceled out (to the extent that it remained constant throughout successive reversals). As the coefficient of resistance was of greater interest than the absolute values of resistance, the potentiometer was calibrated in terms of an arbitrary unit by a method of internal comparison of coils.[4] With this calibration, emf *ratios*, and hence α, could be obtained accurately without knowledge of the relation between the arbitrary unit of emf used and the absolute unit of emf.

[3] By "residual" emf is meant the emf that would still exist in the sample and leads were the current through the sample reduced to zero, as well as the emf that the potentiometer would register if the input terminals were short-circuited with copper. These are largely, if not entirely, thermal. The former result mostly from strain inhomogeneity in the leads in regions where a temperature gradient exists and may amount to as much as several microvolts. The latter usually results from lack of temperature uniformity throughout the galvanometer circuit. In these experiments, it was negligible.

[4] For an analogous method employed with bridges see Wheatstone bridges and some accessory apparatus for resistance thermometry by E. F. Mueller, Bul. BS **13**, 553 (1916-17) S288.

945247—51——3

Routine measurements of the thermal emf of test wires versus the Bureau's platinum thermoelectric standard, Pt–27, are usually made with the wires inserted in porcelain insulating and protection tubes with the hot and cold junctions at 1,200° and 0° C, respectively. For the present measurements, it was desired to evaluate the effect of strain on the thermal emf. In order that annealing should not occur during the measurement, a hot-junction temperature lower than the lowest reported temperature for rapid annealing of platinum (400° C) was required. For this measurement the sample tube was lowered into a vertical tube-furnace. Measurements of all except the hard-drawn wires were made at 300° or 400° C. Experiments showed that, with the time of measurement used, the thermoelectric power of these wires was independent of the hot-junction temperature over the above range. The measurements with hard-drawn wires (samples 5 and 7) were made at either 100° or 200° C, as the initial rate of change of electrical properties of such wire due to annealing is rapid at 300° C or above.

In measuring the thermal emf, a switch was used to reverse simultaneously the unknown emf and the potentiometer current and thus eliminate the effect of residual emfs in the measuring circuit. Careful handling of the sample and leads is important, since a portion of wire that has been cold-worked by bending may have thermoelectric properties differing slightly from those of the unworked portion. If the region where the resulting physical inhomogeneity exists is placed in a temperature gradient, it becomes the seat of a thermal emf, which may amount to as much as several microvolts, and, in these experiments, was difficult to reduce below 0.1 μv. The effect may be detected by changing the temperature distribution along the sample, for example, by varying the immersion of the sample in the ice bath, steam bath, or furnace. If the measured thermal emf remains constant in such a test, it is probable (though not certain) that there is no emf due to inhomogeneity in the wires. The effect was minimized by avoiding bending of the wires AXY and CY. The most reliable measurements of thermal emf were those made after annealing the sample in the furnace. After such annealing, the sample was raised a few inches in the furnace for the thermal emf measurement, thus bringing annealed (homogeneous) wire into the region of the temperature gradient at the top of the furnace while keeping the junction Y in the isothermal hot zone. In cases where the properties of the lower part of the sample wire AXY were changed by annealing in the furnace, while the part outside the furnace remained unchanged, a correction, which in most cases was nearly negligible, was applied to the measured thermal emf to make it correspond to its value if the annealing had extended all the way to the cold junction.

All values of emf were measured to the nearest 0.02 μv. Because of the difficulty of completely eliminating residual emf in the platinum, the reported thermal emfs may be in error by as much as 0.1 to 0.2 μv. The resistance measurements were reproducible within about 1 part in 10^5 (corresponding to a few hundredths of a microvolt out of a measured emf of 4,000 μv). Values of α measured in this investigation may be in error by as much as 5×10^{-7}.

With the samples and measuring equipment used, the thermal emf provided a more *sensitive* index of physical changes in the wire than did the coefficient of resistance. However, the latter is a more *reliable* index because of the cancellation of the residual emfs by reversal of the measuring current.

At first, annealing at 1,450° C was carried out in vacuum in order to avoid atmospheric contaminants. This was done by removing the sample from its tube and suspending it from binding posts in a bell jar, using leads A and either B′ or B″ to carry the annealing current. The other leads and the reference wire CY remained attached but carried no current and were not heated appreciably in this process. The residual pressure in the bell jar was in the range 1 to 10 μ of mercury. A liquid-air trap was used to remove mercury vapor originating with the mercury-vapor pump. Following such annealing the sample was carefully mounted in its glass tube with the tube open to the air, and the coefficient of resistance and the thermal emf were measured. Following the first anneal of 0.020-in. wire at 1,450° C in vacuum (table 1, sample 4 item C), it was found that α had decreased slightly but that the decrease was very much less than Meyers had found with 0.003-in. wire in air. The rate at which the wire had cooled from 1,450° C, following cutting off of the annealing current, was relatively slow, due, on the one hand, to the absence of convective heat loss and, on the other hand, to the relatively large size of the wire. It was realized that the effect noted by Meyers might depend on the rate at which the wire was cooled from high temperatures. In subsequent experiments, the rate of cooling was varied by filling the bell jar with air or helium at about atmospheric pressure for the cooling period. Later it was found that annealing could be carried out in the open air of the laboratory without contamination, and more rapid cooling was obtained by directing a fan at the sample. In order to test the reversibility of the changes in electrical properties produced by these treatments, the samples were annealed at 500° C in air (in the tube-furnace) following each high-temperature electrical anneal, as Meyers' experiments had indicated that the limiting maximum value of α would be attained after such treatment.

3. Materials

Samples 3 and 4 were from different lots of platinum wire of thermocouple grade that had been annealed for 1 hr at 400° C by the manufacturer. Sample 5 was from one lot and samples 7, 8, and 9 were from another lot of thermocouple platinum, both of which had been furnished hard-drawn (cross-sectional area reduced 99+% in drawing). Two

other samples of annealed 0.020-in. platinum wire from the same source as the other samples gave results similar to those with sample 4 but were omitted from this paper because the measurements were preliminary and were considered less reliable. All samples used in this investigation were furnished by the Sigmund Cohn Corp.

4. Results

The various experiments relating to the initial objectives of this investigation are listed in table 1 in the order in which they were performed on each wire.

In order to put the values of the thermal emf of the samples versus the reference wire on a common basis, they have been calculated for a hot-junction temperature of 400° C (next to last column, table 1). In the last column of table 1 are given values of the thermal emf of the samples versus Pt-27 based on a measurement of the thermal emf of the reference wire versus Pt-27. In computing the last two columns of table 1, it was assumed that the thermal emf was linear with temperature between 0° and 1,200° C.

Effect of annealing at 1,450°. With regard to the first objective of this investigation, the results in table 1 indicate that hard-drawn platinum wire of high purity almost completely recovers its electrical properties after 1 hr at 400° or 500° C, though a slight further recovery occurs with increase of the

TABLE 1. *Effect of various treatments on the electrical properties of platinum*

"Cooling time" is the time required for the sample to cool to the disappearance of incandescence.

Treatment	R_0	$R_{100}-R_0$	α, $\left(=\frac{R_{100}-R_0}{100\,R_0}\right)$	$E_{0^\circ}^{400^\circ C}$ vs. ref	$E_{0^\circ}^{400^\circ C}$ vs. Pt. 27
Sample 4, 0.020-in. diameter					
	Ohms	*Ohms*		*μv*	*μv*
A. As received; annealed by manufacturer 1 hr at 400° C	0.189162	0.074248	0.0039251	+0.8	−4.3
B. 3 hr at 500° C in air	.189092	.074245	.0039265	.0	−6.7
C. 1 hr at 1,450° C in vacuum; cooling time in vacuum = 16 sec	.189248	.074301	.0039261	−.5	−8.2
D. 2 hr at 500° C in air	.189228	.074298	.0039263	−.7	−8.8
E. 1 hr at 1,450° C in vacuum; cooled in He at 1 atm; cooling time = 1½ sec	.189533	.074328	.0039216	+2.2	−0.1
F. 2 hr at 500° C in air	.189302	.074333	.0039267	−0.7	−8.8
G. 1 hr at 1,450° C in vacuum; cooled in air at 1 atm; cooling time = 4 sec	.189531	.074373	.0039241	+.6	−4.9
H. 2 hr at 500° C in air	.189096	.074385	.0039275	−.9	−9.4
I. 1 hr at 1,450° C in air; cooling time = 2½ sec	.190078	.074585	.0039239	+.8	−4.3
J. 2 hr at 500° C in air	.189633	.074584	.0039268	−1.1	−10.0
K. 1 hr at 1,450° C in an atmosphere of dusty air				+1.5	−2.2
L. 2 hr at 500° C in air	.190495	.074812	.0039272	−1.2	−10.3
Sample 5; 0.003-in. diameter					
A. As received; hard-drawn; reduction of cross-sectional area in drawing = 99+%	5.119	1.954	0.00382	+96	+280
B. 2 hr at 500° C in air	4.9816	1.9548	.0039240	+3.6	+5
C. 15 min at 1,450° C in air; cooling time = about 0.1 sec	5.1460	2.0081	.0039023	.....	.....
D. 2 hr at 500° C in air	5.1168	2.0091	.0039265	.....	.....
Sample 7; 0.020-in. diameter					
A. As received; hard-drawn; reduction of cross-sectional area in drawing = 99+%	0.1936	0.07472	0.00386	+63	+182
B. 1 hr at 400° C in air	.190437	.074774	.0039264	+0.3	−5.8
C. 2 hr at 500° C in air	.190412	.074761	.0039262	+.1	−6.4
D. Coiled on 25-mm diameter mandrel and straightened again	.190730	.074882	.0039261	.....	.....
E. Coiled on 5-mm diameter mandrel and straightened again	.193569	.075899	.0039210	+3.1	+2.6
F. 2 hr at 400° C in air	.193410	.075927	.0039257	+1.6	−1.9
G. 2 hr at 500° C in air	.....	.....	.....	+1.1	−3.4
H. 4 hr additional at 500° C in air	.193387	.075932	.0039264	+1.0	−3.7
I. 1 hr at 800° C in air followed by slow reduction of temperature over period of about ½ hr	.193334	.075934	.0039276	−0.5	−8.2
J. 2 hr at 800° C in vacuum followed by slow reduction of temperature over period of about ½ hr	.193359	.075931	.0039269	−.2	−7.3
K. 1 hr at 1,450° C in air followed by slow reduction of temperature over period of about ½ hr	.193799	.076107	.0039271	−1.1	−10.0
L. Quenched from 400° C in quiet air	.193790	.076108	.0039273	−0.9	−9.4
M. Quenched from 800° C in quiet air	.193775	.076112	.0039278	−1.3	−10.6
N. Quenched from 1,500° C in quiet air; cooling time = 3.4 sec	.194034	.076143	.0039242	+1.0	−3.7
O. Quenched from 1,400° by fan in air; cooling time = 0.7 sec	.194213	.076132	.0039200	+2.5	+0.8
P. 2 hr at 400° in air	.193940	.076144	.0039261	−0.4	−7.9
Q. 2 hr at 500° in air	.193880	.076141	.0039272	−1.2	−10.3
Sample 3; 0.020-in. diameter					
A. As received; annealed by manufacturer for 1 hr at 400° C	0.190009	0.074565	0.0039243	.....	.....
B. 1 hr at 1,450° C in vacuum followed by 7 hr at 500° in air	.190032	.074623	.0039269	.....	.....
C. 1 hr at 1,450° C in air followed by 9 hr at 500° C in air	.190586	.074845	.0039271	.....	.....
D. Cooled from 1,450° C in helium over period of about ½ hr	.190580	.074843	.0039269	.....	.....
E. 4 hr at 500° C in air	.190581	.074849	.0039274	.....	.....

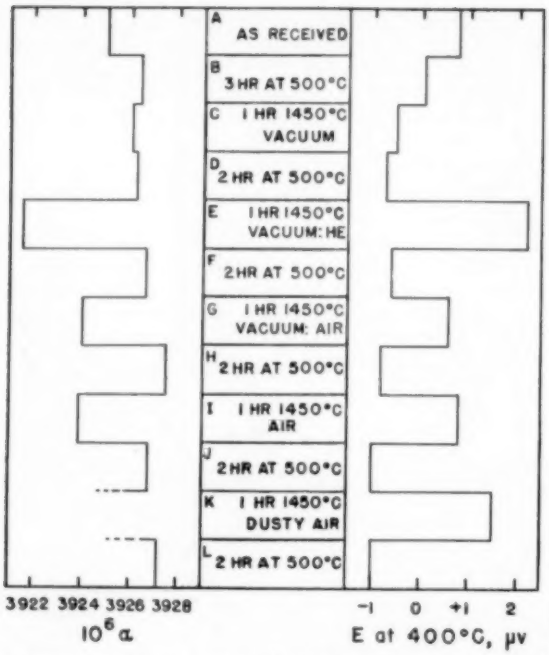
A AS RECEIVED
B 3 HR AT 500°C
C 1 HR 1450°C VACUUM
D 2 HR AT 500°C
E 1 HR 1450°C VACUUM: HE
F 2 HR AT 500°C
G 1 HR 1450°C VACUUM: AIR
H 2 HR AT 500°C
I 1 HR 1450°C AIR
J 2 HR AT 500°C
K 1 HR 1450°C DUSTY AIR
L 2 HR AT 500°C
3922 3924 3926 3928
10⁶ α
−1 0 +1 2
E at 400°C, μv

FIGURE 2. *Effect of various heat-treatments on the electrical properties of sample 4.*

See table 1 for the numerical data and a description of the experimental conditions.

annealing temperature up to 1,450° C.[5] However, this conclusion should not be applied without qualification to platinum of lower purity. The initial values obtained for samples 3 and 4 indicate that these were not completely annealed when received. However, this may have resulted from the strain of coiling and other handling that intervened between the manufacturer's anneal and the determination of the initial results in table 1.

Effect of quenching. Figure 2 illustrates graphically the data on sample 4. It will be noted that with the exception of item C, the simultaneous changes in α and E are of opposite sign and roughly proportional to each other. This proportionality is also displayed in figure 3.

After each quench from 1,450° C the values of α and E were restored by the subsequent anneal for 2 hrs at 500° C in air to approximately the values 0.003927 for α and -1 μv for $E^{400°}_{0°}$ vs reference wire, the latter value corresponding to -10 μv versus Pt-27 at 1,200°. These values may thus be regarded as limiting values for this very pure platinum in the annealed state. The most extreme values previously

[5] B. G. Dammers (Thesis, Leiden, 1936. A brief summary is given by W. H. Keesom and B. G. Dammers, Physica **2**, 1051 (1935)) and W. Meissner (Ann. Phys. [5] **29**, 264 (1937)) have reported the existence of an optimum annealing temperature of about 800° C. According to these authors, a maximum coefficient of resistance was obtained by annealing at this optimum temperature with lower values obtained after annealing at either higher or lower temperatures. This result was not confirmed by the present investigation. Since the variation of coefficient of resistance with annealing temperature was not demonstrated to be reversible by these authors, it is possible that their samples became contaminated at the higher temperatures.

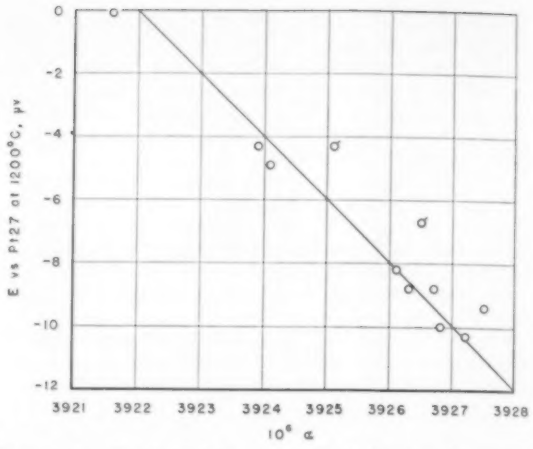

FIGURE 3. *Graph of data on sample 4 showing the proportionality of thermal emf with coefficient of resistance throughout the various heat-treatments.*

See table 1 for a description of the experiments. ○′, Before first anneal at 1,450° C; ○, on quenching from 1,450° C to room temperature at various rates; the diagonal line represents the equation $\alpha = 0.003922 - 0.5 \times 10^{-6} E^{1,200° C}_{0° \text{ vs. Pt-27}}$.

recorded at the Bureau were 0.003926 for α and -8μv for $E^{1,200°}_{0° \text{ vs. Pt-27}}$. Since, in all known cases, impurities lower the coefficient of resistance of platinum and (with the exception of gold) make the emf more positive, it is presumed that the repeated attainment of 0.003927 for α and -10 μv for $E^{1,200°}_{0° \text{ vs. Pt-27}}$ throughout the measurements with the 0.020-in. samples indicates that the wire was exceptionally pure and that no appreciable contamination occurred during the experiments.[6]

The decrease in α and increase in E from the above limiting values, which occur on quenching in various atmospheres, are greater the more rapid the quenching. This is shown in table 2, which summarizes the pertinent data from table 1. The time of cooling from 1,450° C (the temperature was measured with an optical pyrometer assuming an emissivity of 0.30 at the effective wavelength of 0.65 μ) to the dis-

[6] Because the value 0.003927 for α is higher than any previously recorded at this Bureau, the experimental procedure was examined with special care to make sure that the result was not due to an experimental error. As a further check, the value of α for sample 3 was determined on three separate occasions by M. Waxman and Johanna Busse of the resistance thermometry group at the Bureau. These determinations involved ways of measuring resistance and of realizing the temperatures that were completely different from those used by the author. A Mueller bridge was used for the resistance measurement. The value of R_0 was obtained from measurements at the triple point of water, while the steam point was realized by the use of a closed steam-point apparatus operating under a controlled pressure. On the other hand, the results by the author were obtained, using a potentiometer, an ice bath, and a hypsometer open to the atmosphere. The three comparisons gave the following results:

Comparison number	α	
	RJC	MW and JB
1	0.0039243	0.0039244
2	.0039270	.0039263
3	.0039273	.0039275

The differences are less than the sum of the individual uncertainties which were about 5×10^{-7} for RJC and 2 or 3×10^{-7} for MW and JB.

TABLE 2. *Effect of rate of quenching on electrical properties of platinum*

Treatment [a]	Atmosphere during cooling	Average cooling time [b]	α	$E_{0°\text{ vs. Pt-27}}^{1,200°}$
		sec		*μv*
Limiting values obtained following anneal for 2 hours at 500° C in air.			0.003927	−10
Temperature reduced over a period of about ½ hour by gradual reduction of annealing current.	Air, 1 atm	ca 1,000	.003927	−10
Do	Helium, 1 atm	ca 1,000	.003927	Not measured
Normal cooling after abrupt cutting off of annealing current	Vacuum (1 micron)	16	.003926	−8
Do	Air 1 atm	3	.003924	−4
Do	Helium, 1 atm	1.5	.003922	0
Forced cooling in fan blast after abrupt cutting off of the annealing current.	Air, 1 atm	0.7	.003920	+1
Normal cooling; 3-mil wire	do	ca 0.1	.003902	Not measured

[a] Except for last entry, all values are for 0.020-in.-diameter wire.
[b] Time of cooling from about 1,450° to disappearance of incandescence.

appearance of incandescence was used as a comparative index of the cooling rate. Table 2 shows that the particular gaseous atmospheres used do not exert an appreciable influence on the electrical properties, and that the rate of cooling alone is of primary importance.

It appears that this effect is an indication of strain produced by the surface of the wires cooling more rapidly than the interior. As is pointed out later, Matthiessen's rule is obeyed throughout the experiments. In other words, the increase in resistivity due to quenching is approximately temperature-independent, and this implies an increase in the residual resistance (resistance at 0° K). Such an increase results from increasing the number of lattice defects and is characteristic of strain due to cold-working.

To examine the extent to which the effect of quenching is analogous to a strain, the experiments upon sample 7 involving coiling and straightening of the wire were made. These results show that annealing at 400° C almost completely overcame the effect of a bending strain on α, but that the thermal emf was only partially restored and that further decrease in E occurred with stepwise increase of the annealing temperature up to 1,450° C. Thus the effect on α and E of annealing after a bending strain was not fully consistent with that obtained on annealing after quenching.

In another experiment (not included in table 1) a sample of 0.020-in. wire was rolled to a thickness of about 0.001 in. It was annealed in a flame between passes. The last reduction in thickness amounted to about 20 percent. It was found that 2 hr at 500° C brought α to the value characteristic of complete annealing. The thermal emf was not measured. The maximum value of α obtained with this sample was 0.003908, indicating relatively low purity.

Matthiessen's rule. The values of R_0 and $R_{100}-R_0$ given in table 1 have been included in order to illustrate the extent to which the resistance changes that result from quenching and annealing obey Matthiessen's rule [8]. This rule may be stated in the following general way: *Slight variations in the purity or physical state of a metal cause variations in resistivity that are nearly independent of temperature.* The rule will be seen to be valid to the extent that the quantity, $R_{100}-R_0$, remains constant throughout treatments that cause changes in R_0. In certain of the experiments, changes in physical state are combined with changes in dimensions of the wire due to coiling or volatilization. The latter effect changes both R_0 and $R_{100}-R_0$ in the same proportion, and here the validity of Matthiessen's rule cannot be determined by simple inspection of the data. In general, the rule is seen to hold approximately, since changes in $R_{100}-R_0$ are much smaller than the changes in R_0 in those experiments where no dimensional change occurred.

Rate of evaporation of platinum. It is known that platinum volatilizes more rapidly in air than in vacuum [9]. This is thought to be due to the formation in air of a volatile oxide that is unstable. This effect is apparent in the data on R_0 in table 1. After allowing for the effect of quenching, these data show that the rate of increase of R_0 at 1,450° C is several times greater in air than in vacuum. Assuming that the increases in R_0 in air are largely due to evaporative decrease of the cross-sectional area of the wire, it is calculated that the rate of volatilization at 1,450° C of a wire hanging vertically in air is roughly 20 times the rate of volatilization in vacuum found by Jones, Langmuir, and Mackay [10].

Relation between α and E. In the past 15 years, the values of α and $E_{0°\text{ vs. Pt-27}}^{1,200°}$ have been determined at this Bureau for nearly 100 samples of platinum from various sources. Any differences between these samples may be attributed to differences in purity, as all were annealed for 1 hr at 1,450° C in air before testing. The results are plotted as open circles in figure 4. Although there is considerable scattering, much of the data can be represented by the following simple equation, which is represented by the solid straight line in figure 4. E is in microvolts.

$$\alpha = 0.003922 - 0.5 \times 10^{-6} E_{0°\text{ vs. Pt-27}}^{1,200°}. \quad (1)$$

This relation was noted by Wm. F. Roeser some years ago and is published here for the first time. Unfortunately, there were only a few samples where a single impurity predominated, so that it is not

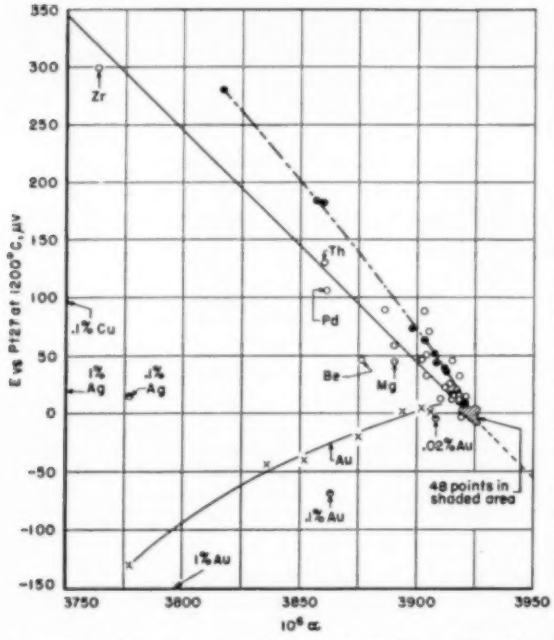

FIGURE 4. *Electrical properties of platinum and various alloys.*

○, Annealed samples of various purities. Where a given impurity was known to predominate its chemical symbol is given. ×, Data of Wm. F. Roeser on alloy with gold (see table 3); ◒, data on alloys with gold and silver—this investigation; ●, data for hard-drawn platinum in various stages of annealing. (See table 1, samples 5 and 7 and table 5). The diagonal solid line represents the equation

$$\alpha = 0.003922 - 0.5 \times 10^{-6} E_{0^\circ \text{ vs. Pt-27}}^{1,200^\circ\text{C}}$$

possible to judge to what extent the equation is generally valid. These samples with predominant single impurities are separately identified in figure 4. Because there is no reason to suppose that the effect of different impurities on the relation between α and E is the same, the above equation ought to be used with caution. In fact, the effect of gold as an impurity is known to be entirely different. While addition of gold lowers α in the usual way, it makes the thermal emf more negative. This is illustrated by the lowest curve in figure 4, which represents unpublished data obtained by Wm. F. Roeser in 1935 (table 3). The points are shown by crosses.

The change of electrical properties with time at 1,500° is believed to be due to preferential volatilization of gold. Spectrochemical analysis of the sample at the end of the experiment showed that the gold content had been reduced to 0.02 percent. (The sample also contained 0.01 percent of Zr at both start and finish plus traces of Ca, Al, Mg, Si, and Fe. These impurities probably account for the final values of $E_{0^\circ \text{ vs. Pt-27}}^{1,200^\circ}$ being positive.)

TABLE 3. *Electrical properties of platinum containing small amounts of gold*

	α	$E_{0^\circ \text{ vs. Pt-27}}^{1,200^\circ}$
Platinum containing 0.25% gold; initial values	0.003777	μV −131
After 3 hr at 1,500° C	.003836	−44
After 5 hr total at 1,500°	.003852	−40
After 8 hr total at 1,500°	.003875	−20
After 12 hr total at 1,500°	.003894	+2
After 16 hr total at 1,500°	.003906	+2
After 22 hr total at 1,500°	.003902	+5

Mott [7] has explained some of the properties of palladium in terms of the quantum theory of metals and his discussion may be applied to platinum, which has a similar electronic structure. The explanation of the effect of dissolved gold in making the thermoelectric power of platinum more negative is particularly interesting in view of the singularity of this effect. However, it appears that copper and silver, being isoelectronic with gold should produce a similar effect. In order to test this, the electrical properties of a number of alloys of gold, silver and copper with platinum were determined. [8] The data obtained and descriptions of the alloys are given in table 4. The alloys were in the form of 0.020-in.-diameter wire and were annealed for 5 min at 1,450° C in air before testing.

The data in table 4 have been plotted in figure 4, insofar as the range of the plot allows, and are represented by half-shaded circles. The isolated position of "Ag" in figure 4 is a consequence of the decrease of thermal emf of the silver alloys at the higher temperatures. The positive emf of the copper and silver alloys is contrary to prediction. Thus, gold remains the only impurity that has been found to lower the thermoelectric power of platinum.

The data for samples 5 and 7 in the hard-drawn state fall far outside the range of figure 3 but would

[7] N. F. Mott, The resistance and thermoelectric properties of the transition metals, Proc. Roy. Soc. (London). [A]**156**, 368 (1936). The characteristic feature of the transition metals on which this treatment is based, is the existence of a nearly filled *d*-band overlapped by an *s*-band. The treatment of the effect of impurities on the thermoelectric power has been extended to aluminum by J. K. Galt, Phil. Mag. [7] **40**, 309 (1949).

[8] The measurements of thermal emf were made by Henry Shenker.

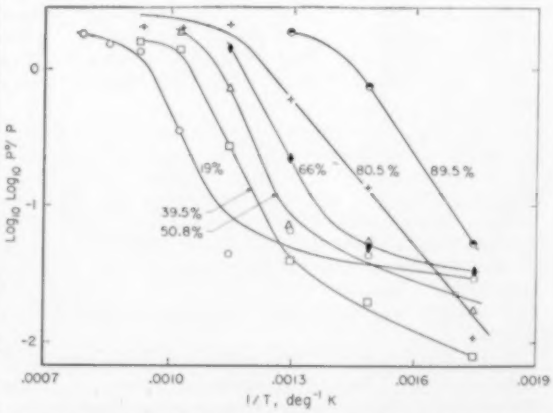

FIGURE 5. *Data of Wise and Vines on isochronal annealing of platinum*

Number give the percentage thickness-reduction in rolling. P is the hardness number at temperature T minus the hardness number of the fully annealed sample. P_0 is the value of P before annealing.

TABLE 4. *Electrical properties of some platinum alloys*

Nominal composition	α	$E^{t}_{0^\circ \text{ vs. Pt-27}}$					
		$t=200^\circ$ C	$t=400^\circ$ C	$t=600^\circ$ C	$t=800^\circ$ C	$t=1000^\circ$ C	$t=1200^\circ$ C
Weight %		μv	μv	μv	μv	μv	μv
Pt—0.1% Cu	0.003590	+29	+67	+100	+129	+155	+183
Pt—1.0% Cu	.001938	234	508	822	1085	1348	1625
Pt—5.0% Cu	.0005375	429	1071	1751	2489	3299	4211
Pt—0.1% Ag	.003777	11	18	21	20	18	15
Pt—1.0% Ag	.002797	86	152	177	170	148	126
Pt—0.02% Au	.003908	0	−1	−2	−2	−3	−4
Pt—0.1% Au	.003863	−10	−21	−32	−45	−57	−68
Pt—1.0% Au	.003404	−86	−185	−293	−407	−521	−631

lie somewhat above the extended line of eq 1. The equation is represented in figure 3 by the diagonal line and is seen to represent the data on quenching of sample 4. The data on the quenching of sample 7 (items K through Q, table 1) are also closely represented by eq 1. However, the data on cold-working by coiling followed by annealing at temperatures below 1,450° would lie above the line representing the equation in figure 3.

It is seen, therefore, that eq 1 is a good representation of the relation between α and E for (a) pure platinum quenched at various rates and (b) annealed platinum, which is contaminated by various impurities other than gold, silver, and copper.[9] The equation is only approximately correct for cold-worked platinum that has not been annealed at 1,450°C.

Kinetics of annealing. Krupkowski and Balicki [11], Balicki [12], and Brindley [13] have shown that many features of the annealing process for copper can be interpreted in terms of the kinetics of a first-order process. In this theory it is postulated that the rate of annealing, $-dx/dt$, is proportional to x, which is the fraction of cold-worked metal remaining at time t, and to a factor $e^{-Q/RT}$, in which Q is an activation energy. It is assumed further, that the quantity P, defined as the difference between the value of some property (resistivity, thermoelectric power, hardness, etc.) at a given stage of annealing and in the fully annealed state is proportional to x. That is,

$$-\frac{dx}{dt}=cxe^{-Q/RT}, \tag{2}$$

where c is a constant, and $P \propto x$, whence

$$\frac{P}{P^\circ}=e^{-cte^{-Q/RT}} \tag{3}$$

where P° is the value of P at $t=0$. On the other hand, Cook and Richards [14], in order to arrive at a form of equation that would fit their hardness measurements on cold-rolled copper, found it necessary to assume a two-step process, namely, "recovery" followed by "recrystallization". Richards states ". . . it is assumed that the degree of recovery is *always very small*, our conception is that recovery is shorter in range than recrystallization and small recovered regions serve as points at which recrystallization can commence". The result of this treatment is a formula similar to eq 3, except that t appears squared and in place of Q there appears the sum of the activation energies for recovery and recrystallization. Values of Q for copper in the range 11.5 to 33 kcal/mole (0.5 to 1.4 ev) have been reported.

A test of the applicability of these equations to the data on the annealing of platinum by Wise and Vines [2] is illustrated in figure 5. (The annealing procedure of these authors may be termed "isochronal", since annealing was carried out for a fixed time at various temperatures.)

As figure 5 shows, the data are apparently incompatible with eq 3 and with Cook and Richards' equation, both of which require that the lines be straight. From the slopes of the straight midportions of the curves are derived values of Q ranging from 16 to 31 kcal/mole without any obvious dependence on the percentage of reduction. It is difficult to base any interpretation on these data, because for each curve there is only one point at or near half-recovery. All the other hardness values are within a few hardness numbers of either the initial or final values, and hence log P°/P has low accuracy at these points.

In order to test eq 3 further, two isothermal annealing curves for platinum were obtained experimentally. The samples were from the same stock as sample 7. Measurements of the coefficient of resistance, α, and of the thermal emf $E^{100^\circ C}_{0^\circ}$ versus the same annealed reference wire used previously were made in the same way as before, except that the lead, AX (fig. 1), was a length of annealed wire similar thermoelectrically

[9] Relations between α and E of similar form exist for silver and iron of relatively high purity. The following equations are derived from unpublished work at this Bureau by Wm. F. Roeser. E is in microvolts.

$$\text{Ag: } \alpha=0.00409-6\times10^{-6}\,(E^{100^\circ}_{0^\circ \text{ vs. Pt-27}}-730)$$

$$\text{Fe: } \alpha=0.00651+4.8\times10^{-6}\,(E^{100^\circ}_{0^\circ \text{ vs. Pt-27}}-1980).$$

The values 0.00409 and 0.00651 are the maximum values of α obtained for silver and iron, respectively, and correspond to the purest samples in the annealed state. With silver, strain or decrease of purity resulted in decreased α and increased E as was the case with platinum, while with iron, α and E decreased together. Here, again, the consistency of the results for samples of different purity was probably fortuitous or due to the narrowness of sample selection. In Mott's theory the positive sign of the coefficient of E in the equation for iron, would be related to the fact that $\partial N(\epsilon)/\partial\epsilon$ is positive for iron (J. C. Slater, Phys. Rev. **49** 537 (1936), where $N(\epsilon)$ is the number of d-levels of energy ϵ. This is in contrast to platinum for which the coefficient of E and the quantity $\partial N(\epsilon)/\partial\epsilon$ are both negative. Matthiessen's rule was obeyed throughout the range of purity and cold-work covered by these experiments, namely, down to values of α of 0.00387 for silver and 0.00542 for iron.

TABLE 5. *Annealing of hard-drawn platinum wire*

Total time, t	R_0	$R_{100}-R_0$	α	$E_{0°}^{100° C}$ vs ref	$P/P°$		
					From $E_{0°}^{100°}$	From α	From R_0
Sample No. 9, annealed at 301° C							
hr	*Ohm*	*Ohm*		μV			
0	.....	.....	[a] 0.003857	[a] +15.9	1	1	1
0.17	0.188000	0.073281	.0038979	6.7	0.42	0.41	0.41
.50	.187752	.073288	.0039034	5.9	.37	.33	.33
1.5	.187563	.073290	.0039075	4.9	.30	.27	.28
5.5	.187318	.073289	.0039125	3.6	.23	.20	.20
29.5	.186761	.073285	.0039240	.6	.04	.03	.04
151.	.186640	.073282	.0039264	.0	0	0	0
Sample No. 8, annealed at 352° C							
0	0.196363	0.075737	0.003857	+15.9	1	1	1
0.13	.193851	.075761	.0039082	4.2	0.26	0.26	0.26
.27	.193680	.075762	.0039117	3.9	.24	.21	.21
1.23	.193236	.075761	.0039206	1.3	.08	.08	.08
6.2	.192973	.075761	.0039260	0.2	.01	.01	.00[9]
31.2	.192958	.075763	.0039264	.1	0	0	0

[a] Not determined experimentally. Values assumed to be the same as for the sample used at 352°.

to the reference wire, CY. This placed the effective cold junction of the thermocouple, AXYC, at point X. (The temperature of this point was measured by replacing BX with a platinum 10-percent rhodium wire and measuring the emf of the platinum-platinum 10-percent rhodium thermocouple, BXA. This procedure avoided bringing inhomogeneous wire into the region of temperature gradient during the measurements. Samples were annealed at 301° and 352° C. The results are given in table 5.

Values of 12 $E_{0°}^{100° C}$ are plotted versus α as filled circles in figure 4 for the samples annealed at 301° and 352° C. The dashed curve drawn through these points also represents the data for samples 5 and 7 (table 1) in the hard-drawn state and for sample 7 after coiling.

Table 5 shows that there is little difference whether $P/P°$ refers to changes in R_0, α, or E. Values of $P/P°$ calculated from α are plotted in figure 6.

Two noteworthy features of the data may be pointed out: (1) the marked decrease in $P/P°$ in the first few minutes is much greater than is required by a simple exponential dependence on t, that is eq 3

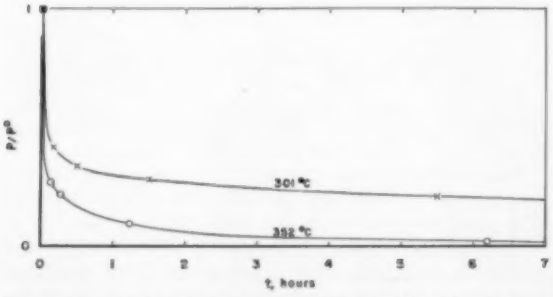

FIGURE 6. *Isothermal annealing of two samples of hard-drawn platinum*

Values of $P/P°$ were calculated from changes in α (table 5).

and the equation of Cook and Richards do not apply, (2) the limiting values that α and E approach as t increases are the same regardless of the annealing temperature. Others (see footnote 5 and reference [13]) have found the limiting values to be a function of the annealing temperature. Since the present experiments are distinguished by the very high purity [10] of the samples used, it is suggested that the dependence of limiting value on temperature that others have found may be due to the presence of impurities.

We may picture annealing to be the result of diffusion of dislocations and their cancellation through encounters with dislocations of opposite sign. If this were the case, the rate of recombination would be proportional to the *square* of the concentration of dislocations and to their diffusion velocity. The latter would contain a factor, $e^{-Q/RT}$, in which Q may be regarded as an activation energy for a displacement over a distance of one atomic diameter. Assuming further that P is proportional to the concentration of dislocations, the equation

$$\frac{P°-P}{P}=kte^{-Q/RT}$$

is obtained. This equation, however, also fails to fit the experimental data. According to the above mechanism, we may suppose that the final stages of annealing (when the local density of dislocations is everywhere low) would be the same regardless of whether the metal had been initially cold-worked to a high degree or not. This is at variance with a body of evidence [2, 13, 14] showing that the final stages of annealing are slower the less the amount of prior cold-work.

Returning to Cook and Richards' assumption of an intermediate stage, the mathematics for such a

[10] Spectrochemical analysis and other considerations indicated that the total content of impurities did not exceed 10 parts per million, and probably was much less.

wo-step process may be carried through rigorously, hat is without these author's assumption that the xtent of the primary process is always small. The esult of this treatment is that P/P° is equal to the um of two exponential terms, each having the form f the right side of eq 3. Indeed, the curves of fig- ire 6 can be fitted by sums of a number of exponential erms of the form of eq 3. However, at least three terms are required to fit the upper curve. Since Brindley [13] and Balicki [12] have shown that Q for copper is practically independent of the degree of cold-work, it seems reasonable to inquire whether the present data might be fitted by summing terms like the right side of eq 3 over a range of values of c while taking Q to be constant. Proceeding in this way we have

$$P=\int_0^{c_m} p^\circ e^{-cte^{-Q/RT}} f(c)dc, \tag{4}$$

where $f(c)$ expresses the density of the terms $p^\circ e^{-cte^{-Q/RT}}$ as a function of c. Depending on the form of $f(c)$, c_m may be either finite or infinite.

Simple functions such as $f(c)=ac^n e^{-bc}$; $n\geq 0$, $b\geq 0$ did not lead to a representation of the data, but the saddle-shaped function

$$f(c)=me^{-\alpha c}+qce^{-bc}$$

gave a satisfactory result. a, b, m, and q are constants. Inserting this function in eq 4 and integrating to $c_m=\infty$ gave

$$\frac{P}{P^\circ}=\frac{k_1}{1+\frac{te^{-Q/RT}}{a}}+\frac{k_2}{\left(1+\frac{te^{-Q/RT}}{b}\right)^2} \tag{5}$$

where $k_1=mp^\circ/aP^\circ$, and $k_2=qp^\circ/b^2P^\circ$. The second term describes the decrease in P/P° at small values of t, the first term remaining constant at the value, k_1. With further increase of t, the first term, which by now predominates, also decreases. The agreement was improved by taking the limiting value of α to be 0.0039274 instead of 0.0039264. In calculating Q from the values of the constants at the two temperatures, one finds that different values result in each term of eq 5. The resulting constants are $k_1=0.328$, $k_2=0.672$, $a=1.4\times10^{-14}$ hr, $b=2.9\times10^{-9}$ hr, $Q_1=39$ kcal/mole, $Q_2=20$ kcal/mole.[11]

[11] After this paper had been prepared, C. H. Meyers kindly furnished the author with unpublished data on the annealing of hard-drawn platinum wire at 100° and 530° C. The samples used were 0.003-in. wire from the same lot as sample 5. At 100° C, only the initial part of the annealing was observed (to $P/P^\circ=0.93$ at $t=11$ hr.) This change in P/P° is given by the second term of eq 5, the first term remaining constant at the value $k_1=0.328$. On the other hand, at 530° C only the final stages of annealing could be observed beginning with $P/P^\circ=0.008$ at $t=0.146$ hr). This change is given by the first term of eq 5, the second term being already zero. It was found that eq 5 with the constants given above did not represent these data. However, by altering the constants to the values, $Q_1=28$ kcal/mole, $Q_2=16$ kcal/mole, $a=1.4\times10^{-10}$ hr, $b=8.1\times10^{-4}$ hr, these data were well represented. This change introduced systematic differences between the calculated and observed values of α at 301° and 352° C that were as large as 2×10^{-4}. Thus, using the altered constants, the representation by eq 5 of all the annealing data from 100° to 530° C is fairly good, although somewhat outside the range of experimental error.

Whether or not eq 5 is generally valid, we may at least conclude that it is apparently not possible to fit the curves of figure 6 on the basis of temperature-activated processes having a single value of Q. It may be supposed that Q depends upon the local stress existing in the region of a given dislocation. A complete treatment, taking dn in eq 4 to be a function of both c and Q has not been carried out, since a larger body of experimental data would be required in order to establish the form of the required function.

Several helpful discussions with Bert Brenner, of the Sigmund Cohn Corp., are acknowledged, and the cooperation of that concern in supplying the samples of platinum for these experiments is much appreciated.

5. References

[1] H. F. Stimson, The International Temperature Scale of 1948, J. Research NBS **42,** 209 (1949) RP1962.
[2] E. M. Wise and R. F. Vines, Effect of cold-work upon hardness and recrystallizing behavior of pure platinum, Trans. Am. Inst. Min. Met. Eng. **137,** 464 (1940).
[3] G. Tammann and K. L. Dreyer, Ann. Phys. [5] **16,** 111 (1933).
[4] G. Tammann and G. Bandel, Ann. Phys. [5] **16,** 120 (1933).
[5] O. Feussner, Metallwirtschaft **7,** 470 (1928); see also, R. F. Vines, The platinum metals and their alloys, p. 31 (The International Nickel Co., Inc., New York, N. Y., 1941).
[6] Wm. F. Roeser and H. T. Wensel, Methods of testing thermocouples and thermocouple materials, J. Research NBS **14,** 253 (1935) RP768; also Temperature, its measurement and control in science and industry, p. 289 (Reinhold Publishing Corp., New York, N. Y., 1941).
[7] Bert Brenner, Changes in platinum thermocouples due to oxidation, chapter in Temperature, its measurement and control in science and industry, p. 1281 (Reinhold Pub. Corp., New York, N. Y., 1941).
[8] W. Matthiessen and C. Vogt, Pogg. Ann. **122,** 47 (1864).
[9] See for example, H. H. Uhlig, ed., Corrosion Handbook, p. 700 (John Wiley & Sons, Inc., New York, N. Y., 1948).
[10] H. A. Jones, I. Langmuir, and G. M. J. Mackay, Phys. Rev. **30,** 201 (1927).
[11] A. Krupkowski and M. Balicki, Rev. de Metallurgie, Memoires **36,** 21 (1939).
[12] M. Balicki, J. Iron & Steel Inst. **151,** 181 (1945).
[13] G. W. Brindley, Report of a Conference on Strength of Solids, p. 95 published by The Physical Society, London (1948).
[14] M. Cook and T. Ll. Richards, J. Inst. Metals **73,** 1, and discussion p. 705 (1946).

Washington, November 29, 1950.

Journal of Research of the National Bureau of Standards Vol. 47, No. 2, August 1951 Research Paper 2233

Potential and Current Requirements for the Cathodic Protection of Steel in Soils

W. J. Schwerdtfeger and O. N. McDorman

Potentials of steel in 20 air-free soils varying in pH from 2.9 to 9.6 were determined in the laboratory. These data and the potential-pH relation for the hydrogen electrode were used in fixing the optimum potential for the cathodic protection of the steel against corrosion. The effectiveness of this potential for the cathodic protection of steel in soils was confirmed by weight-loss measurements on electrodes that were maintained at the selected potential in five corrosive soils. Cathodic polarization curves are interpreted in terms of the potential and current requirements for the cathodic protection of steel in soils.

1. Introduction

Cathodic protection of underground steel structures usually is accomplished by applying direct current of such magnitude that the structure assumes a certain potential with respect to a standard reference electrode. Experience with piping systems has indicated that the optimum potential for this protection is approximately −0.85 v referred to a copper-copper sulfate electrode [1].[1] As potentials are measured while the applied current is flowing, an indefinite IR drop between the reference electrode and the electrical boundary of the corrosion circuits may be included. Consequently, the true potential of the corroding surface is not known. Although underground structures maintained at this potential are probably not materially affected by corrosion, the theoretical and experimental basis for −0.85 v as applicable to all soil environments has never been stated.

By applying electrical theory to the behavior of galvanic couples, Mears and Brown [2] deduced that cathodic protection is achieved when the potentials of the local cathodes are brought by polarization to the open-circuit potential of the most anodic element. In soils, differences in potential exist on the surface of buried steel structures, in effect forming galvanic couples. The problem then is that of determining a critical potential generally applicable to steel in soils.

The concentration of ferrous ions in equilibrium with iron in water is very small in the alkaline range [3, 4, 5]. Gatty and Spooner [6] cite references indicating that the potential of iron in air-free solutions is a function of the hydrogen-ion concentration of the solution, the potential increasing in the anodic direction with increasing values of pH. Consequently, it appears that the rate of corrosion of iron in a solution may be reduced to a negligible value by polarizing the surface of the metal to a potential corresponding to a pH value at which the concentration of ferrous ions is small. Although no exact relation would be expected between the potential of iron and hydrogen-ion concentration in air-free soils differing widely in composition, an approximate evaluation of the critical potential at which iron would be subject to negligible corrosion appears feasible. This requirement for cathodic protection may be subjected to experimental verification by maintaining weighed electrodes exposed to normal corrosion in soils at the selected potential for a considerable period of time.

[1] Figures in brackets indicate the literature references at the end of this paper.

2. Potential of Steel in Air-free Soils

Potentials of steel electrodes[2] were measured in 20 air-free soils ranging in pH from 2.9 to 9.6 and in resistivity from 60 to 17,800 ohm-cm. Each soil was finely ground and saturated with water, and then mechanically worked and carefully packed into a Lucite cylinder 1.75 in. (45 mm) inside diameter by 2 in. (51 mm) long. The steel electrode was a disk 1.73 in. (44 mm) in diameter by 0.125 in. (3.2 mm) thick with machined surfaces. One surface of the disk after degreasing was scratched with 1G French emery paper. With this surface adjacent to the soil at one end of the cylinder while the other end rested on a flat surface, the disk was manually pressed with an oscillatory motion until the soil began to ooze out around the edge, indicating that good contact between steel and soil had been secured. After removing the excess soil from the edge of the disk and cylinder, molten asphalt was applied around the edge of the disk to hold it and to serve as an air seal. A circular piece of No. 16 mesh stainless steel screen with a 0.25-in. (6.4-mm) hole in the center was pressed against the soil at the other end of the cylinder. Then molten asphalt was applied over this entire area excepting the hole, which permitted release of the soil pressure and served as an area of contact for the reference electrode. The soil cells were individually confined in a water-saturated atmosphere and removed only for such time as was required for daily potential measurements which were made with a potentiometer. The

[2] Composition of steel in percent: 0.23 C, 0.58 Mn, 0.008 P, 0.025 S, 0.095 Si, 0.077 Cu.

potentials of triplicate cells became relatively steady and varied less than ±5 mv, indicating that oxygen had been effectively excluded or consumed by corrosion. Stabilization at the most anodic potentials occurred within a period of 10 days.

The values of the potentials of the steel electrodes in the different air-free soils versus the pH values of the corresponding soils are shown in figure 1. Each point represents the average of four potential measurements made on as many consecutive days after stabilization of the electrodes. The rather wide dispersion of the values for soils having approximately the same hydrogen-ion concentration results from the fact that the potential of steel in aqueous electrolytes is determined by the composition, as well as by the hydrogen-ion concentration of the electrolyte. The curve is similar to curves representing the potential of iron as a function of hydrogen-ion concentration in different aqueous electrolytes [6]. In fact, it may be considered as a composite of the potential-pH curves for different salt solutions reported in the literature.

Corey and Finnegan [5] report that the hydrogen-ion concentration of waters in which iron is in equilibrium with ferrous hydroxide is between 8.3 and 9.6, depending on the composition of the waters and other factors. Since the curve in figure 1 is a composite for various soils it would be reasonable to select a critical potential based on the average pH value reported in the literature, such as pH 9. It will also be observed in figure 1 that at this value the potential curve for the standard hydrogen electrode at atmospheric pressure intersects the potential curve for steel. According to Holler [7] corrosion is reduced to a negligible amount at this point, since there is no difference of potential between the hydrogen and steel electrodes. The potential at this intersection, approximately −0.77 v, therefore is considered as the protective potential. (This potential is equivalent to −0.53 v. on the standard hydrogen scale).

3. Properties of the Soils Used in the Study of Cathodic Protection

The samples of soil for the study of cathodic protection were taken from five of the National Bureau of Standards soil-corrosion test sites. The soils vary considerably with respect to their physical properties and the composition of the water-soluble matter (table 1). All of these soils are severely corrosive toward ferrous metals, as is evidenced by their low resistivities. Specimens of 1.5-in. (38-mm) steel pipe of standard wall thickness 0.145 in. (3.7 mm) were perforated within 8 years in soil No. 64.

4. Experimental Methods

The experimental corrosion cell in which the test electrode [3] was subjected to corrosion by differential aeration is shown in figure 2. The cell was made

[3] See footnote 2 for composition.

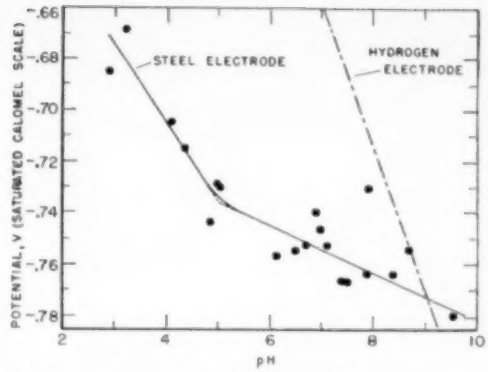

FIGURE 1. *Relation between the potential of steel in air-free soils and the* pH *values of the soils*

up with four Lucite sections. Differential aeration was accomplished by puddling half the soil of the top section and wetting the other half under a suction of 30 cm of mercury. The soil of the other three sections also was moistened under suction. The suction apparatus consisted of flasks fitted with buckner funnels of the fritted-glass type. After packing the puddled soil into one-half of the top section, the four sections were set up inside the funnels. Dry soil, previously passed through a No. 20 mesh sieve was packed into each section. Water dispensers that provided for uniform distribution of distilled water were set up over the dry soil of each section. The rate of moistening the soil was controlled by the degree of suction and by the characteristics of the soil. The perforated steel electrode (fig. 2) was the auxiliary anode, the perforations permitting air to pass through to the test electrode from the bottom of the cell. The stainless steel screen kept the soil intact. The component parts were held together by asphalt, which also served as a sealer. The

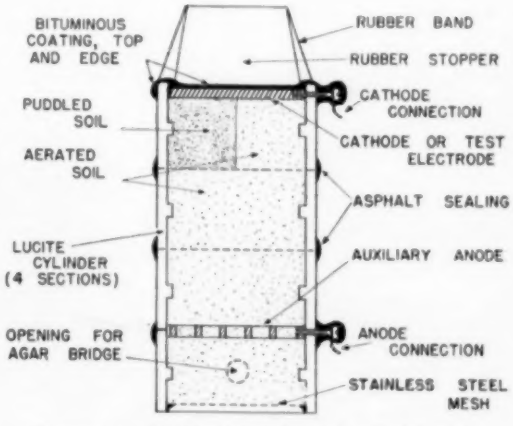

FIGURE 2. *Details of experimental corrosion cell.*

TABLE 1. *Properties of the soils*

Soil			pH	Resistivity at 60° F	Aeration [b]	Total acidity (Mg-eq/100 g of soil) [c]	Composition of water extract—milligram equivalents per 100 g of soil					
Number [a]	Type	Location of test site					Na+K as Na	Ca	Mg	CO_3	HCO_3	Cl	SO_4
				Ohm-cm									
13	Hanford very fine sandy loam	Bakersfield, Calif	9.5	280	G	A	6.23	0.09	0.13	0.00	1.12	1.64	3.76
60	Riffe peat	Plymouth, Ohio	2.9	218	P	297.4	2.91	10.95	2.86	.00	0.00	0.00	56.70
64	Docas clay	Cholame, Calif	7.9	62	F	A	28.10	2.29	0.76	.00	.80	28.80	0.26
78	Caddo fine sandy loam	Latex, Tex	4.5	821	P	24.0	1.06	0.18	.31	.00	.00	0.82	.74
79	Tidal marsh	Freeport, Tex	7.9	324	P	A	6.22	.40	.31	.00	3.42	2.99	1.01

[a] Soil number also refers to site number as specified in Bureau soil-corrosion tests.
[b] Aeration of soils: G, good; F, fair; P, poor.
[c] A indicates absence of acidity because of alkaline reaction.

rubber band placed longitudinally around the cell applied pressure to the test electrode through the rubber stopper. Since the asphalt was pliable, this pressure assured contact between steel and soil. The only part of the test electrode subject to corrosion was the machined surface adjacent to the soil. The surface was prepared by degreasing and scratching with 1G French emery paper. The edge and top side were coated with a bitumastic compound. Electric connections to the electrodes were made through steel screws that had wires soldered to the heads. Potential measurements were made through an agar bridge at the lower side of the cell. The cell was stored in a friction top can containing a small quantity of water to keep the air saturated with moisture. The cell was placed above the water level and was not removed for the duration of the study. Wires from the electrodes were brought through holes in the side of the can. The can also was fitted with a hole for insertion of the agar bridge. When potential measurements were not being made, the bridge was removed and the hole was sealed.

Each cathodic protection test was of 60-days duration. Several cells were assembled with each soil, and cells for any one soil were operated concurrently. The corrosion rates in such a group of cells were reproducible within a standard error of about 8 percent. All the cells were permitted to react freely for a period of approximately 48 hours before applying protective currents. The weight losses that occurred during this period were calculated from cathodic and anodic polarization curves such as described by Holler [7] and Pearson [8]. The cathodic polarization curves also are interpreted in connection with the current required for protection, to be discussed later. Cathodic polarization data obtained at the conclusion of the 60-day period were similarly plotted. In obtaining the data it was found necessary to apply approximately equal increments of current at regular intervals. An arbitrary interval of 3 minutes was used.

Dry cells (1.5 v) were used as a source of external power. The test electrode (cathode) was maintained at the desired potential by applying a constant voltage between the cathode and the auxiliary anode. The voltage was obtained from a variable voltage divider connected across the dry cell. The voltage was adjusted to provide the required current, which was measured with a zero-resistance milliammeter. Thus, the amount of current flowing to the cathode depended on the potential of that electrode. A change in chemical polarization of the cathode affected the applied current in such a way so as to oppose that change. The auxiliary anode was comparatively unaffected by anodic polarization at the desired current, and the cell resistance was relatively constant. Current and potential measurements were made approximately every 48 hours. The protective potential, in general, was maintained within ± 15 mv. All potential measurements were made by the Hickling interrupter method as adapted for use with soils [9].

5. Protection Obtained by Maintaining a Fixed Potential

The degree of cathodic protection that was obtained by maintaining the potential of the cathode at -0.77 v with respect to the saturated calomel electrode is indicated by the weight losses given in table 2. The weight losses of the cathodes attributable to the freely corroding period have been deducted from the losses shown in the table. Because the potentials of nearly all the cathodes departed more or less from the critical potential of -0.77 v for different periods of time, the extent of the departures with respect to potential and time are given in table 2. It will be observed that the weight losses of the cathodes in all the soils are small compared with the weight losses of the controls, especially of those cathodes whose potential deviated little, if at all, from -0.77 v. As may be expected, the results summarized in table 2 show that larger weight losses for any given soil are associated with the greater deviations less negative than the critical potential (-0.77 v). Figures 3 and 4 show some of the cathodes and their corresponding controls for which data are included in table 2. Some of the corrosion shown in the photographs of the protected specimens of course occurred during the freely corroding period of 48 hours. The fact that corrosion was not completely prevented in any of the soils is consistent with the results of Mears and Bialosky [10] who reported small residual weight losses for cathodically protected specimens. These investi-

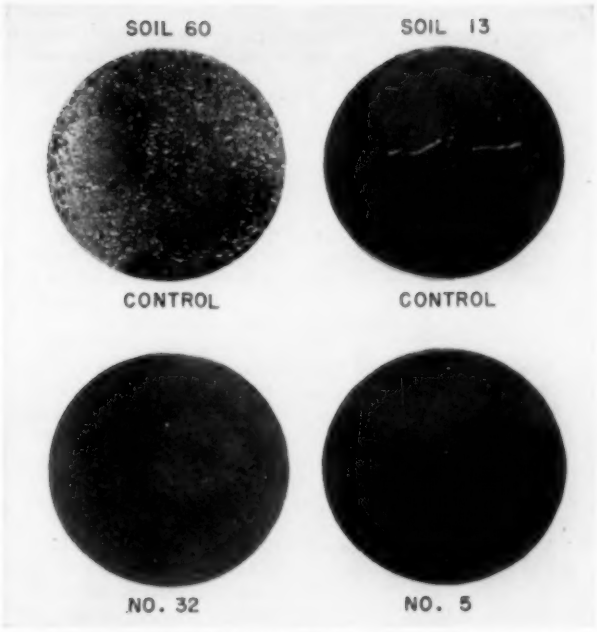

FIGURE 3. *Unprotected (control) and protected steel electrodes in soil 60* (pH *2.9*) *and soil 13* (pH *9.5*)—*exposure 60 days.*

Protected cathodes 32 (soil 60) and 5 (soil 13) were maintained at potential −0.77 v (saturated calomel scale) after 48 hr without protection.

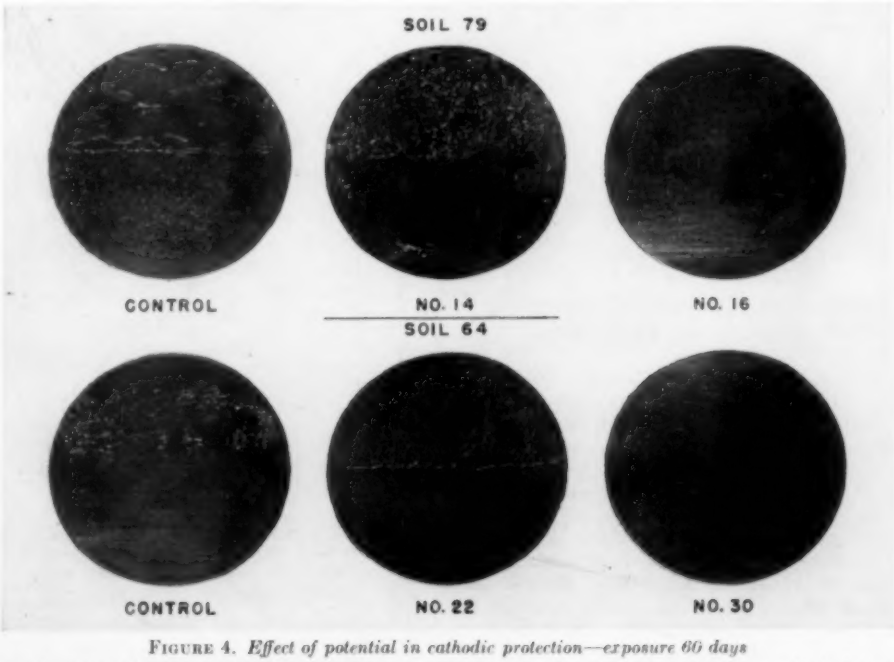

FIGURE 4. *Effect of potential in cathodic protection—exposure 60 days*

Partially protected cathodes 14 (soil 79) and 22 (soil 64) failed to polarize. Protected cathodes 16 (soil 79) and 30 (soil 64) were maintained at −0.77 v (saturated calomel scale) after 48 hr without protection.

gators attributed such losses to incomplete protection during the period before cathodic protection became wholly effective. The weight loss in soil 60 of a cathode having a somewhat different potential (−0.69 v) than the critical potential (−0.77 v) for 12 of the 60 days was 84 mg (table 2—cathode 1), while a change to only −0.75 v for 18 of the 60 days resulted in a weight loss of 40 mg (table 2—cathode 32). However, the weight loss accompanying a greatly increased potential (in a negative direction) to −1.0 v for almost the entire 60 days was 27 mg table 3—cathode 2), which is not materially less than that for cathode 32. These results indicate that corrosion cannot be entirely prevented and that −0.77 v is the approximate optimum protective potential.

This is in accord with Kuhn's statement that polarizing an iron structure to potentials greater than −0.85 v (ref. $Cu-CuSO_4$) represents wasted electric energy [1]. How much IR drop is included, if any, in the designated potential of −0.85 v cannot be definitely stated. (The value of −0.77 v referred to saturated calomel, which is free of IR drop outside of the electrical boundary, is equivalent to −0.85 v referred to a copper-copper sulfate reference electrode apart from any equivalent IR drop).

TABLE 2. *Weight losses of cathodes maintained at approximately −0.77 v (referred to saturated calomel) for 60 days*

Soil number	Cathode number	Weight loss of electrodes		Average potential of the cathodes during the period of departure from −0.77 v	
		Cathode	Control	Days of departure	Potential
		mg	*mg*		*v*
13	5	8	431	0	−0.77
64	30	6	196	5	.76
78	19	19	111	3	.75
60	32	40	519	18	.75
60	1	84	519	12	.69
79	16	19	364	7	.74
79	13	28	364	14	.69

6. Interpretation of Cathodic Polarization Curves in Cathodic Protection

Breaks in cathodic polarization curves have been interpreted by Ewing [11], Pearson [12], Denison and Romanoff [13], and Holler [7] in terms of the current and potential requirements for cathodic protection in soils. However, the data pertaining to significant changes in potential or current noted by these investigators have been based chiefly on theoretical considerations. Also, the effect of time on chemical polarization as related to critical current densities has received scant attention. Limitations of polarization curves in certain environments for determining the current required for cathodic protection have been pointed out by Mears and Bialosky [10]. These investigators concede that breaks in cathodic polarization curves have definite significance when the rate of corrosion is determined wholly by the cathode reaction (cathodic control). For the special condition that the observed potential of a corroding metal is the same as that of the anode on open-circuit the break in the curve indicates that the entire surface has become cathodic. However, under most natural environmental soil conditions, the potential of iron with respect to a standard reference electrode is considerably less negative than the potential of iron in the same environment with air excluded. For such natural conditions the significance of breaks in cathodic polarization curves with respect to cathodic protection is not so readily understood.

In a study of the polarizing characteristics of dissimilar metals, Brown and Mears [14] showed that breaks in a composite cathodic polarization curve of a series of metals connected together in an electrolyte coincided with the open-circuit potential of the more anodic metal. Hence, in a differential aeration cell, a break in the cathodic polarization curve would be expected to occur at the open-circuit potential of the anode. Experimental verification of this was obtained with a corrosion cell set up similar to those already described, except that the electrode was cut into equal segments that were separated to permit measurement of the cell current. Figure 5 illustrates the electrical relations that were observed. It will be noted that a change in the polarization rate occurred around the open-circuit potential of the

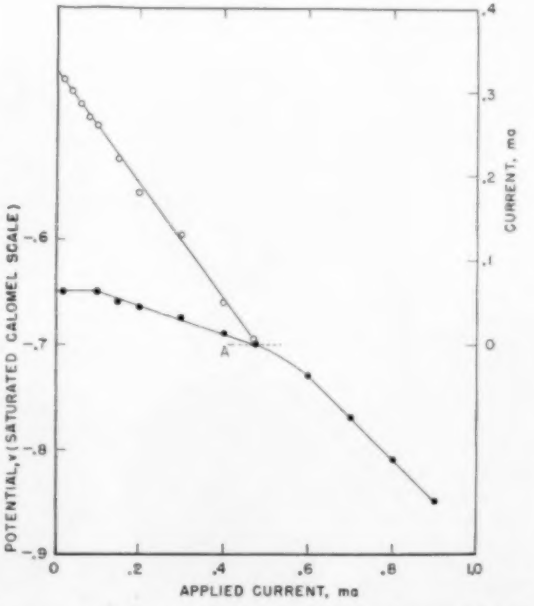

FIGURE 5. *Current and potential relations of separated steel electrodes in a differential-aeration cell during cathodic polarization.*

○, Cell current; ●, couple potential; A, open-circuit potential of anode = −0.70 v.

anode, namely, −0.70 v, at which potential the cell current was reduced to zero. Because the potential of −0.70 v was the average potential of a large number of local couples on the anode, polarizing the couple to this potential would not eliminate local couples whose potentials were greater (more negative) than −0.70 v. In order to effectively inhibit corrosion it would have been necessary to increase the potential of the experimental couple to −0.77 v.

Typical cathodic polarization curves obtained on the solid electrode of one of the experimental cells, plotted on both rectangular and semilogarithmic coordinates are shown in figure 6, a, and b, respectively. Two breaks are indicated in figure 6, a; point *A* corresponding to the average open-circuit potential of the anode of the cell, and point *B* corresponding to the beginning of the hydrogen-overvoltage portion of the curve. An approximation of the current indicated by *A* (fig. 6, a) is obtained from the semilogarithmic curve (fig. 6, b) by the intersection of the extended dashed straight-line portions of the curve. The straight-line part of the semilogarithmic curve at currents greater than the extrapolated value represents the hydrogen overvoltage. The beginning of the hydrogen-overvoltage curve does not always appear as a distinct break (*B*) in the rectangular plot but sometimes appears as a gradual decrease in the polarization rate. Although the current indicated by *A* (fig. 6, a) would not be sufficient initially to eliminate all local corrosion on the surface of an electrode it is reasonable to expect that the drift in potential caused by the continuous application of the current indicated by the break would be sufficient to polarize the surface to the protective potential and thereby to provide cathodic protection.

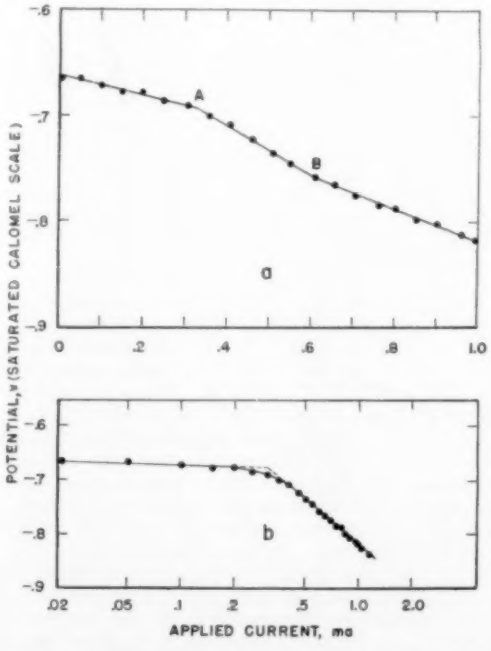

FIGURE 6. *Cathodic polarization curves of a single steel electrode in a differential-aeration cell, (a) plotted on rectangular coordinates, (b) on semilogarithmic coordinates.*

In order to determine the effectiveness of the current indicated by the break *A* (fig. 6, a) as a requirement for cathodic protection, corrosion cells were set up as described in section 4, and currents indicated by the breaks *A* in the cathodic polarization curves for the five soils studied were applied to the previously weighed cathodes. In four of the soils the cathode potentials drifted to the protective value of −0.77 v in from 3 to 21 days (table 3). The cathodes of two of these cells were allowed to drift to potentials greater than the protective potential, whereas the cathodes of the other two cells were maintained at −0.77 v. A comparison of weight losses of the cathodes with losses of the respective control electrodes (excepting in soil 64, which will be discussed later) shows that the degree of protection is good. The data for cathode 6 furnish additional evidence that polarization to a potential greater than −0.77 v produces no appreciable further reduction in weight loss. This will be noted by comparison with the data for cathode 5 in table 2, in which case no actual benefit is indicated. Cathode 2 has already been referred to in section 5 in this same connection.

The rapid drift in potential of cathodes 2, 21 and, 25 (table 3) to the protective value is consistent with the low weight losses of these electrodes. On the other hand, electrode 6, exposed to the very corrosive soil 13, lost negligible weight in spite of the fact that its average potential (−0.72 v) for 21 days was considerably less negative than the protective potential. This apparent anomaly is to be explained by the fact that local corrosion in soil 13 is generally negligible. The relative absence of local corrosion is well illustrated by comparing the photographs of the control electrodes (soils 13 and 60) in figure 3. However, even in alkaline and well aerated soils such as soil 13, the possibility of pitting cannot be ignored. Should air be totally excluded from the surface of steel in such soils, polarization to the protective potential would be required.

TABLE 3. *Potential changes and weight losses of cathodes receiving current indicated by the break in cathodic polarization curves—exposure 60 days*

Soil number	Cathode number	Weight loss of electrodes		Potential at the break	Average potential of the cathode[a]			
					Less than −0.77 v		Greater than −0.77 v	
		Cathode	Control		Days	Potential	Days	Potential
		mg	*mg*	*v*		*v*		*v*
78	21	5	111	−0.69	3	−0.74	57	[b] −0.77
79	25	14	364	.71	7	.75	53	[b] .77
60	2	27	519	.74	3	.76	57	1.00
13	6	9	431	.72	21	.72	39	1.50
64	22	119	196	.73	60	.68	0	------

[a] Potential referred to the saturated calomel half-cell.
[b] Current reduced to maintain potential indicated.

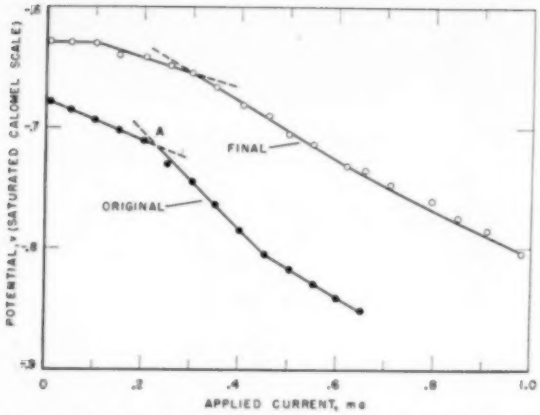

FIGURE 7. *Cathodic polarization curves of a steel cathode (22) in soil 64 before and after the application of external current A for 60 days.*

Protection was incomplete, as indicated by a weight loss of 119 mg and reoccurrence of a break in the final curve. Note: In four of the five soils tested the current at A was sufficient to polarize the cathode and provide protection.

The fact that the potential of cathode 22 (soil 64) did not drift to the protective potential during the period of the test is not an indication that the current corresponding to the break in the cathodic polarization curve is insufficient for cathodic protection. The failure of the potential of cathode 22 to reach the protective value is attributed to selecting the applied current before the maximum rate of corrosion developed. Therefore, the current applied for cathodic protection was insufficient. The increase in the corrosion rate of cathode 22 during the course of the test is shown by the fact that the break in the cathodic polarization curve obtained at the conclusion of the test indicated a greater current requirement than the curve obtained at the beginning (fig. 7).

In maintaining the cathodes in the five soils at the protective potential the effect of chemical polarization resulted in a reduction of the applied current (table 4). In four of the soils a steady value of current, indicated as the minimum in table 4, was reached in from 14 to 21 days after the current was initially applied. The reduction of current in the case of cathode 30 (table 4) although slight, occurred progressively over the 60-day period. Elimination of local couples by diffusion of alkali over the surface of this cathode progressed slowly because of the preponderance of soluble chloride in soil 64. It is probable that the applied current could have been reduced even more had the length of the test period been extended.

The average corrosion currents calculated from the weight losses of the control electrodes by the application of Faraday's law (table 4) indicate in most cases that the minimum current required for cathodic protection is about equal to the average current associated with corrosion. Thus, the high initial currents required for protection are partly attributable to the higher initial corrosion rates.

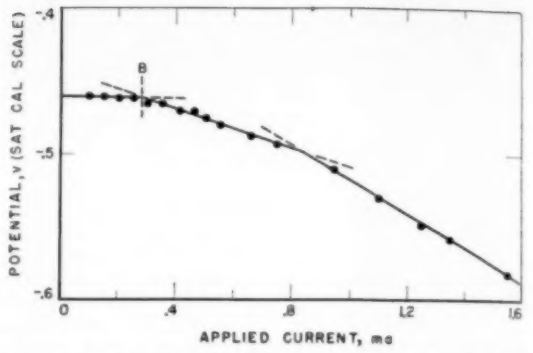

FIGURE 8. *Cathodic polarization curve of a steel cathode (8) in soil 13 before the application of protective current.*

B, Minimum protective current, which maintained a cathode potential of −0.77 v.

Denison and Romanoff studied the behavior of zinc-steel couples underground [13], and their results suggested that no more current is required for the cathodic protection of steel than that calculated by Faraday's law for loss in weight produced by normal corrosion.

TABLE 4. *Current required for cathodic protection—exposure 60 days*

Soil number	Cathode number	Weight loss of electrodes		Protective current applied to cathode [a]		Average current calculated from weight loss of control by Faraday's law	Current indicated by departure from relatively constant potential on original cathodic polarization curve of cathode
		Cathode	Control	Initial	Minimum		
		mg	*mg*	*ma*	*ma*	*ma*	*ma*
13	8	12	431	3.90	[b] 0.28	0.29	0.28
60	32	40	519	1.27	[b] .24	.35	.30
78	19	19	111	0.20	[b] .05	.07	.06
79	16	19	364	.88	[b] .24	.24	.16
64	30	6	196	.68	[c] .55	.13	.15

[a] Cathode maintained at −.77 v ±0.015 v (referred to saturated calomel).
[b] Minimum steady current after 14 to 21 days.
[c] Minimum current after a progressive decrease for 60 days.

At low values of applied current the potential of a corroding electrode is relatively constant (fig. 8). The currents at which the corresponding potentials depart from relatively constant values are given in the last column of table 4. For cathode 8 this value is shown at B in figure 8, which is characteristic of the curves used for obtaining the other values in the last column. In the case of the four cathodes that had stabilized after 21 days, there is fair agreement between the minimum current that actually maintained protection and the values in the last column. Apparently the point of departure on the initial cathodic polarization curve of the electrode potential from a relatively stable value, designates the applied current necessary to maintain a balance between the consumed and available oxygen after a cathodically protective alkaline film has been established on the electrode surface.

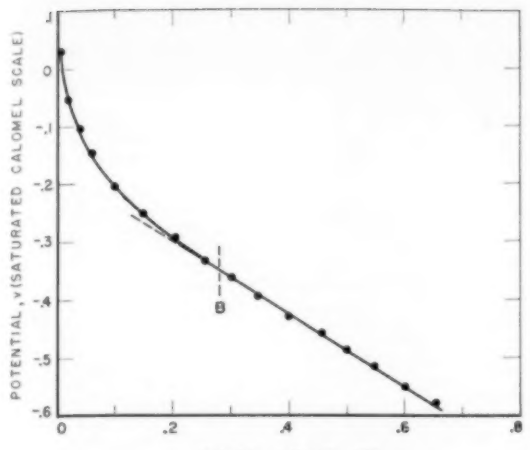

FIGURE 9. *Cathodic polarization curve of cathode 8 in soil 13 (see fig. 8) after the application of protective current for 60 days.*

B, Minimum protective current, which maintained a cathode potential of −0.77 v. Weight loss=12 mg.

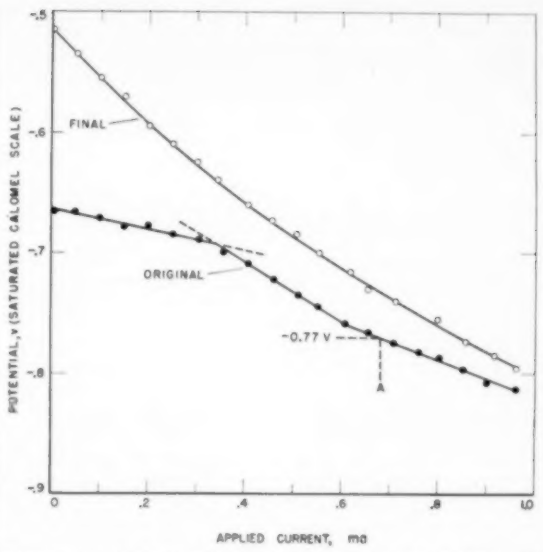

FIGURE 10. *Cathodic polarization curves of a steel cathode (30) in soil 64 before and after the application of protective current for 60 days.*

A, Current initially applied, subsequently varied, to maintain potential of −0.77 v. Weight loss=6 mg.

The close relation between the current required for protection and that associated with corrosion was probably applicable over the greater part of the 60-day period, therefore suggesting that initially applied currents smaller than those indicated would not have been sufficient for protection. Consequently, the minimum current finally required for cathodic protection must not be confused with the current initially required. To verify this statement additional cells were assembled with soils 78 and 79 and the respective minimum currents, as indicated by the departure of cathode potentials from relatively constant values on the original cathodic polarization curves, were applied to the electrodes for the duration of the 60-day test period. The weight losses of these electrodes were as large as the losses associated with the corresponding controls. The potential of the cathode in soil 78 remained substantially unchanged during the test period while the potential of the cathode in soil 79 actually became less negative. The cathode in soil 79 (No. 14), together with the corresponding control, is shown in figure 4. Field investigations in soils with pipe coupons show that a change in pipe potential to a more negative value is essential for a reduction in corrosion [15].

At the conclusion of the 60-day test period all cathodes were placed on open-circuit. After a period of about 15 hours, required for stabilization of the cathode potentials, a cathodic polarization curve again was obtained on each electrode. The curve for cathode 8 shown in figure 9, is typical of all the curves obtained on the completely protected electrodes. The noble potential on open-circuit is due to the formation of an oxide film on the electrode surface. The polarization curve shown in figure 9 is typical of a true cathode and, of course, reveals the absence of corrosion. It will be noted that, here again, *B* denotes the minimum current required for protection and that an inflection occurs at this point. It cannot be ascertained whether this inflection has any significance, because it was not apparent on the final curves for all protected specimens (fig. 10). Here again in figure 10, the absence of a break in the final curve is consistent with the negligible weight loss that occurred on cathode 30. The occurrence of a break, after having applied current for a period, shows that the current was insufficient for protection (fig. 7) or that a state of corrosion has been resumed. A photograph of cathode 22 on which the curves of figure 7 were obtained is shown in figure 4.

7. Summary

The cathodic protection of steel in five corrosive soils was investigated in the laboratory, using a specially designed differential-aeration cell.

The most significant requirement for cathodic protection was found to be the maintenance of a critical potential on the surface of the cathode. This potential, defined by the point of intersection of the potential-pH curve for steel in air-free soils and the potential-pH curve for the hydrogen electrode at atmospheric pressure, was approximately −0.77 v, referred to the saturated calomel electrode; or −0.53 v referred to the standard hydrogen electrode.

Electrodes maintained for 60 days at −0.77 v lost negligible weight under conditions that produced severe corrosion of unprotected electrodes simultaneously exposed in the same soils.

Referred to the copper-copper sulfate electrode, the protective potential is approximately −0.85 v, which is in agreement with the practice for cathodic protection used by many corrosion engineers, in those cases where the measurements are free of IR drop external to the electrical boundary of the corrosion circuit.

The current required to maintain the protective potential (−0.77 v) diminished to fairly stable values after about 3 weeks for four of the five soils tested. This limiting value of current, which just maintains the protective potential, differs for different soils. These limiting values were in good agreement with the average current associated with the normal rates of corrosion of the unprotected electrodes.

A characteristic break in the cathodic polarization curve for steel in soil is interpreted as indicating the minimum current initially required for cathodic protection. Although the electrode potential corresponding to this current may be considerably less negative than the protective potential, it was found that the potential generally drifted to the critical protective value before appreciable corrosion occurred.

Cathodic polarization curves obtained for protected electrodes at the conclusion of the test were similar to those obtained for insoluble electrodes, thereby indicating that cathodic protection had been achieved.

8. References

[1] Robert J. Kuhn, Proc. Am. Petroleum Inst. **14,** Sec. IV, 153 (Nov. 1933).
[2] R. B. Mears and R. H. Brown, Trans. Electrochem. Soc. **74,** 519 (1938).
[3] John R. Baylis, Ind. Eng. Chem. **18,** 370 (1926).
[4] K. Murata, J. Soc. Chem. Ind. (Japan) **35,** 532 (1932).
[5] Richard C. Corey and Thomas J. Finnegan, Proc. ASTM **39,** 1242 (1939).
[6] O. Gatty and E. C. R. Spooner, The electrode potential behavior of corroding metals in aqueous solutions p. 310 (Oxford University Press, London, 1938).
[7] H. D. Holler, J. Electrochem. Soc. **97,** 277 (Sept. 1950).
[8] J. M. Pearson, Trans. Electrochem. Soc. **81,** 485 (1942).
[9] Robert B. Darnielle, J. Research NBS **25,** 421 (1940) RP1336.
[10] R. B. Mears and J. M. Bialosky, Cathodic Protection Symposium, Electrochem. Soc. and Nat. Assn. Cor. Engrs. **37** (1949).
[11] Scott Ewing, Proc. Am. Gas Assn. 613 (1940).
[12] J. M. Pearson, Petroleum Engr. **15,** 6, 7, 8 (1944).
[13] Irving A. Denison and Melvin Romanoff, J. Research NBS **40,** 301 (1948) RP1876.
[14] R. H. Brown and R. B. Mears, Trans Electrochem. Soc. **81,** 455 (1942).
[15] D. Holsteyn, Elec. News (Petroleum Ind. Elec. Assn.) **13,** No. 3 (1943).

Washington, February 14, 1951.

urnal of Research of the National Bureau of Standards Vol. 47, No. 2, August 1951 Research Paper 2234

A Monte Carlo Method for Solving a Class of Integral Equations[1]

R. E. Cutkosky

This note describes a random walk equivalent to the Neumann series solution of an integral equation. A diffusion analogy and the problem of importance sampling are discussed briefly.

Certain types of matrices can be inverted by a Monte Carlo method that was devised by J. von Neumann and S. M. Ulam, and that appears in a paper written by G. E. Forsythe and R. A. Leibler.[2] In the following it is shown that this method, when suitably generalized, can be used to approximate the Neumann series solution of an integral equation. This procedure is then shown to be similar to those used to solve certain problems dealing with scattering of particles, which can be formulated in terms of a nonhomogeneous integral equation, and which have been described by Herman Kahn.[3]

We wish to solve the following equation for $\phi(x)$

$$\phi(x)=f(x)+\lambda\int_a^b K(x,y)\phi(y)\,dy, \tag{1}$$

where we assume, for convenience, that $K(x,y)$ is uniformly continuous and a and b are finite. A formal solution of (1), which is valid if λ is smaller in absolute value than the eigenvalue of the corresponding homogeneous equation, which is smallest in absolute value, is given by Neumann's series [4]

$$\phi(x)=f(x)+\lambda\int_a^b K(x,y)f(y)dy$$

$$+\lambda^2\int_a^b K^{(2)}(x,y)f(y)\,dy+\cdots, \tag{2}$$

where

$$K^{(n)}(x,y)=\int_a^b K^{(n-1)}(x,\xi)K(\xi,y)d\xi.$$

We may write this as

$$\phi(x)=f(x)+\lambda\int_a^b L(x,y)f(y)\,dy,$$

where

$$L(x,y)=K(x,y)+\lambda K^{(2)}(x,y)+\lambda^2K^{(3)}(x,y)+\cdots.$$

We need consider hereafter only the series (2)—if we wish to obtain the resolvent kernel L, we may use the fact that L satisfies the following equation

$$L(x,y)=K(x,y)+\lambda\int_a^b K(x,\xi)L(\xi,y)\,d\xi.$$

The series (2) can be evaluated by a Monte Carlo procedure consisting of two steps: first, a random process by which a particular term of the series is selected, and second, a random process by which the multiple integral defining the term selected is approximated (see footnote 3). This, when multiplied by a suitable weighting factor, will provide an estimate of the value of $\phi(x)$ for a particular x. We notice, however, that in series (2) each term is obtained by a simple operation on the preceding one, and this allows us to construct a simple random walk for approximating (2).

This random walk is defined by a sequence of functions $P_n(x,y)$, defined for $a\leqq x\leqq b$, $a\leqq y\leqq b$, and $n=0, 1, 2, \ldots$, where $P_n(x,y)>0$ and

$$\int_a^b P_n(x,y)\,dy<1-\delta,\quad \delta>0.$$

In terms of this sequence we also define

$$V_n(x,y)=\frac{\lambda K(x,y)}{P_n(z,y)},$$

and

$$p_n(x)=1-\int_a^b P_n(x,y)\,dy.$$

In addition, we must also require that $|\lambda|$ be smaller than the smallest eigenvalue of $K'(x,y)=|K(x,y)|$. To estimate $\phi(x)$, we start a random walk at the point x of the interval (a,b). With a probability density given by $P_0(x,x_1)$ we jump to the point x_1, or we stop the random walk, with probability $p_0(x)$. Suppose that we have made k jumps, and have reached the point x_k. Then with probability density $P_k(x_k,x_{k+1})$ we jump to the point x_{k+1}, or we stop the random walk with probability $p_k(x_k)$. If our random walk has traversed the path $\gamma: x\to x_1\to\ \ldots\ \to x_{k-1}\to x_k$, stopping at x_k, we define

$$V(\gamma/x)=V_0(x,x_1)\ \ldots\ V_{k-1}(x_{k-1},x_k)\,\frac{f(x_k)}{p_k(x)}, \tag{3}$$

and use $V(\gamma/x)$ as an estimate of $\phi(x)$. The expecta-

[1] The preparation of this paper was sponsored (in part) by the Office of Naval Research.

[2] G. E. Forsythe and R. A. Leibler, Matrix inversion by a Monte Carlo method, MTAC 4, No. 31, p. 127 (July 1950).

[3] Herman Kahn, RAND Corp. Report R-163, Stochastic attenuation analysis (June 14, 1949).

[4] R. Courant and D. Hilbert, Methoden der Mathematischen Physik (J. Springer, Berlin, 1924-36).

tion of $V(\gamma/x)$ is defined by

$$E(V(\gamma/x))=\int_{A_{11\gamma}} V(\gamma/x)\,dP(\gamma/x). \tag{4}$$

Since the probabilities used at each step are conditional probabilities, the probability measure defined in the space of paths with exactly k steps is given by

$$dP(\gamma/x)=P_0(x,x_1)\ \ldots\ P_{k-1}(x_{k-1},x_k)p_k(x_k)dx_1\ \ldots\ dx_k, \tag{5}$$

and thus the integral (4) can be represented by a sum of integrals, the kth of which corresponds to those γ with k steps. In this way we obtain

$$\begin{aligned}E(V(\gamma/x))&=f(x)+\lambda\int_a^b K(x,x_1)f(x_1)\,dx_1\\&\quad+\gamma^2\int_a^b\int_a^b K(x,x_1)K(x_1,x_2)f(x_2)dx_1dx_2+\ldots\\&=\phi(x),\end{aligned} \tag{6}$$

which proves that $V(\gamma/x)$ is an unbiased estimate of $\phi(x)$. Because of the condition on γ, the above integrals and series are absolutely convergent.

Similarly we obtain for the nth moment of the $V(\gamma/x)$, (assuming the nth moment exists),

$$\left.\begin{aligned}\nu_n(x)=E(V^n(\gamma/x))&=\frac{f^n(x)}{P_0^{n-1}(x)}+\lambda\int_a^b K(x,x_1)V_0^{n-1}(x,x_1)\,\frac{f^n(x_1)}{P_1^{n-1}(x_1)}\,dx_1\\&+\lambda^2\int_a^b K(x,x_1)K(x_1,x_2)V_0^{n-1}(x,x_1)V_0^{n-1}(x_1,x_2)\,\frac{f^n(x_2)}{P_2^{n-1}(x_2)}\,dx_2\,dx_1\\&+\cdots.\end{aligned}\right\} \tag{7}$$

In the particular case that $P_n(x,y)$ is independent of n, that is the probabilities depend only on where we are, and not on how many steps we have taken, (7) reduces to a rather simple form. In fact, if we define $K_n(x,y)=K(x,y)V^{n-1}(x,y)$ the nth moment satisfies the following equation

$$\nu_n(x)=\frac{f^n(x)}{p^{n-1}(x)}+\lambda\int_a^b K_n(x,y)\nu_n(y)\,dy, \tag{8}$$

(assuming $|\lambda|$ is sufficiently small).

Let us now turn our attention briefly to the problem of finding a set of functions $P_n(x,y)$ such that the variance of the estimate of $\phi(x)$ will be as small as possible. We might expect that if we knew $\phi(x)$ we could find a Monte Carlo procedure that would give us the correct answer with probability 1 (see footnote 3). It is convenient to use an argument based on the two-step method mentioned earlier. In the series (2) denote the nth term by $I_n(x)$. Our Monte Carlo process gives us a set of functions $P(n,x)$ and $v(n,x)$; where $P(n,x)v(n,x)=I_n(x)$, and $P(n,x)$ is the probability of taking exactly n steps if we start at the point x. Referring to (5), we see that

$$P(n,x)=\int_a^b\cdots\int_a^b P_0(x,x_1)\cdots P_{n-1}(x_{n-1},x_n)P_n(x_n)\,dx_1\cdots dx_n.$$

We would like to choose $P(n,x)$ so that $P(n,x)=I_n(x)/\phi(x)$, as then $v(n,x)=\phi(x)$. To estimate $I_n(x)$ correctly with probability 1, we must have $K(x,y)$ and $f(x)$ non-negative, as we cannot allow negative probabilities. It may be convenient to introduce a sequence $\{U_n(x)\}$, which has a known sum $S(x)$, and estimate $\phi(x)+S(x)$ by the quantity $v^*(n,x)=v(n,x)+U_n(x)/P(n,x)$.

The above discussion is of course of little more than academic interest, but it gives an insight into the problems involved in minimizing the variance of the estimate. One thing we notice in particular is that the optimum choice of the sequence $\{P_n(x,y)\}$ will depend, in general, on the point x at which we wish to find ϕ.

As promised in the introduction, this method can be shown equivalent to Monte Carlo techniques often used to solve problems formulated in a different manner. Suppose we consider the problem, important in certain applications, of the diffusion of the neutrons through a thick slab of scattering material. Let the slab lie between the planes $x=0$ and $x=a$. Let $f(E,\theta,\phi,x)$ give the number of neutrons incident with energy E, at an angle given by θ and ϕ, which make their first collision at a distance x from the front of the slab. Let $K(E',\theta',\phi',x',E,\theta,\phi,x)$ give the probability that a neutron that makes a collision a distance x from the front of the slab, and has an initial energy E and an initial direction of travel (θ,ϕ), will proceed in the direction (θ',ϕ'), have energy E', and make its next collision at a distance x' from the front. A collision at $x>a$ corresponds to a neutron passing through the slab, and a collision at $x<0$ corresponds to a neutron reflected back, which we assume stops the process. Let $\psi(E,\theta,\phi)$ give the number of neutrons

that penetrate the slab with energy E, and have the direction of motion θ, ϕ.
Then clearly

$$\psi(E,\theta,\phi)=\int_a^\infty f(E,\theta,\phi,x)dx$$
$$+\int_{x=a}^{x=\infty}\int_{x'=0}^{x'=a}\int_{E',\theta',\phi'}K(E,\theta,\phi,x,E',\theta',\phi',x')$$
$$\cdot f(E',\theta',\phi',x')dE'd\theta'd\phi'dx'dx \qquad (9)$$

+higher terms representing multiple collisions. This is very similar to equation (2).

The usual Monte Carlo method for evaluating (9) is to consider a randomly selected incident particle and trace its path thru the slab, using some chance device to determine the result of a collision (see footnote 3). The method we have found for evaluating series (2) corresponds to choosing a particular particle that has penetrated the slab, tracing its path backward thru the slab, and then multiplying by the density of particles that have the same entrance characteristics. Although both the position of the particle making the random walk and its final weight must be remembered from step to step, only the final weight is needed for the answer in our method, while in the other both the final position and final weight are needed, and a histogram must be plotted. Thus if an answer is desired for only a few points, our method may be simpler.

Los Angeles, August 16, 1950.

Journal of Research of the National Bureau of Standards Vol. 47, No. 2, August 1951 Research Paper 2235

Study of Degradation of Polystyrene, Using Infrared Spectrophotometry

Bernard G. Achhammer, Mary Jane Reiney, and Frank W. Reinhart

Since polystyrene is a widely used plastic and styrene is an integral part of the most widely used synthetic rubber (GR–S), it appears necessary to know something of the process of degradation of polystyrene to assist in interpreting the degradation of these materials in service. Polystyrene films were exposed to heat at 100° C in a forced-draft air oven and to ultraviolet radiant energy at 60° C in air. Chemical structural changes in the polymer as a result of these treatments were analyzed by study of the infrared spectra between 2 and 16 microns, obtained with a Baird recording infrared spectrophotometer. Ultraviolet exposure for 200 hours resulted in absorptions at 2.9 and 5.8 microns, which are attributed to hydroxyl and carbonyl groups, respectively. Heating of the film for 270 hours at 100° C produced no significant change in the infrared spectrum. Prolonged heating at 125° C resulted in the destruction of the films by flow. The literature and theory on the degradation of polystyrene are discussed. Several mechanisms are postulated to account for the production of hydroxyl and carbonyl products in the polymer.

1. Introduction

The hydroperoxide theory of the oxidation of olefinic systems, which resulted from studies by Farmer and his coworkers [1, 2, 3],[1] has led to various attempts to explain the oxidation and degradation of polymeric materials with related chemical structure [4 to 7]. According to this theory, hydroperoxidation occurs on the carbon atom alpha to the double bond. Although the complex decomposition of hydroperoxides with heat and light is not understood completely, it is thought that the hydroperoxide is converted to hydroxyl and there is some evidence that carbonyl may also be formed [5, 8]. Cole and Field [8] have applied these theories to the oxidation of butadiene-styrene copolymers and other elastomers and have suggested that the formation of carbonyl and hydroxyl absorptions in the infrared spectra, which they found, is a result of the breakdown of hydroperoxides. Work in this laboratory has verified that hydroxyl and carbonyl absorptions occur in the infrared spectra of butadiene-styrene copolymer (75:25) as a result of exposure at 100° C in an air oven and to ultraviolet radiant energy at 60° C in air.

Since polystyrene is a widely used plastic and styrene is also an integral part of butadiene-styrene elastomeric copolymers, it appears necessary to know something of the mechanism of the oxidation of polystyrene to assist in interpreting the degradation in service of this plastic and of the synthetic rubber-like materials containing styrene.

The following structure is generally accepted and thermodynamically likely as predominant in polystyrene:

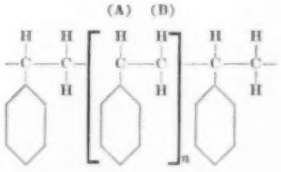

where n determines the molecular weight of the particular polystyrene and is dependent on the conditions of polymerization. This gives polystyrene a relatively simple chemical structure to be considered in regard to degradation. The components of the chemical structure may be divided into three parts: (1) The benzene ring, (2) the tertiary carbon atom bearing a single hydrogen atom (A) and attached to the benzene ring, and (3) the methylene connecting bridges in which the secondary carbon atom holds two hydrogen atoms (B).

It is generally agreed that the C—H bond energy values are in the order primary greater than secondary greater than tertiary. The C—H bond energy is reduced when the hydrogen atom is attached to a carbon atom adjacent to a double bond [9]. From oxidation studies on simple hydrocarbons, it appears that a hydroperoxide group is likely to be formed at site (A).

Staudinger and Steinhofer [10] showed that the unsaturated di- and tri- styrene fractions obtained on high vacuum distillation of polystyrene were oxidized by glacial acetic acid containing chromic trioxide with the formation of ketones of the following type:

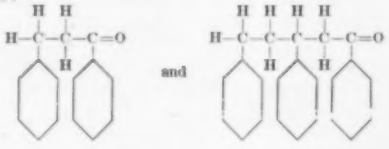

[1] Figures in brackets indicate the literature references at the end of this paper.

linek [11] suggested that the results of thermal gradation of polystyrene in the presence of oxygen dicate that a hydroperoxide mechanism may be sponsible for the degradation. Although the infrared absorption spectrum of polystyrene is available in the literature [12, 13], infrared techniques have apparently not been used to follow the degradation of polystyrene.[2]

In the investigation described in this report polystyrene films were exposed in the presence of air to heat and to ultraviolet radiant energy and changes in the chemical structure of the polymer as a result of the treatments were detected by infrared spectrophotometry. Infrared analysis is suitable for this study since both the hydroxyl and carbonyl groups, which might be expected on oxidative degradation, have strong absorptions in the infrared region and are known to occur at approximately 3μ and 5.7 to 6.0μ, respectively, [14, 15]. The hydroxyl and carbonyl groups may be situated independently on the polymer molecule or be adjacent to each other as in carboxyl groups.

2. Materials

The samples of polystyrene studied are described in table 1. Samples A, B, C, D, E, E1, and G1 are commercial resins that do not contain any compounding ingredients. These samples were not subjected to any purification procedures but were used as received.

TABLE 1. *Description of samples of polystyrene*

Sample designation	Approximate molecular weight [a]	Average oxygen content [b]
		Percent
A	295,000	0.048
B	340,000	.096
C	290,000	.064
D	370,000	.033
E	360,000	.26
E1	290,000	.27
G1	230,000	.12
[c] X	[d] 230,000	.11

[a] Weight average molecular weight as determined by light scattering (unpublished work of William A. Crouse).

[b] The oxygen content was determined by the direct method of Walton, McCulloch, and Smith (W. W. Walton, F. W. McCulloch, and W. H. Smith, Determination of small amounts of oxygen in organic compounds, J. Research NBS **40**, 443 (1948) RP1889). The samples were dried in a stream of purified helium at 100° C for 16 hr before being analyzed.

[c] The molecular weight and oxygen content were determined after purification. The oxygen content before purification was 0.13%.

[d] Number average molecular weight as determined by osmotic pressure (unpublished work of Guy A. Hanks).

The sample designated X was prepared by polymerizing purified monomer without catalyst or solvents in a nitrogen atmosphere at 120° C for 48 hr. It was subjected to the following purification prior to use: The sample was dissolved in benzene and precipitated with methanol, and the liquid was decanted. This treatment was repeated. The twice-precipitated material was dissolved in benzene and the solution frozen. The benzene was removed with a vacuum pump while the frozen mixture was slowly brought to 24° C. The light fluffy sample was kept under vacuum while being raised to 60° C and finally held there for 24 hr to remove essentially all the volatile materials. The sample was then stored in a dark glass bottle until used. This procedure was designed to remove impurities, low molecular weight polymer, and monomer. Other studies showed that the dried product contained less than 1 percent of benzene. Although the purified sample X was considered to be polystyrene hydrocarbon, it is evident from the data shown in table 1 that some oxygen is incorporated in the polymer molecules in spite of the precautions taken to exclude it.

Samples C, E1, and X were studied more extensively than the others. Samples C and E1 are representative of the two types into which the commercial samples can be classed according to their infrared absorption spectra. Sample C is representative of samples A, B, C, D, and G1. Samples E and E1 are similar.

3. Film Preparation

Films of various thicknesses ranging from 0.0009 to 0.010 in. were made for the tests. The thinner films were made from 5- and 10-percent solutions of the sample in distilled toluene or benzene. The solution was poured on a clean, level piece of plate glass and spread to an even thickness with a doctor blade. A dust shield was placed above the solution, and the film was allowed to form in air. When the film was dry, the plate was immersed in water and the film floated from it. In most cases the film was then dried in a vacuum chamber for about 8 hr followed by exposure to the room atmosphere until used.

The thicker films were made from 15-percent or more concentrated solutions of the samples in distilled solvent. The amount of solution necessary to form a film of the desired thickness was poured into a brass ring which was laid on a clean, level piece of plate glass. A dust shield was placed above the solution in the ring and the film allowed to form in air. Slower drying was necessary for uniform film formation when highly volatile methyl ethyl ketone was used and, therefore, the whole assembly was placed in a desiccator with two outlets open to the air. When the film was dry, the plate was immersed in water, the ring jarred loose from the plate, and the film floated from the plate. The film was then dried in a vacuum chamber for about 8 hr and stored in air until used. Nevertheless, some solvent remained in the film resulting in carbonyl absorption in the infrared spectrum, and the use of methyl ethyl ketone as a solvent was abandoned. Some toluene and benzene were retained by the films, but their presence did not interfere with the observation of infrared absorptions caused by carbonyl or hydroxyl resulting from degradative treatment.

Thickness measurements of the films were made in some cases with a Mikrokator gage that has a scale

[2] Since this paper was written, Matheson and Boyer reported at the Chicago meeting of the American Chemical Society in September 1950, concerning work using infrared absorption to follow carbonyl formation in polystyrene.

range of 0.0014 in. with graduations of 0.00002 in. In other cases the films were measured with a Carson electronic micrometer or with an ordinary micrometer.

4. Experimental Methods

4.1. Measurement of Absorption in the Infrared Region

The infrared absorption spectra of the films were measured between 2.0 and 16.0 μ with a Baird recording infrared spectrophotometer with a sodium chloride prism [16]. This instrument is a double-beam type operating on the optical null principle. Using the atmosphere as a reference, the infrared absorption at each wavelength was recorded through a bolometer, amplifier, and mechanical drive system. A graph of percentage transmission of the film versus wavelength is obtained by this method. Changes in chemical structure of the polystyrene film on exposure to degradative treatment were observed by comparing the infrared absorption spectrum before treatment with the spectrum of the same film after treatment.

The use of the Baird spectrophotometer on this project was necessarily intermittent. Because of changes in the sensitivity of the instrument introduced between periods of use on this project, some of the spectra show differences in resolution and intensity of the bands. These spectra have not been superimposed for comparison, as have the others. No attempt is made in this report to compare or observe minor changes in the infrared absorption spectra, and changes in the absorption bands resulting from the various treatments are considered qualitative rather than quantitative.

4.2. Heat and Ultraviolet Exposure of Films

The film holders, in which the films were exposed to the various treatments, were designed to fit the aperture of the Baird recording spectrophotometer. These holders were made of chromium-plated brass and had a 2⅝-in.-diameter aperture for the film.

Polystyrene films inserted in these holders were exposed at 100° C in a laboratory forced-draft oven. Ultraviolet exposure in air was made by placing the films on a revolving table 6 in. from an S–1 sunlamp.[3] The temperature of the air at the revolving table was about 60° C. This sunlamp equipment is described in Method No. 6021 of Federal Specification L–P–406a [17].

4.3. Outdoor Exposure of the Films

Several films inserted in metal holders were exposed outdoors in Washington, D. C., on racks at an angle of 45°, facing south. This exposure was started in early December 1949, and was continued 5 months, through April 1950.

[3] It is recognized that the radiant energy from the S–1 sunlamp includes infrared and visible wavelengths as well as those of the ultraviolet. However, it is assumed that in the short periods of exposure used in these experiments the ultra-violet radiant energy is chiefly responsible for the observed effects.

5. Results

The infrared absorption spectra of polystyrene films, both untreated and after exposure to heat and to ultraviolet radiant energy in the presence of air, are shown in figures 1 to 8, inclusive. The many individual absorption bands of polystyrene, as shown in the untreated films (figs. 1 to 4, inclusive), are not discussed in this report. Interpretation is attempted only in the case of bands in which changes are observed as a result of degradative treatment.

5.1. Untreated Films

A comparison of the infrared absorption spectra of untreated films of samples A, B, C, D, E, E1, and G1 was made as the initial phase of this work. The absorption spectra showed that samples E and E1 could be differentiated from samples A, B, C, D, and G1 by a comparison of absorption at 5.75 μ for films at least 0.0009 in. thick. Infrared absorption spectra of untreated films of samples C and E1 are shown in figures 1 and 2, respectively, as representative of the two classes. Comparison of these spectra shows that sample E1 has greater absorption at 5.75 μ, indicated by an arrow on the graph. Absorption in this region generally results from the type of structures represented by

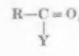

where Y is R, H, OR, or OH.

The infrared absorption spectra of untreated films of sample X are shown in figures 3 and 4, the Baird spectrophotometer having been set at a low sensitivity. Figure 3 shows the spectrum of a film of sample X cast from a benzene solution. The absorption at 5.75 μ is very slight. Figure 4 shows the spectrum of a sample X film cast from methyl ethyl ketone solution. The stronger absorption at 5.85 μ is attributed to the presence of some residual methyl ethyl ketone in the film.

5.2. Films Exposed to 100° C in an Air Oven

Films of polystyrene samples C, E1, and X were exposed for various periods in a laboratory forced-draft air oven at 100° C. No extensive changes in the infrared absorption spectra of the films were observed as a result of this treatment, that is, no new bands were created or old bands removed. Figure 5 shows the infrared absorption spectra of a film of sample X after 200 hr at 100° C in air superimposed on the absorption spectra of the same film after 50 hr at 100° C in air. Only insignificant changes in the absorption spectra are shown as a result of this exposure. No chemical changes have occurred that are detectable by infrared spectrophotometry. This is also representative of the results obtained with films of samples C and E1 exposed for 270 hr. These results differ from those suggested by Jellinek [11] for pyrolytic conditions.

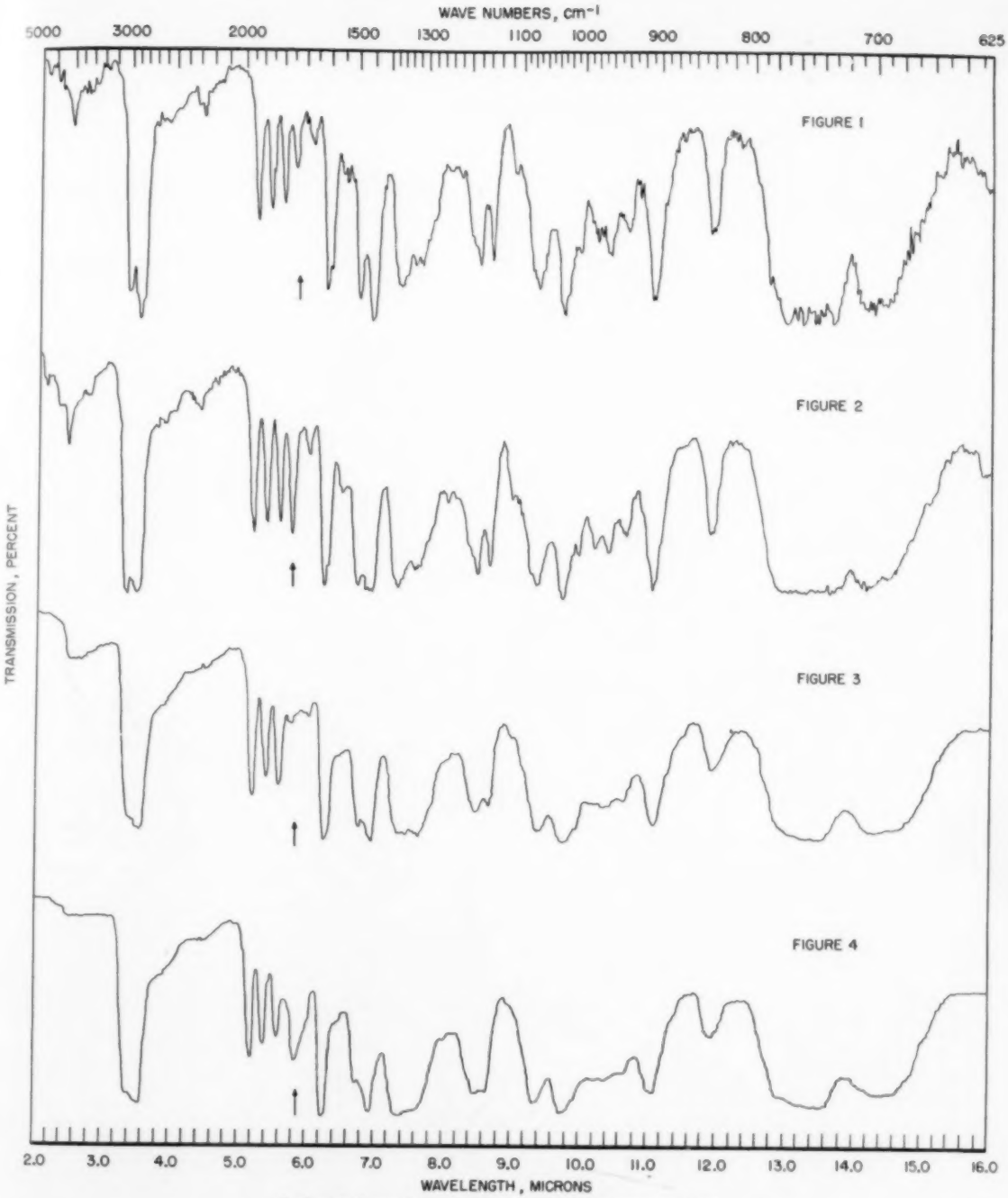

Infrared absorption spectra of untreated polystyrene films

Figure	Sample	Thickness	Solvent	Figure	Sample	Thickness	Solvent
		in.				*in.*	
1	C	0.007	Toluene	3	X	0.007	Benzene
2	E1	.007	Toluene	4	X	.007	Methyl ethyl ketone

5.3 Films Exposed to Ultraviolet Radiant Energy at 60° C in Air

A comparison of the absorption spectrum of sample X after 50 hr of exposure to ultraviolet radiant energy at 60° C in air with the absorption spectrum after 200 hr at these conditions is shown in figure 6. Definite increases in absorption at approximately 2.9 and 5.8 μ after 200 hr of treatment indicate the formation of hydroxyl and carbonyl groups, respectively.

The absorption spectrum of an untreated film of sample C is compared in figure 7 with the absorption spectrum of the same film after 200 hr of exposure to ultraviolet radiant energy at 60° C in air. The formation of hydroxyl and carbonyl groups is indicated by the definite increases in absorption at 2.9 and 5.8 μ, respectively. The elimination of the absorption at 13.7 μ is attributed to loss of residual toluene solvent. A rather general increase in the background absorption results from the treatment.

Comparison of figures 7 and 8 shows that polystyrene sample E1 exhibits similar changes in infrared absorption when exposed to ultraviolet radiant energy in air.

5.4. Films Exposed to Outdoor Weathering

In order to determine whether outdoor weathering would produce hydroxyl and carbonyl groups in polystyrene, films of samples A, E1, and X were exposed outdoors for 5 months in Washington, D. C. Measurements made every month show that oxidation occurs progressively in all three samples and produces hydroxyl and carbonyl groups. The change in absorption attributed to the formation of hydroxyl groups is relatively weak. The superimposed initial and 4-month transmission curves for samples X and E1 are presented in figures 9 and 10, respectively.

6. Discussion of Results

The infrared absorption spectra show that hydroxyl and carbonyl groups are formed in the polystyrene polymer on exposure to ultraviolet radiant energy from both natural and experimental sources. The oxidation resulting in these products probably occurred through the formation of a hydroperoxide on the tertiary carbon in the polystyrene chain. This mechanism can be postulated as follows:

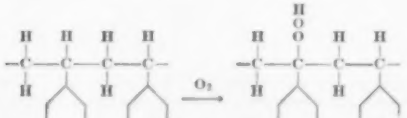

The hydroxyl and carbonyl groups could result from subsequent breakdown of this hydroperoxide under ultraviolet radiant energy.

George and Walsh [18] have studied the decomposition of tertiary alkyl peroxides. Milas and Surgenor [19] have shown that the following scheme can be applied to the thermal decomposition of tertiary butyl hydroperoxide:

$$(CH_3)_3COOH \xrightarrow{95 \text{ to } 100^\circ \text{ C}} (CH_3)_3COH + O\cdot$$

$$(CH_3)_3COOH \xrightarrow{250^\circ \text{ C}} (CH_3)_2CO\cdot + \cdot OH$$

$$(CH_3)_2CO\cdot \longrightarrow (CH_3)_2C{=}O + CH_3\cdot$$

$$CH_3\cdot + \cdot OH \longrightarrow CH_3OH$$

The decomposition of the tertiary hydroperoxides in polystyrene may lead to carbonyl and hydroxyl groups by a similar mechanism:

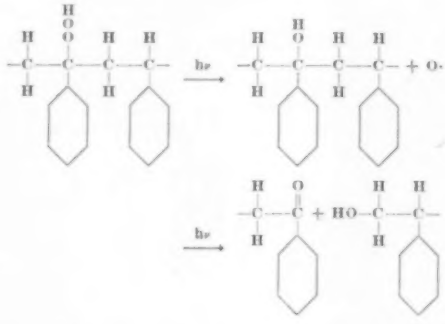

This mechanism would also presumably be of a free radical nature.

Although no evidence of oxidation was observed in the infrared spectra after heating the polystyrene films for 270 hr at 100° C in air, this does not necessarily infer that longer exposure or higher temperature would not produce oxidation resulting in hydroxyl and carbonyl groups. The infrared pattern after 100 hr at 125° C in an air oven showed no extensive changes from the initial pattern, although the films were starting to sag and flow. Continued exposure resulted in destruction of the films due to flow and development of holes. Films exposed to 150° C in an air oven (after previous exposure to 100° C for 270 hr) developed holes and flowed after 1 hour's treatment. The necessary energy to cause oxidation is supplied, however, on exposure to ultraviolet radiant energy at a temperature as low as 60° C. The carbonyl group absorption is definitely present after 70 hr of exposure and the hydroxyl absorption after 100 hr. This is compatible with the hypotheses of Jellinek and others [10 and 11] that hydroperoxide formation may be responsible for the degradation of polystyrene.

Assuming random scission, the formation of carbonyl groups would decrease the molecular weight of the polymer since the formation of each carbonyl would cause a break in the chain molecule. An increase in solubility would be expected as a result. Ultraviolet-treated samples of C and E1 in table 2 show that oxidation resulting in the formation of hydroxyl and carbonyl groups is accompanied by an

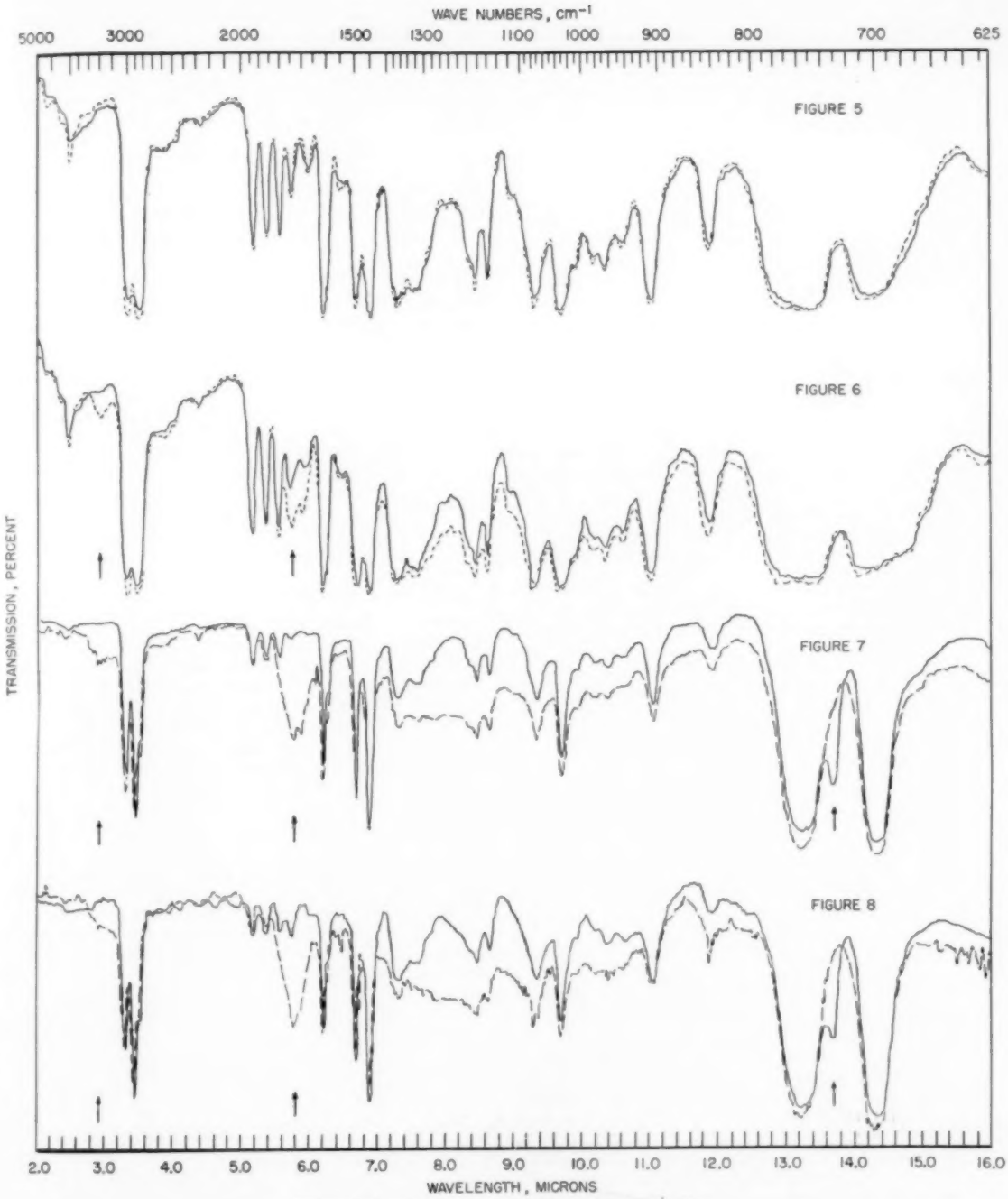

Infrared absorption spectra of treated polystyrene films

Figure	Sample	Thickness	Solvent	Treatment
5	X	0.007 in.	benzene	—, 50 hr at 100° C in air; - - - -, 200 hr at 100° C in air.
6	X	.007	benzene	—, 50 hr S-1 sunlamp at 60° C; - - - -, 200 hr S-1 sunlamp at 60° C.
7	C	0.001 in.	toluene	—, Untreated; - - - -, 200 hr S-1 sunlamp at 60° C.
8	E1	.001	toluene	—, Untreated; - - - -, 200 hr S-1 sunlamp at 60° C.

TABLE 2. *Solubility of polystyrene samples*

Sample designation	Treatment	Solvent used	Thickness of film	Apparent solubility *	Condition of film	Color of film
			in.			
X	Untreated	a. Methyl ethyl ketone	0.0009	Soluble immediately	Not brittle	Colorless.
		b. do	.007	Soluble	Brittle	Do.
		c. Benzene	.007	do	do	Do.
C	do	Toluene	.001	Soluble immediately	Not brittle	Do.
E1	do	do	.001	do	do	Do.
X	200 hours at 100° C in air	a. Methyl ethyl ketone	.008	do	Slight flow; brittle	Do.
		b. Benzene	.007	do	do	Do.
C	238 hours at 125° C in air	Toluene	.010	Soluble	Film not intact; evidence of flow; brittle.	Slightly yellow.
E1	216 hours at 125° C in air	do	.007	do	do	Do.
X	200 hours S-1 sunlamp at 60° C in air.	a. Methyl ethyl ketone	.007	Soluble immediately	Very brittle	Yellow.
		b. Benzene	.008	do	do	Do.
C	do	Toluene	.001	Insoluble (yellow particles remain).	Splitting; very brittle	Do.
E1	do	do	.001	Some insolubility (yellow particles remain).	do	Do.

* Soluble immediately = soluble within 5 min with shaking; soluble = soluble within approximately 1 hr with occasional shaking.

apparent decrease in solubility. The formation of carbonyl groups may, therefore, not be concomitant with chain scission; or a competitive cross-linking may be overshadowing chain scission. It is also possible that the groups in question are formed by reaction at chain ends or by oxidation of the benzene ring. The latter type of oxidation can be postulated as follows:

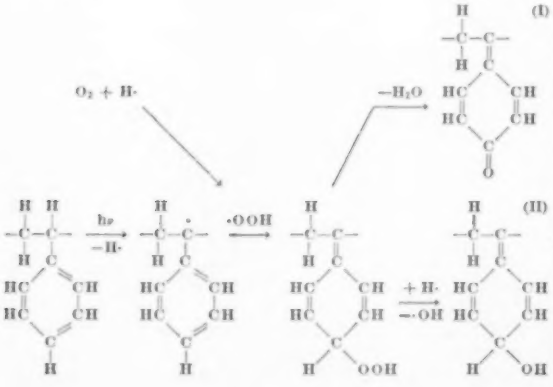

The (I) structure, which is basically a quinone, contains the requirements such as conjugated double bonds and carbonyl conjugate with a double bond to explain the discoloration of the polymer observed on exposure to ultraviolet radiant energy. On the other hand, a sufficient number of quinoid carbonyl groups to account for the absorption at 5.8 μ in figures 6, 7, and 8 after treatment should also be accompanied by noticeable absorptions characteristic of the quinoid structure. The absence of noticeable differences at 6.2 μ is not very good negative evidence, since the absorption may be obscured by that of the unchanged benzene structure.

If it is assumed that some benzene rings may exist as part of the linear polymer chain, the following structure is suggested for the polymer:

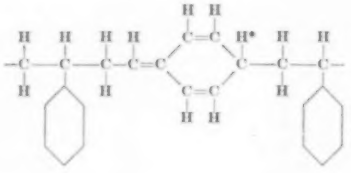

The hydrogen of a tertiary carbon atom (*) is available for the hydroperoxidation as are double bonds in a ring that may be oxidized singularly without subsequent scission of the linear chain. However, the likelihood of such a structure forming in the polymer is very slight, and consequently the amount would be too small to account for the results obtained in this study; but it might be considered as a contributing influence. Oxidation at the double bond also seems probable in the structures (I) and (II).

Table 1 shows that the polystyrenes used in this study contain oxygen. This oxygen was probably introduced in the polymerization stage. One possible structure likely to be formed when the double bond of the monomer is opened in the presence of oxygen is as follows:

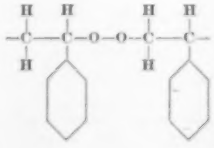

With oxygen in this form in the polymer, the production of carbonyl and hydroxyl groups on exposure to ultraviolet radiant energy can be postulated as follows:

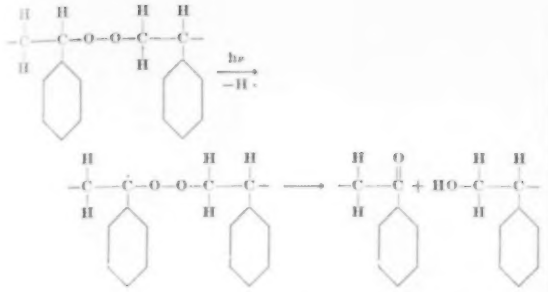

This process also causes a decrease in molecular weight and may result in products similar to those postulated for the breakdown of hydroperoxide on the tertiary carbon atom.

Since sample X was polymerized from purified styrene in a nitrogen atmosphere, the oxygen may have been taken on after the polymerization stage. In this case, as well as for all the other samples, it may be that the oxygen will react with an unsaturated group at the end of a molecule to give the following structures, which may react on exposure to ultraviolet radiant energy as indicated:

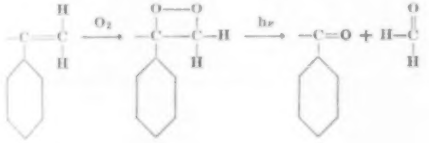

or

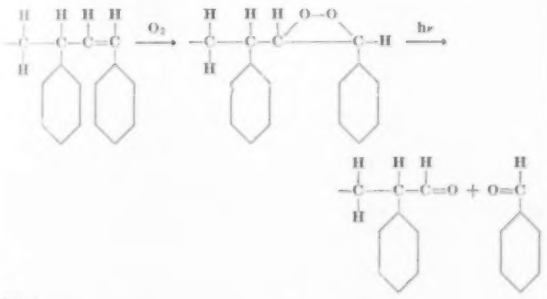

or

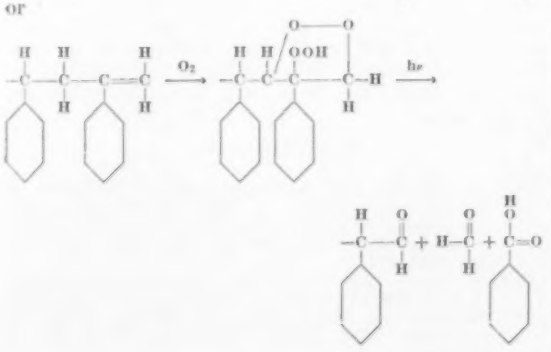

or

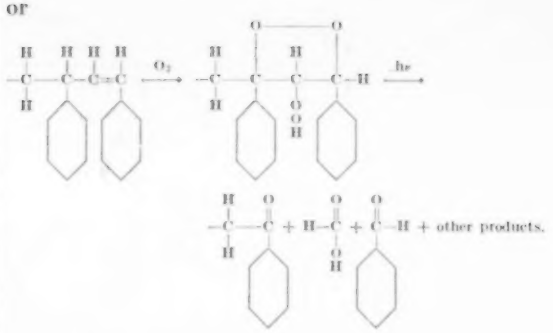

All these mechanisms show that the oxidation of a double bond chain end is likely to produce a carbonyl group on the end of the polymer molecule. The diperoxide structure given above has been suggested by Bolland and Hughes for squalene [20]. Chain end oxidation could be expected to produce a relatively smaller number of carbonyl groups than hydroperoxide chain scission, and the latter would appear to conform better to the solubility effects for sample X in table 2.

In regard to the hydroxyl absorption in the infrared spectra, the absorption band is found in the region of hydrogen-bonded hydroxyl rather than at the somewhat shorter wavelength attributed to free hydroxyl [14, 15]. Intermolecular bridging between hydroxyls in adjacent chains seems probable as shown below:

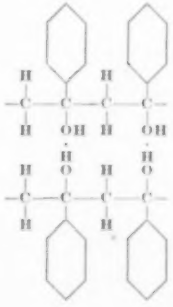

This suggests the possibility of crosslinking of chains by loss of water forming the ether linkage between chains. Also it is possible to postulate both peroxide and carbon to carbon crosslinking at the carbon bearing the tertiary hydrogen. Such crosslinking and intermolecular bridging would help to explain the increased brittleness and decreased solubility of the polystyrene on exposure to ultraviolet radiant energy. With sufficient fundamental background data it might be possible to identify some of the existing absorption bands in the spectrum of ultraviolet-treated films as due to ether or peroxide linkages.

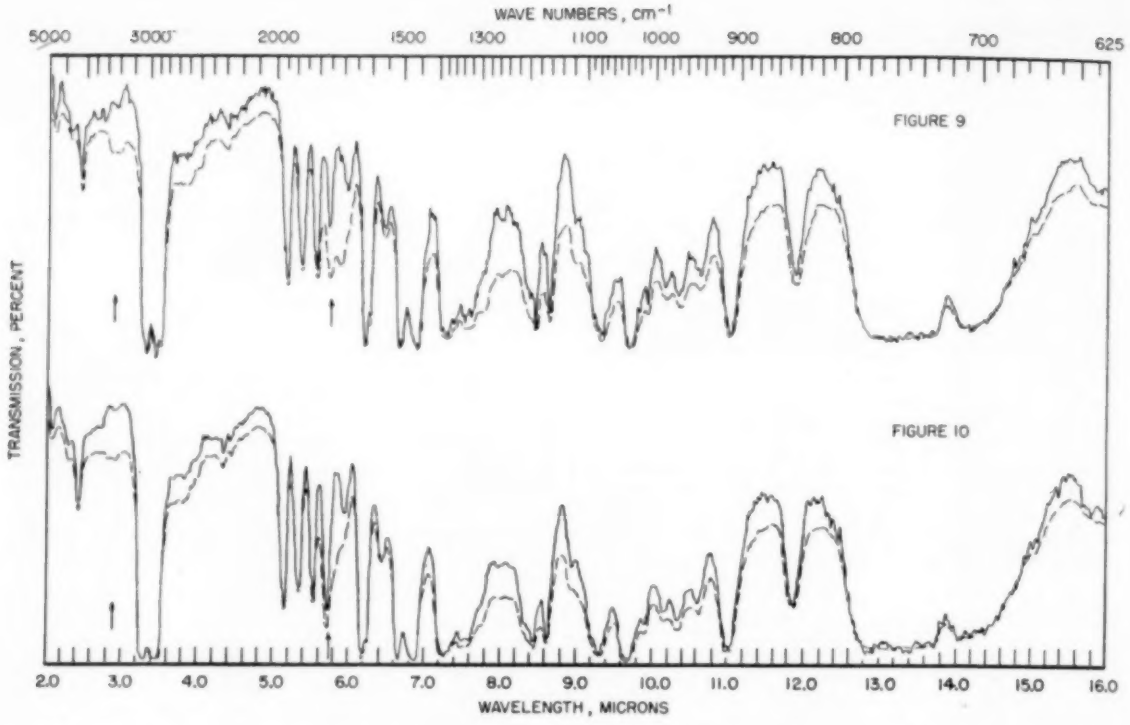

Infrared absorption spectra of treated polystyrene films

Figure	Sample	Thickness	Solvent	Treatment
		in.		
9	X	0.007	toluene	—, Untreated; ——, 4 months' outdoor exposure.
10	E1	.008	toluene	—, Untreated; ——, 4 months' outdoor exposure.

7. Summary and Conclusions

Polystyrene films oxidize when exposed to ultraviolet radiant energy in air. Absorptions characteristic of hydroxyl and carbonyl groups are found in the infrared spectra of the exposed films.

Exposure of polystyrene films in an air oven at 100° C for 270 hr does not result in hydroxyl or carbonyl absorption in the infrared spectra. Oxidation resulting in the formation of these groups might occur on longer exposure or exposure at higher temperature; however, the films were destroyed by flow at prolonged exposure at 125° C.

The degradation of polystyrene film by ultraviolet radiant energy in the presence of air probably occurs through the formation of a hydroperoxide and subsequent breakdown and rearrangement to give hydroxyl and carbonyl products in the polymer. These carbonyl groups are most likely in the form of ketones; however, by means of the infrared spectra it is not possible to differentiate between the carbonyls of the ketone, aldehyde, and acid, all of which might be present to some degree.

This investigation was sponsored by and conducted with financial assistance from the Office of the Quartermaster General, Department of the Army.

The courtesy of C. J. Humphreys, Chief of the Radiometry Section, in making the Baird Recording Spectrophotometer available for this work is appreciated.

The work of E. K. Plyler of the Radiometry Section on another project, in which he found that the commercial grades of polystyrene are of two types as shown by differences in absorption at 5.75 μ, was used as a basis for selecting samples C and E1 for this work; his help and encouragement are appreciated.

8. References

[1] E. H. Farmer and A. Sundralingam, The course of autoxidation reactions in polyisoprenes and allied compounds. Part I. The structure and reactive tendencies of the peroxides of simple olefins, J. Chem. Soc. **1942,** 121.

[2] E. H. Farmer, G. F. Bloomfield, A. Sundralingam, and D. A. Sutton, The course and mechanism of autoxidation reactions in olefinic and polyolefinic substances, including rubber, Rubber Chem. and Tech. **15,** 756 (1942).

[3] E. H. Farmer, Peroxidation in relation to olefinic structure, Trans. Faraday Soc. **42,** 228 (1946).
[4] E. H. Farmer and A. Sundralingam, The course of autoxidation reactions in polyisoprenes and allied compounds. Part VI. The peroxidation of rubber, J. Chem. Soc. **1943,** 125.
[5] E. H. Farmer, Oxidative breakdown of rubber, IRI Trans. **21,** 122 (1945).
[6] H. S. Taylor and A. V. Tobolsky, Radical chain processes in vinyl and diene reactions, J. Am. Chem. Soc. **67,** 2063 (1945).
[7] A. V. Tobolsky, Oxidative degradation of polymeric materials, Discussions of the Faraday Soc. No. 2, 384 (1947).
[8] J. O. Cole and J. E. Field, Oxidation of GR–S and other elastomers, Ind. Eng. Chem. **39,** 174 (1947).
[9] H. S. Taylor and J. O. Smith, Jr., The reactions of methyl radicals with benzene, toluene, diphenyl methane, and propylene, J. Chem. Phys. **8,** 543 (1940).
[10] H. Staudinger and A. Steinhofer, Über hochpolymere Verbindungen. 107. Mitteilung, Polystyrole. Ann. chem. **517,** 35 (1935).
[11] H. H. G. Jellinek, Thermal degradation of polystyrene, Part II, J. Polymer Sci. **4,** 1 (1949).
[12] H. W. Thompson and P. Torkington, The infrared spectra of compounds of high molecular weight, Trans. Faraday Soc. **41,** 246 (1945).
[13] R. B. Barnes, U. Liddel, and V. Z. Williams, Synthetic rubber. A spectroscopic method for analysis and control, Ind. Eng. Chem., Anal. Ed. **15,** 83 (1943).
[14] R. B. Barnes, R. C. Gore, U. Liddel, and V. Z. Williams, Infrared spectroscopy—industrial applications and bibliography (Reinhold Publishing Corp., New York, N. Y., 1944).
[15] R. B. Barnes, R. C. Gore, R. W. Stafford, and V. Z. Williams, Qualitative organic analysis and infrared spectrometry, Anal. Chem. **20,** 402 (1948).
[16] W. S. Baird, H. M. O'Bryan, G. Ogden, and D. Lee, Automatic recording infrared spectrophotometer, J. Opt. Soc. Am. **37,** 754 (1947).
[17] Plastics, organic: general specifications, test methods. Federal Specification L–P–406a (Government Printing Office, Washington 25, D. C., Jan. 24, 1944).
[18] P. George and A. D. Walsh, A note on the decomposition of tertiary alkyl peroxides, Trans. Faraday Soc. **42,** 94 (1946).
[19] N. A. Milas and D. M. Surgenor, Studies in organic peroxides. VIII. *t*-Butyl hydroperoxide and di-*t*-butyl peroxide, J. Am. Chem. Soc. **68,** 205 (1946).
[20] J. L. Bolland and Hilda Hughes, The primary thermal oxidation product of squalene, J. Chem. Soc. **1949,** 492.

WASHINGTON, July 14, 1950.

U. S. GOVERNMENT PRINTING OFFICE: 1951